Short-term Motion Prediction of floating offshore wind turbine Based on Muti-input LSTM Neural Network

Wei Shi[1,2,3], Lehan Hu[1], Zaibin Lin[4], Lixian Zhang[1], Jun Wu[5], Wei Chai[6*]

[1]DeepWater Engineering Research Centre, Dalian University of Technology, China;

[2] State Key Laboratory of Coastal and Offshore Engineering, Dalian University of Technology, Dalian, China;

[3] Research Institute of Dalian University of Technology in Shenzhen, Shenzhen, China;

[4]School of Engineering, University of Aberdeen, UK

[5] School of Naval Architecture and Ocean Engineering, Huazhong University of Science and Technology, Wuhan, China

[6] School of Naval Architecture, Ocean and Energy Power Engineering, Wuhan University of Technology, Wuhan, China

* Corresponding author: Prof. Wei Chai, Email: chaiwei@whut.edu.cn

Abstract: The motion response of an offshore floating wind turbine (FOWT) platform is closely related to the control operation regarding the safety of a wind turbine. It is affected by various factors such as sea state environments and mooring systems. In practice, how to predict the motion response of the wind turbine platform in the short term has always been a concern of engineering practice. At present, the development of deep learning technology has brought some potential solutions to this problem. In this paper, a Multi-Input Long-Short Term Memory (MI-LSTM) neural network method is proposed to predict the short-term motion response of a floating offshore wind turbine platform. Specifically, the numerical simulation of the 5MW Braceless platform is carried out under different environmental conditions, and the data of

platform motion response, wave elevation, and mooring force are selected as input variables. Then the training and test groups are established after post-processing data. Subsequently, a Single-Input LSTM (SI-LSTM) model and a Multi-Input LSTM (MI-LSTM) model are established to learn the input data. After comparing the overall accuracy of the results, it is found that the additional mooring force and wave elevation positively affects the platform response prediction results. From the aspects of discreteness and overall accuracy, it is verified that the established MI-LSTM model is also applicable, considering the influence of second-order hydrodynamics. Lastly, compared with the prediction results obtained by the multi-input one-dimensional convolutional neural network (MI1D-CNN), the advantages of the two different models are expounded from the perspectives of training time and accuracy, which provides ideas for the optimization of the FOWT motion response prediction model. This study sheds insights on the short-term motion response forecast and platform positioning of a FOWT. Short-term forecasts of a FOWT can be achieved under various sea conditions by combining the global positioning system.

Keywords: Floating offshore wind turbine; deep learning; response prediction; multi-input LSTM model; second-order hydrodynamic

1. Introduction

With the rapid development of the global economy, energy has become a critical factor in determining social and economic development. To meet the Net Zero target by utilizing sustainable energy, the vigorous growth of renewable energy has become an essential part of the development strategy worldwide. Due to its high energy conversion ability, offshore wind power has been gradually installed in various countries recently. Different foundations of floating offshore wind turbines have been proposed, including spar, tension leg platform (TLP) shape, semi-submersible, and barge [1]-[2]. Substantial research has been carried out in terms of hydrodynamics, mooring systems, stability, performance, and survivability of a FOWT [3]-

[6].

Compared with the onshore wind turbine structure, a FOWT encounters a more complex ocean environment. The motion response of a FOWT occurs at six degrees of freedom (6DOF) and leads to significant challenges in design and assessment [7]. Therefore, it is of great significance to propose an accurate prediction method for the motion response of the FOWT to guide the design and assess structural safety. In the deep learning model, motion response prediction is generally based on the historical data of motion response and many other results from numerical and experimental measurements. In general, deep learning technology is applied to predict the motion response of structures in the next few seconds [8]. According to the length of the forecast time, motion response prediction can be categorized as short-term and safe-period motion prediction. Short-term prediction plays a vital role in improving dynamic positioning control performance, and it provides early warning in extreme sea conditions to reduce platform damage to a certain extent. A short-term forecast's prediction advanced time (PAT) is generally a few seconds, and it requires high forecast accuracy [9].

In recent years, the application of deep learning technology in offshore structures has gradually expanded. The research is mainly carried out by the convolutional neural network (CNN) and the recurrent neural network (RNN) methods [10]-[18]. Wang et al. [11] proposed the Low-frequency adds wave-frequency responses (LAWR) method to predict the mooring line tension of a semi-submersible platform. Combined with the LSTM method, accurate results are obtained for predicting mooring line tension under different cases. Pena et al. [15] proposed the Wave-Generative Adversarial Network (Wave-GAN) technology, combined with CNN convolutional neural network and CFD method, to predict the load of nonlinear waves on fixed structural columns. Pena et al. [15] concluded the maximum error between the Wave-GAN predicted value and CFD simulated value of 1.5%-2% by adjusting several parameters, and the mean absolute error (MAE) of the test group is about 0.014. Lian et al. [16] constructed the digital twin of mesh clothing and established the deep neural network (DNN) to predict whether the mesh clothing is damaged. The average accuracy of the final identification model is 94.3%. Bjørni et al. [17] predicted the mooring line tension in the next 30 s by taking the platform motion response in the first 60 s as input and constructed a three-layer deep neural network with bias term. It is concluded that the average error of anchor chain tension is 0.46% through cross-sectional comparisons. According to the combined prediction method of the Extreme Learning Machine (ELM), the Empirical Mode Decomposition (EMD), and LSTM neural network, Zhang et al. [18] proved that the combined prediction method presented higher prediction accuracy than the single LSTM model and ELM-LSTM model. However, when considering the influence of environmental factors and mooring force, there is limited research on predicting the motion response of a FOWT. At the same time, in practice, it needs to assess the motion response of a FOWT under the influence of various complex factors and consider the impact of second-order hydrodynamic force. Moreover, the amount of research on the motion response prediction of a FOWT under the effect of the second-order hydrodynamic force is also limited.

To investigate the short-term motion prediction of a FOWT, the MI-LSTM Neural Network model is used. This paper is organized as follows: Section 2 introduces the basic principles of the RNN. The architecture and differences between the established SI-LSTM model and the MI-LSTM model are explained in detail. The hyperparameters of the model and the selection of the training and test groups are also given in this section. Then, in Section 3, the structure size of the 5 MW Braceless platform model is shown. A detailed comparison is made between the prediction results of the SI-LSTM and MI-LSTM models under different environmental conditions in Section 4. This proves the positive excitation of the increased input factor numbers on the prediction results and illustrates the advantages and benefits of the MI-LSTM model. In Section 5, the applicability of the proposed model is demonstrated when the second-order hydrodynamic force is considered. Given that there are few comparisons between the RNN model and CNN model regarding time domain problems, in Section 6, by comparing the prediction results of the proposed model with the multi-input one-dimensional convolutional neural network (MI1D-CNN) model, the advantages of the two models are illustrated from the perspectives of overall accuracy and training time. Finally, the conclusions and recommendations are made to the future optimization of the platform response prediction model.

2. Long-Short Term Memory (LSTM) Neural Network

2.1. Recurrent Neural Network (RNN)

Recurrent neural network (RNN) is gradually emerging in the interdisciplinary field as a typical representative of deep learning technology. RNN takes time series data as input and performs recursion in the evolution direction of the sequence, where all nodes (cyclic units) are linked in a chain [19]. RNN has memorization, parameter sharing, and turning completeness [20]-[22], so it has clear advantages in learning the nonlinear features in sequences. RNNs are widely used in natural language processing, such as speech recognition, language modeling, and time series prediction. RNN performs outstandingly in solving scheduling problems, and motion response prediction is the typical time domain problem. Therefore, in this paper, RNN is selected for model architecture.

Since the motion of the platform at time t is affected by the motion at the previous time $t-1$, meanwhile, the motion at current time t will also have an impact at forward time $t+1$, platform motion response is a continuous process with time dependence. Considering this characteristic, the traditional deep neural network (DNN) cannot convey information precisely in the time sequence, but the RNN is developed to overcome this problem. Training input data from a FOWT system to predict the motion response in the next few seconds can be viewed as an adaptive function mapping. The input is the previous time series information of different input factors, and the output is the motion response in the future. Hence, the trained deep learning model can achieve prediction in a short time.

The timeline expansion of the RNN is shown in **Figure 1**, where x is the network input layer, s is the network node hiding layer, and o is the network node output layer. After the network receives the input x_t at time t, the value of the hidden layer is s_t and the output value is o_t. The value of s_t depends not only on x_t, but also on s_{t-1}. In other words, s inherits the information from each node.

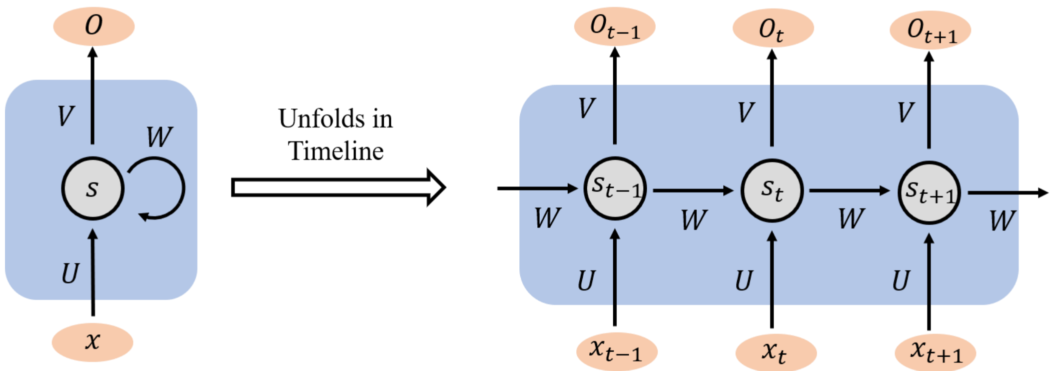

Figure 1. An unfolded RNN network

The calculation method of the RNN network is shown in Equations 1-2:

$$o_t = \boldsymbol{g}(\mathbf{V} \cdot s_t) \tag{1}$$

$$s_t = \boldsymbol{f}(\mathbf{U} \cdot x_t + \mathbf{W} \cdot s_{t-1}) \tag{2}$$

where **V** is the weight matrix of the output layer, ***g*** is the activation function for the output layer, **U** is the weight matrix of the input layer x, **W** is the weight matrix of the last value, which is the input of this time, and ***f*** is the activation function for the hidden layer. Common activation functions, such as sigmoid, tanh, Rectified Linear Unit (ReLU), and linear activation function, can be selected according to data characteristics and experimental effects. The sigmoid activation function is generally selected for hidden layer activation function ***f***, while the linear activation function is generally chosen for output layer activation function ***g***. Equation 1 is the calculation formula of the output layer. The output layer is fully connected, indicating every node in the output layer is connected to every node in the hidden layer. Equation 2 is the calculation formula of the hidden layer.

2.2. Long-Short Term Memory (LSTM) Network

LSTM is first proposed by Hochreiter and Schmidhuber [22]. Compared with traditional RNN, the LSTM network has improved the gradient explosion and gradient extinction. It has been one of the most popular RNN models and is widely applied in many fields, such as speech recognition, image description, and natural language processing. The internal structure of the LSTM node is shown in **Figure 2** [24].

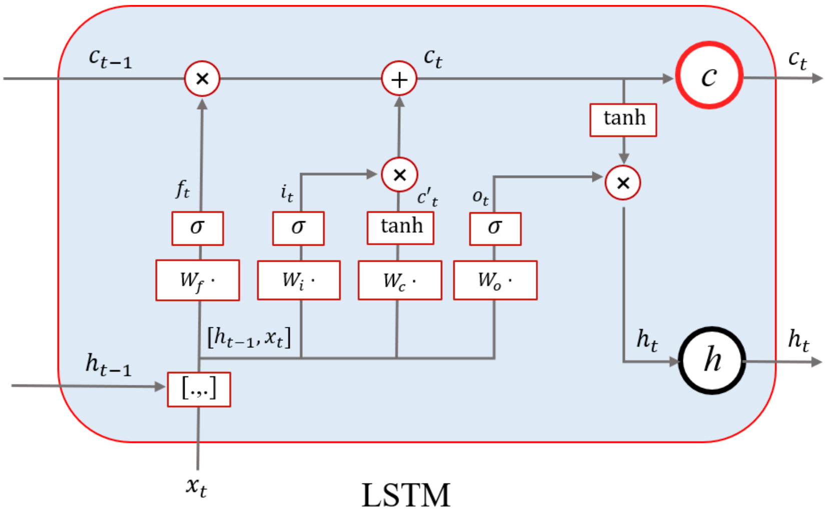

Figure 2. LSTM node unit internal structure

At time t, the LSTM network has three inputs: current time input value x_t, LSTM output value h_{t-1} at the last time, and the unit state c_{t-1} at the previous time. The output of LSTM has two parts: the output value of LSTM at the current time h_t, and the unit state at the current time c_t. x, h, and c are vectors. In addition, LSTM uses the concept of a Gate to control the state of the unit [24]. Gate is a full connection layer which controls information transmission between input and output. Its input is a vector of time series information, and its output is a vector of real numbers between 0 and 1. The gate can be expressed as:

$$G(x) = \boldsymbol{\sigma}(\boldsymbol{W} \cdot x + \mathbf{b}) \tag{3}$$

where $\boldsymbol{W}$ is the weight matrix of the gate, $\mathbf{b}$ is the bias term, and $\boldsymbol{\sigma}$ is the generally sigmoid activation function.

The output vector of the gate is multiplied by the element and the vector is controlled to achieve the gate effect. The gated output is a vector of real numbers between 0 and 1. When the gated output is 0, any vectors multiplied by the output will get the 0 vectors, indicating that no information can pass through. When the gated output is 1, no changes are applied by multiplying, indicating that any information can pass through. Because $\boldsymbol{\sigma}$ has a range of (0,1), the gate is an intermediate state.

LSTM relies on two gates to control the content of the cell state: (1) one is the forget gate that determines the amount of the cell state c_{t-1} at the last moment. c_{t-1} is used to retain the current moment c_t; (2) one is the input gate that determines the amount of the current network input x_t, which is saved to the unit state c_t. Meanwhile, LSTM uses an output gate to control the amount of unit state c_t that is generated from the current output value h_t. The governing equations of each gate are given as follows:

$$f_t = \boldsymbol{\sigma}(\mathbf{W_f} \cdot [h_{t-1}, x_t] + \mathbf{b_f}) \tag{4}$$

$$i_t = \boldsymbol{\sigma}(\mathbf{W_i} \cdot [h_{t-1}, x_t] + \mathbf{b_i}) \tag{5}$$

$$c_t = f_t \cdot c_{t-1} + i_c \cdot tanh(\mathbf{W_C} \cdot [h_{t-1}, x_t] + \mathbf{b_c}) \tag{6}$$

$$o_t = \boldsymbol{\sigma}(\mathbf{W_o} \cdot [h_{t-1}, x_t] + \mathbf{b_o}) \tag{7}$$

$$h_t = o_t \cdot tanh(c_t) \tag{8}$$

where f_t is the forgetting gate equation, $\mathbf{W_f}$ is the weight matrix of the forgetting gate, $[h_{t-1,}x_t]$ is joining two vectors into a longer vector, $\mathbf{b_f}$ is the biased term of the forgetting gate, i_t is the input gate equation, $\mathbf{W_i}$ is the weight matrix of the input gate, $\mathbf{b_i}$ is the offset term of the input gate, c_t is the current moment element state equation, o_t is the output gate control equation, h_t is the final output equation determined by the output gate and unit state.

Existing LSTM network prediction modes mainly fall into the following four types [25]: point-to-point, point-to-sequence, sequence-to-point, and sequence-to-sequence, shown in

Figure 3:

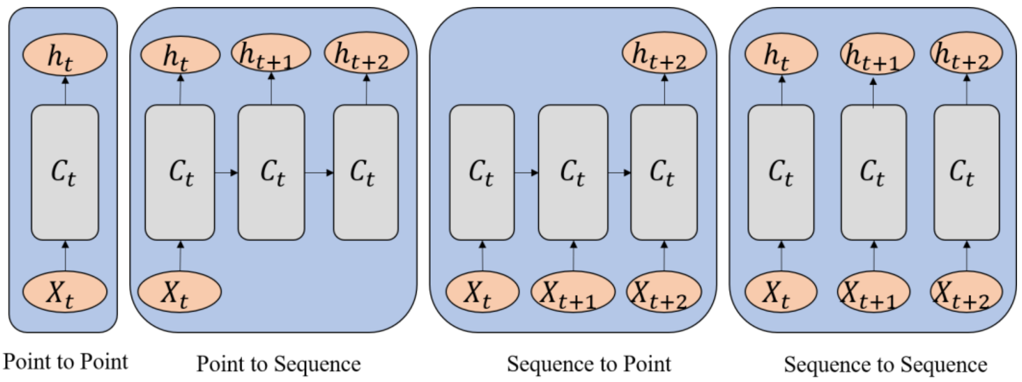

Figure 3. LSTM network prediction modes

The LSTM network in this paper is set up by using sequence-to-point mode for a prediction model, which uses forecasting point response from previous time series after the selected data input mode is adopted in the form of the sliding window. Each window length has 200 time points and the 10 s surge motion. The sliding window form is shown in **Figure 4**, where the mapping relationship between the data input and output is presented when the forecast time is 5 s. Therefore, the response at $t+5$ is predicted based on the response from t-10 to t.

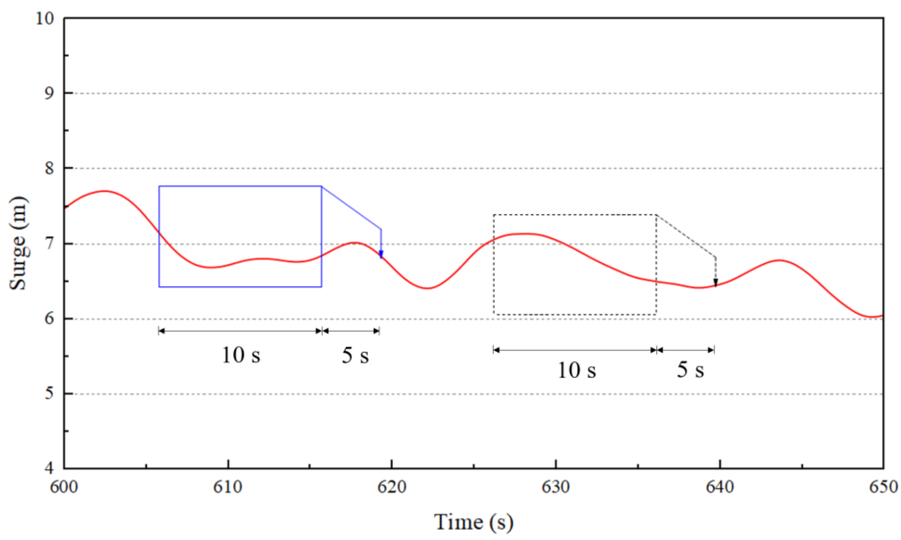

Figure 4. Sliding windows for data input and output

2.3. LSTM Model Structure

The LSTM network model established in this paper has three hidden layers and one fully connected output layer, shown in **Figure 5**. The data sampling frequency is 20 Hz. The input time step of the LSTM network contains 200 time series points with a motion response of 10s. The batch size is set to 256 sample sets, which are also the input for training and updating internal parameters. The number of neurons is set to 200. These two parameters are hyperparameters and can be adjusted according to the performance of the actual test.

Input layer: input time series with a window of 200 data points, representing the motion response of 10s. The input dimension of the single-input model is 1, and that of the multi-input model is 3.

Hidden layer: The hidden layer has 200 nodes.

Output layer: The output layer is dense, the activation function is Linear, and the output result is the motion response at the target time.

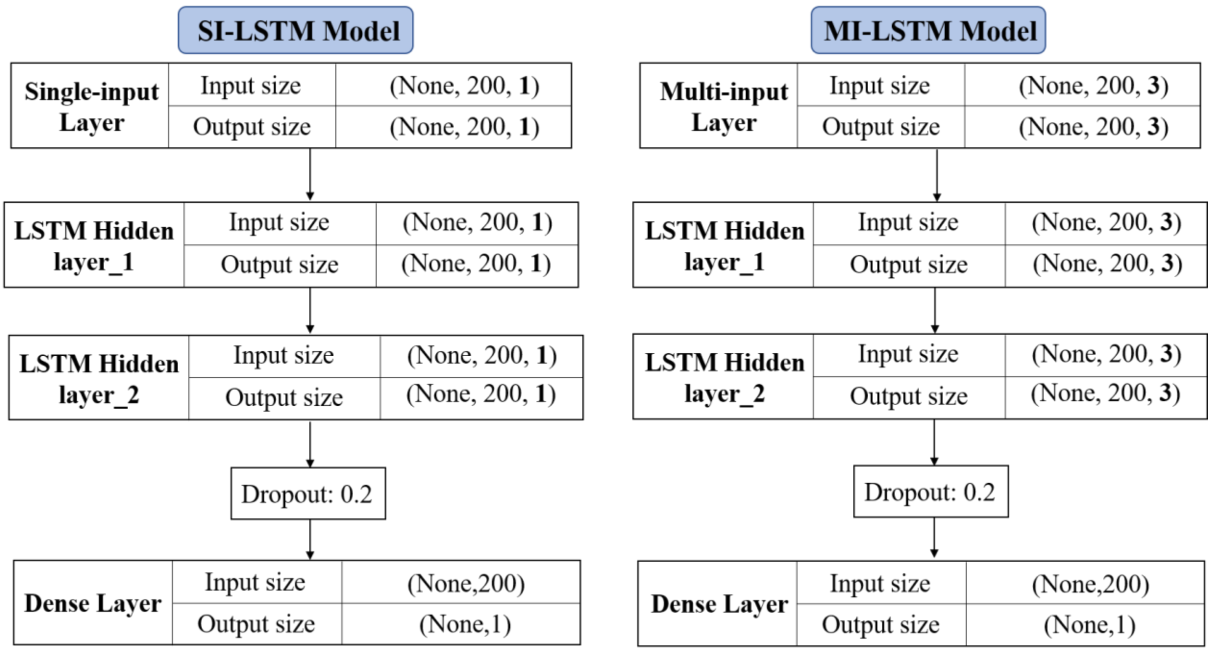

Figure 5. LSTM network model structure and data transfer format

The Adam algorithm is configured for the LSTM network [27]. Adam algorithm is an advanced Stochastic Gradient Descent (SGD) algorithm, which introduces an adaptive learning rate for each parameter. The adaptive learning method and the Momentum method are combined. The learning rate is dynamically adjusted by the first and second moment estimation of the gradient. The gradient descent process is relatively stable and suitable for most non-convex optimization problems in large data sets and high-dimensional space.

Simultaneously, the Dropout layer is added after the input layer and the hidden layer to prevent overfitting [28], and the Dropout_1 and Dropout_2 are set to 0.2. Overfitting may occur due to a large number of unknown network parameters or training times. The principle of dropout is that during the neural network training, some neurons are randomly discarded and not used for training at this round to avoid overfitting and accelerate loss convergence.

In this paper, the LSTM neural network is constructed, and the input data consists of three parts, including time series of previous motion response, mooring force, and wave elevation. And the current motion response is set as the output data. The process of using the LSTM neural network model to predict the motion response is shown in **Figure 6.** The process of predicting motion response by LSTM neural network.

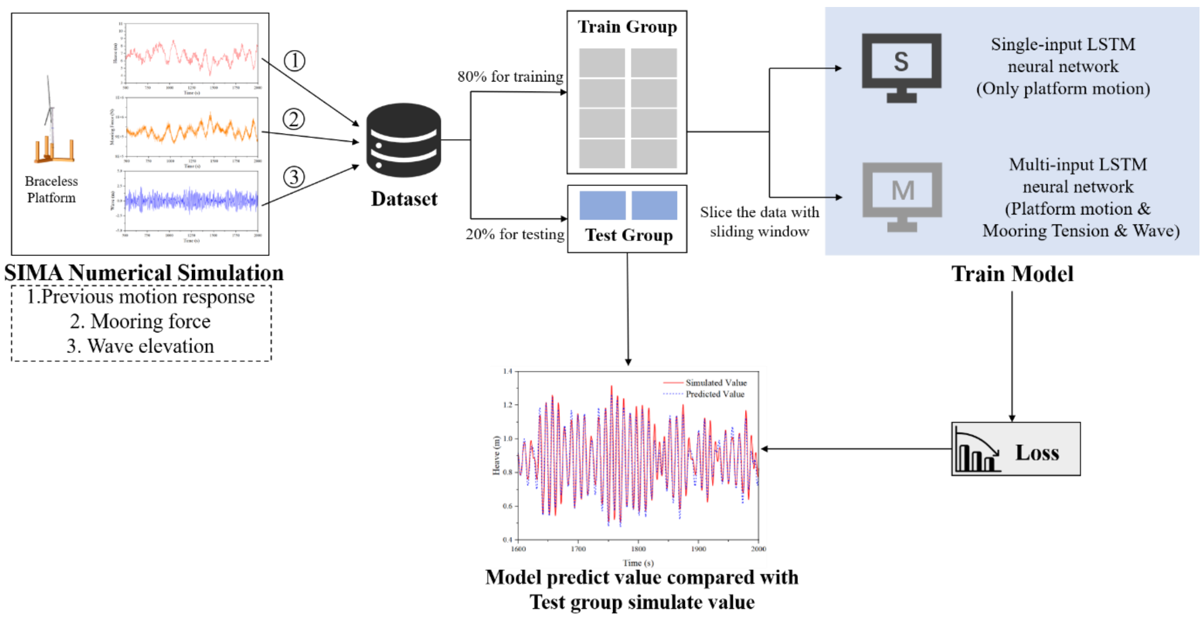

Figure 6. The process of predicting motion response by LSTM neural network

3. Braceless Platform model

The 5 MW Braceless model is established by SIMA, and the time domain response is obtained by numerical simulation. SIMA is developed for the analysis of flexible marine riser systems, but it is also suited for any slender structures, such as mooring lines, and umbilicals, and for steel pipelines and conventional risers. The data used in training in this paper came from the FOWT model of a 5 MW Braceless semi-submersible platform in the water depth of 100 m. The Braceless platform consists of one central column, three side columns, and three pontoons, shown in **Figure 7**.

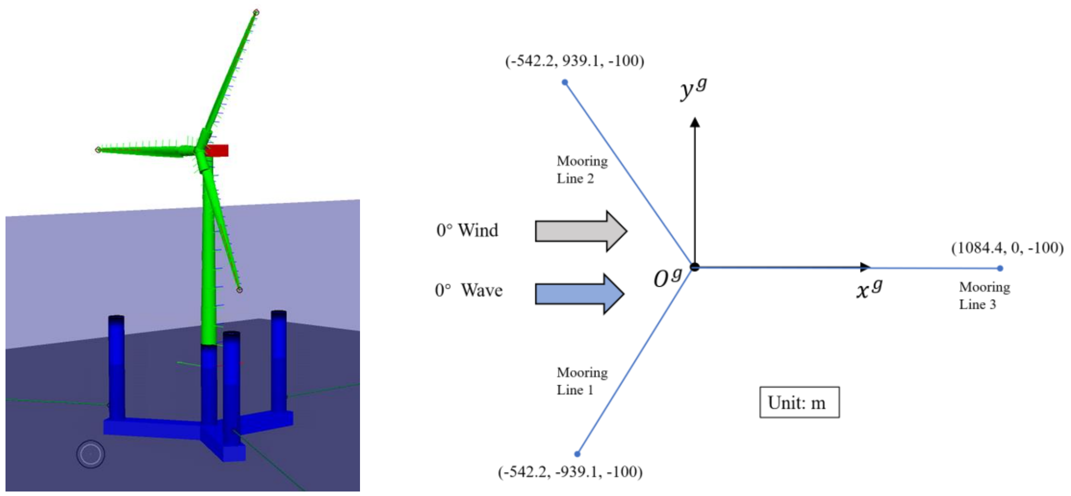

Figure 7. Schematic of 5-MW Braceless platform

Three side columns are evenly distributed around the central column at 120°. They are connected to the bottom of the central column by a floating buoy to form a Braceless semi-submersible platform. The three-point mooring system is adopted, and the anchor chain is set at the bottom of the side column. 0° wave-wind misalignment is considered in the simulation. The main parameters of the Braceless platform are shown in **Table 1.** Parameters of the 5 MW Braceless Platform.

In the following cases, the water depth is 100 m. The average wind speed V_t, effective wave height H_S, and spectrum peak period T_p at the selected cabin height are listed in **Table 2.** Environment matrix (JONSWAP). The significant wave height and spectrum peak period are in 50 years return period. The two-parameter JONSWAP spectrum is used to describe random ocean waves. The Kaimal wind speed spectrum is used to describe the offshore wind conditions.

Table 1. Parameters of the 5 MW Braceless Platform

Parameter	Value
Central column diameter (m)	6.5
Side column diameter (m)	6.5
Buoy height (m)	6
Buoy bottom width (m)	9
Buoy short radius (m)	41
Buoy long radius (m)	45.5
Depth of the draft (m)	30
Displacement (t)	10555
Steel weight (t)	1804
Equivalent thickness (m)	0.03

Table 2. Environment matrix (JONSWAP)

Case	Vt (m/s)	Turbulence intensity (%)	Hs (m)	Tp (s)
EC 1	9.8	10.1	2.9	9.98
EC 2	14.8	15	4.5	11.81
EC 3	16	13	5.3	12.81

4. Single-input and Multi-input

4.1. Data Partitioning and Error Measurement

The sampling frequency of the Braceless platform simulation test is 20 Hz. The total sampling length of motion response (surge, pitch, and sway) is 2000 s. The collected time series

contains 40000 data points. In the training model, the first 32000 points of response data are the training groups and the last 8000 points of response data are the test groups. Three test cases (EC1, EC2, and EC3) are selected, and each test case contained 2000 s surge, pitch, and sway motion data.

The training group data is used to train and obtain the neural network model. The relationship between training Epochs and Loss is observed through the Loss function. Then the test group data is imported into the trained neural network model to verify the accuracy and performance of the trained model.

The Loss function adopted in this paper is the Mean Squared Error (MSE), which is the averaged squared difference between the predicted value and the measured value as shown in Equation 9:

$$MSE = \frac{\Sigma(y_t' - y_t)^2}{n} \tag{9}$$

where $y_t{}'$ is the predicted value of the motion response at time t, y_t is the measured value of the motion response at time t, and n is the total number of predicted values 8000 in this study.

4.2. Single-input Predicted Results

Single-input LSTM (SI-LSTM) model is used to train the motion response data in the training group in terms of the heave, surge, sway, and pitch. The training input of the model is only based on the previous motions. The output of the model is compared and analyzed with the data of the test group. The predicted advance time is set as 2.5 s and 5 s respectively. The actual and predicted values are shown in **Figures 8-10**.

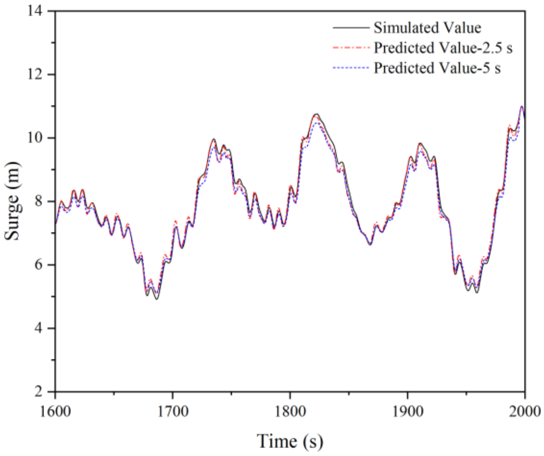

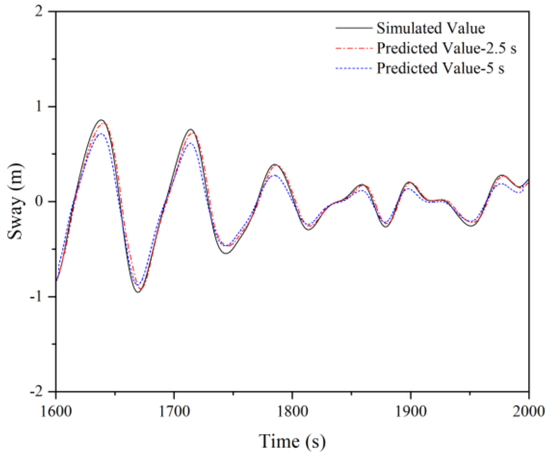

(a) (b)

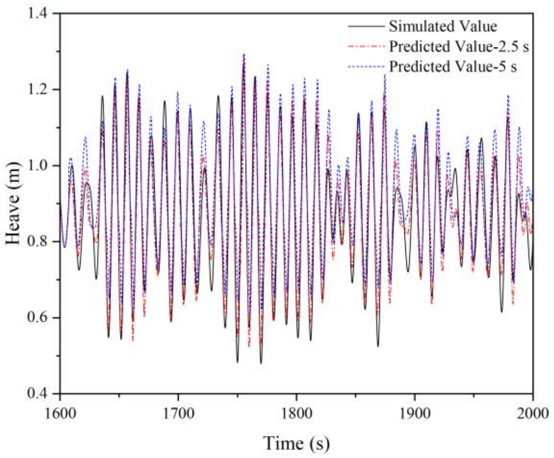

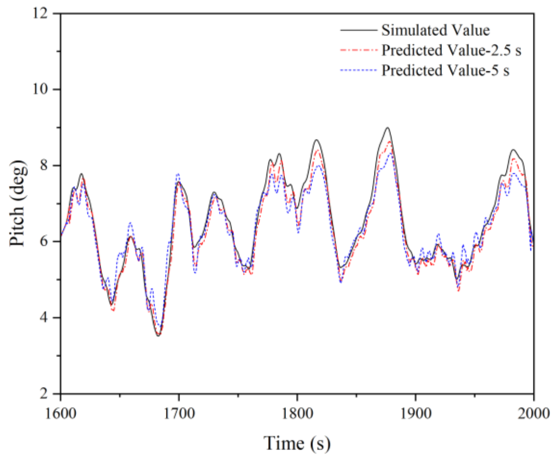

(c) (d)

Figure 8. Simulated and predicted values of EC 1 at 2.5 s and 5 s:

(a) Surge; (b) Sway; (c) Heave; (d) Pitch

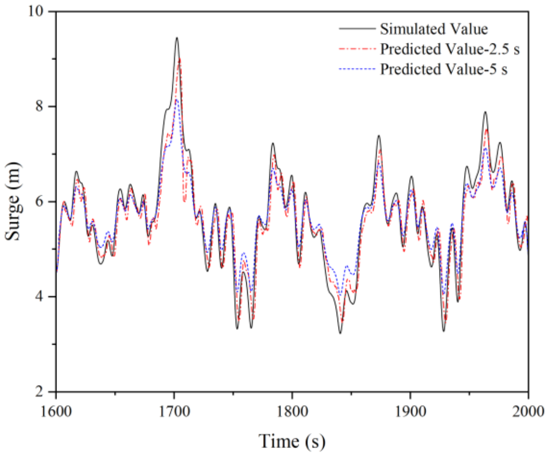

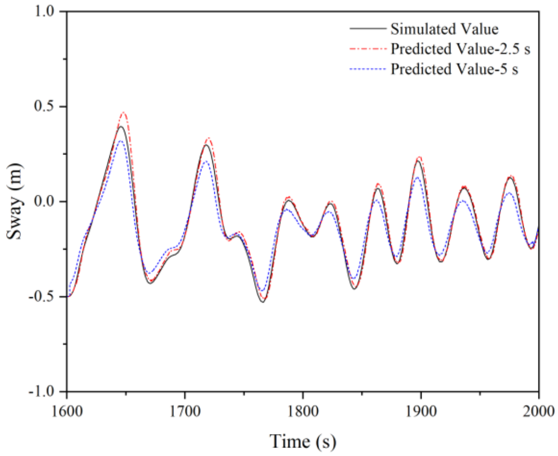

(a) (b)

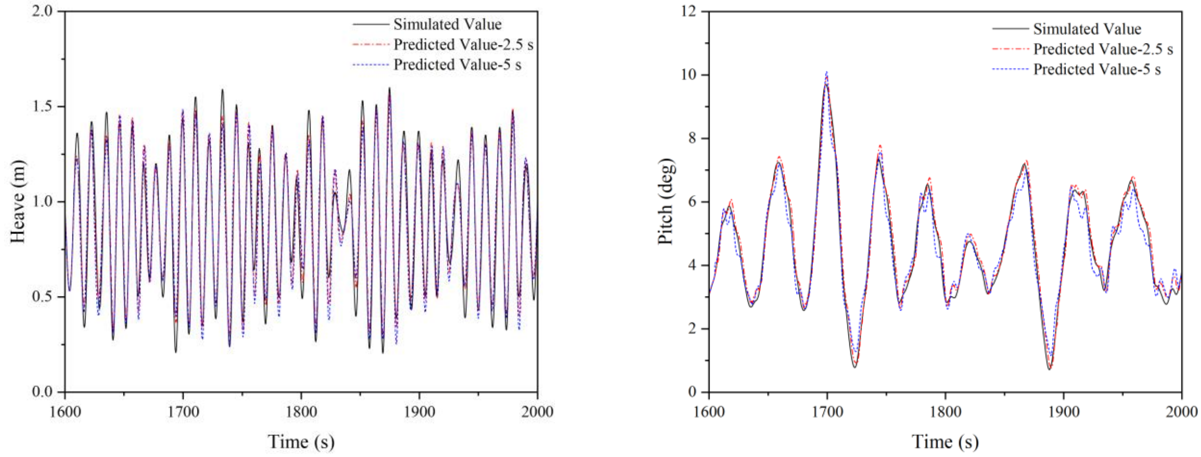

(c) (d)

Figure 9. Simulated and predicted values of EC 2 at 2.5 s and 5 s：

(a) Surge; (b) Sway; (c) Heave; (d) Pitch

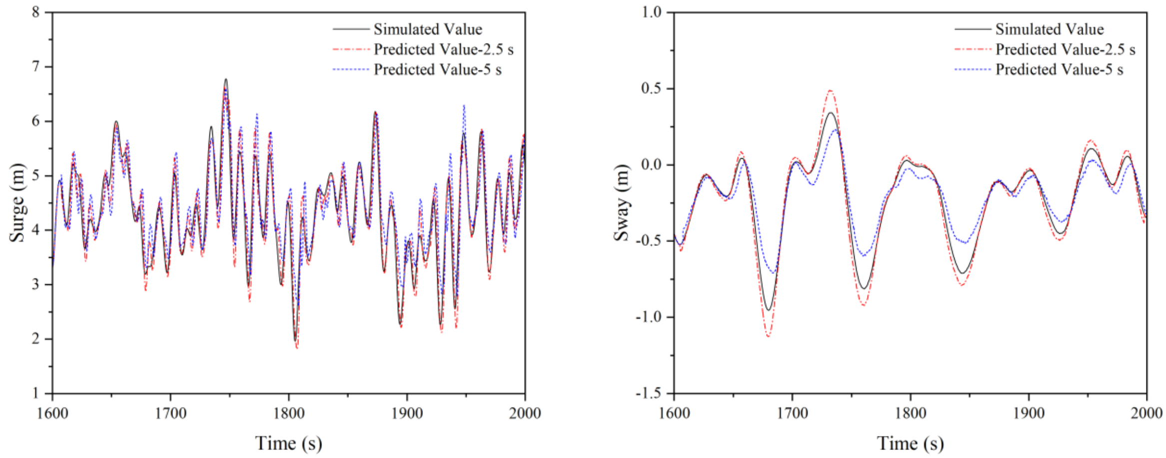

(a) (b)

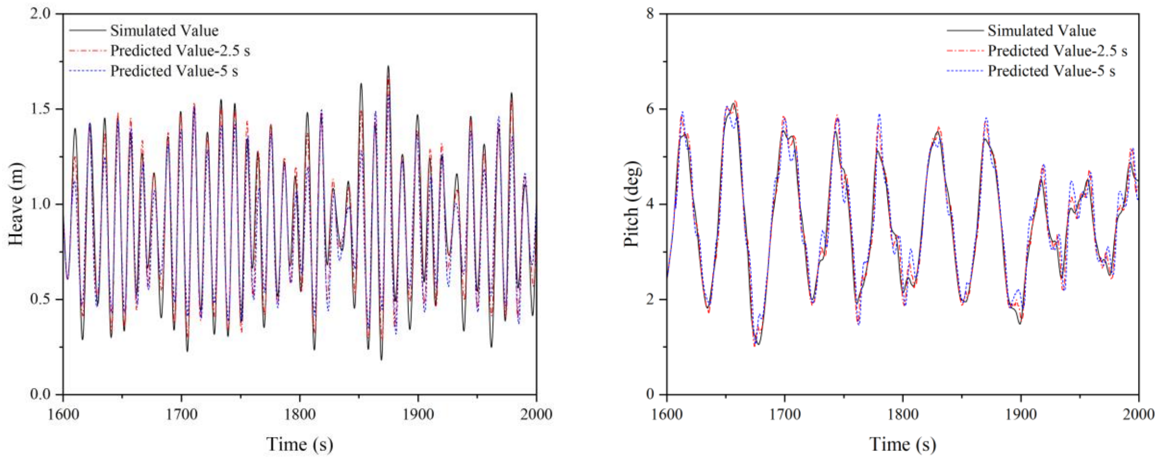

(c) (d)

Figure 10. Simulated and predicted values of EC 3 at 2.5 s and 5 s:

(a) Surge; (b) Sway; (c) Heave; (d) Pitch

It can be seen from **Figures 8-10** that when the previous motion response is used as the single input, the predicted value at PAT of 2.5 s is closer to the simulated value. Due to the large amplitude of motion in the surge, the predicted results in **Figure 8(a)** agree well with the simulation results, apart from the minor discrepancy at the peak of the surge in **Figures 9-10(a)**. Due to the small amplitude in sway, the predicted results under the two PATs generally agree with simulated results compared to the agreement between predicted and simulated surge. Similarly, there is also a minor discrepancy at the peak. The amplitude of heave motion is the smallest among the three motions, but it contains higher frequency components. The predicted heave motion in three test cases in **Figure 8-10** presents better agreement with simulated results at PAT of 2.5 s, but a minor discrepancy can be noted at the peak and trough at PAT of 5 s. The peak value of pitch in **Figures 8-10(d)** is also large, but there is higher-order fluctuation at the peak and trough due to the nonlinear motion induced by wind and waves. Single-input LSTM model learned the nonlinear features from the training data group, so the predicted value agrees well with the simulated results.

In summary, compared with the simulated values, the predicted values in all motions have very minor discrepancies at peak and trough, but a fairly good agreement has been presented. The discrepancy at peak and trough can be attributed to the limited input factors to train the neural network. To unravel this, the multi-input network structure is investigated in detail in Section 4.3.

4.3. Muti-input Predicted Results

A multi-input model is trained to explore the effects of multiple factors as input conditions on the predicted results. Unlike the single-input model, the training input of the multi-input LSTM (MI-LSTM) model is based on the previous motions, mooring forces, and wave

elevation. The output of the model is compared and analyzed with the data of the test group. The predicted advance time is set as 2.5 s and 5 s respectively. The test and predicted results are shown in **Figures 11-13**.

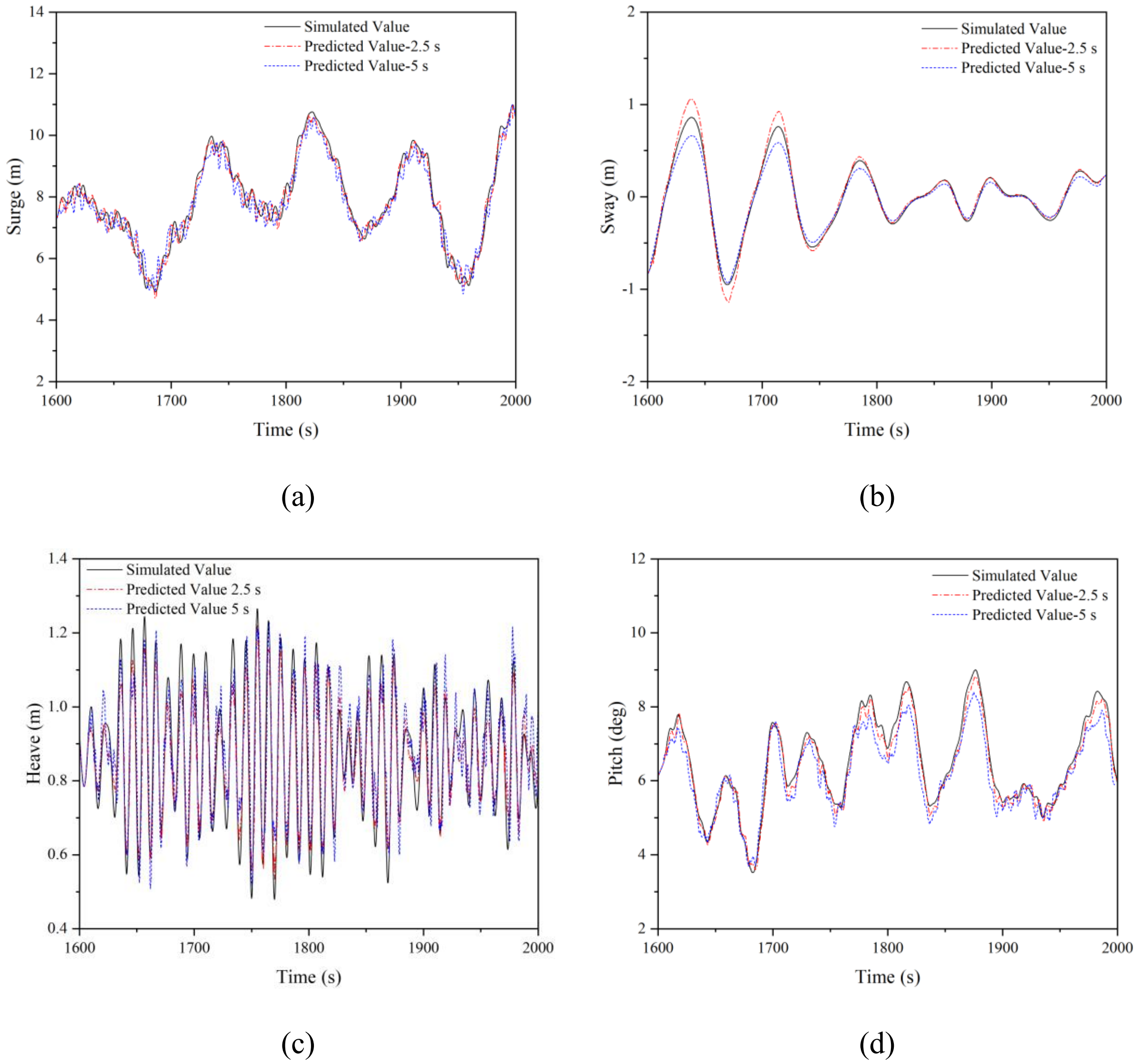

Figure 11. Simulated and predicted values of EC 1 at 2.5 s and 5 s:

(a) Surge; (b) Sway; (c) Heave; (d) Pitch

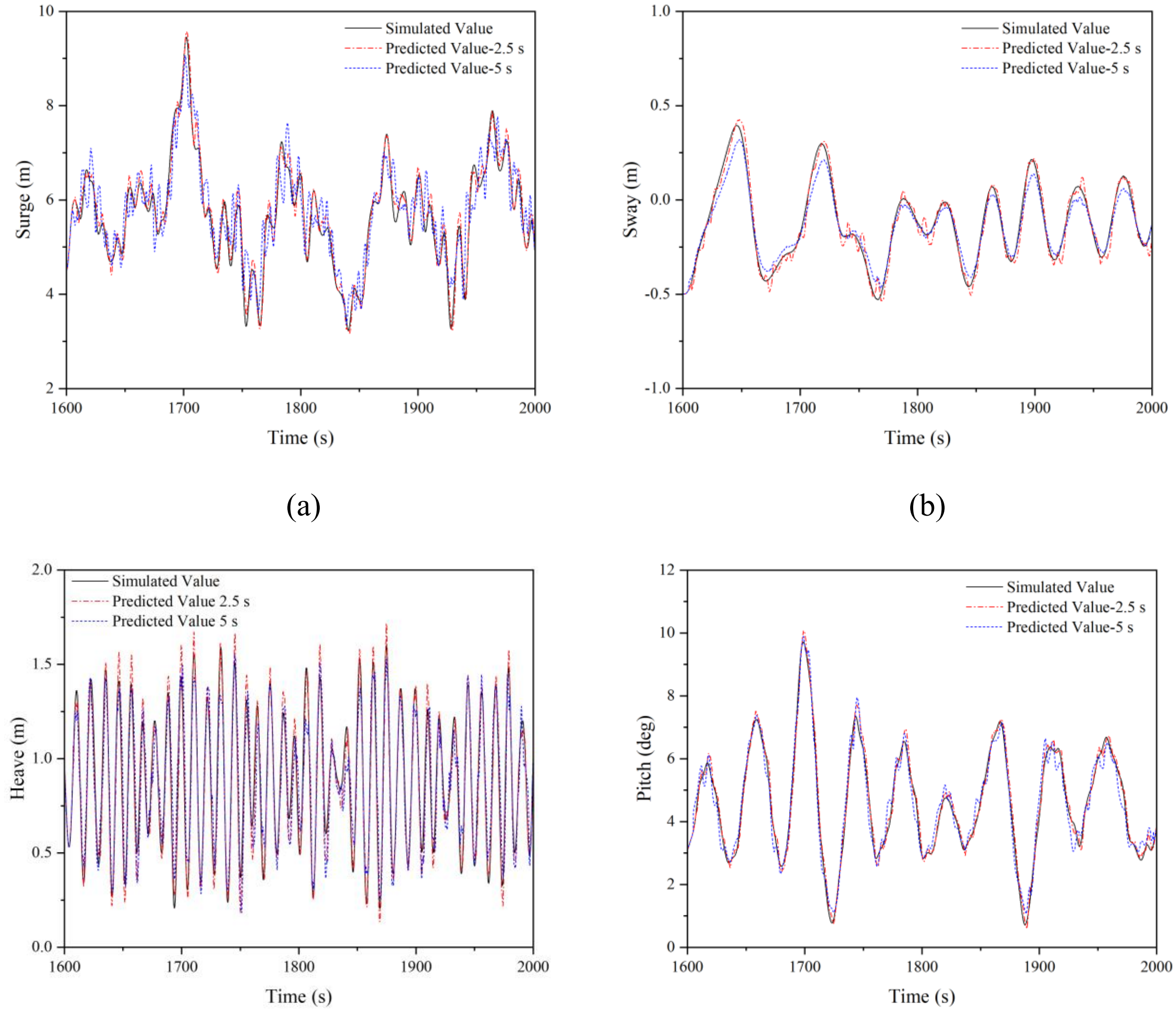

(a) (b)

(c) (d)

Figure 12. Simulated and predicted values of EC 2 at 2.5 s and 5 s:

(a) Surge; (b) Sway; (c) Heave; (d) Pitch

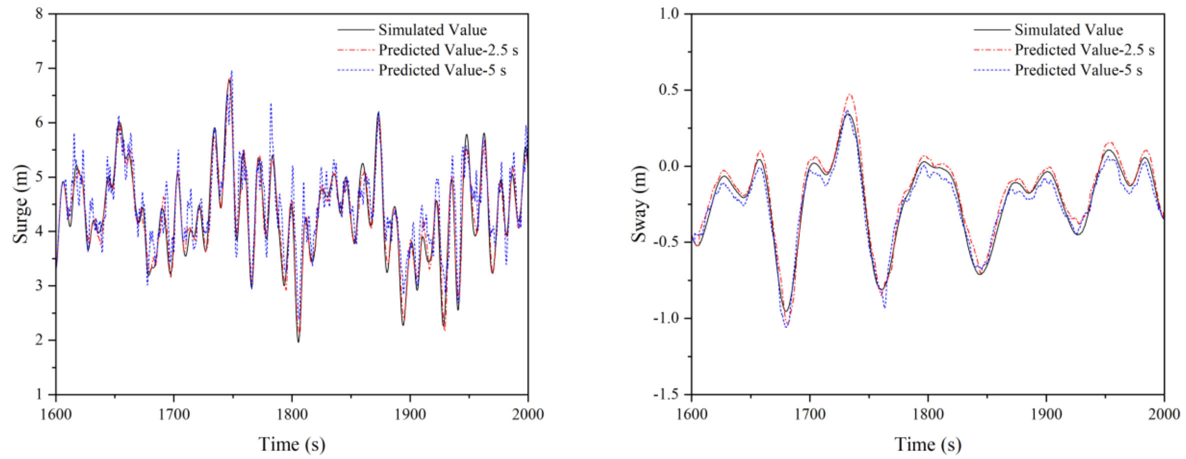

(a) (b)

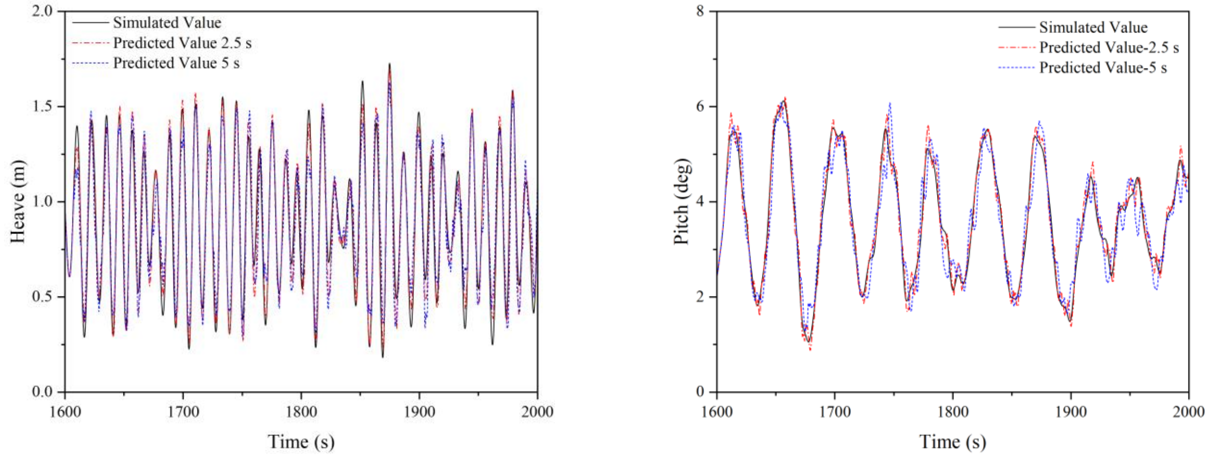

(c) (d)

Figure 13. Simulated and predicted values of EC 3 at 2.5 s and 5 s：

(a) Surge; (b) Sway; (c) Heave; (d) Pitch

When the model input factors become multiple, i.e., adding mooring force and wave elevation, a better agreement between the predicted value and the simulated value is obtained compared with the single input case. Improved agreement of surge prediction at peak in **Figure 12(a)** is presented compared to **Figure 9(a)**. But in the case of multiple inputs, the fluctuations can also be noticed from the predicted surge. Sway and heave are not significantly improved due to their less sensitivity to mooring force. With the additional input factors, the accuracy of the predicted pitch has been improved significantly as pitch motion is sensitive to mooring forces, comparing **Figures 9(d)** and **12(d)**. It can be found that in the period 1900s-2000s, the discrepancy of the single-input model can be found, while the multi-input model presented better performance with additional input data sets. Similar to the pitch, better agreements have been achieved for the predicted surge.

In a word, after adding the additional input factors to train the multi-input model, better performance in predicting the FOWT motion response has been demonstrated. However, the saw-tooth effect of the MI-LSTM model is more obvious, caused by the deep learning of the additional input information. The saw tooth effect is further analyzed after analyzing the scatterplot of discrete situations in Section 4.4.

4.4 Error Analysis

In this study, the number of Epochs is set to 50 rounds. It is shown in **Figure 14** the trend of the Loss function changing with the Epochs is generated and recorded during the training. It can be noted that with the increment of Epochs, Loss decrease rapidly in the beginning. Then after the rapid decrease stage, Loss finally tended to be stable. After the Epochs reaches 50, Loss remains unchanged. It can be concluded that the network training effect will not be further improved after 50 rounds and a neural network model with good accuracy is generated. The model has completed learning about the relationship between the input and output data.

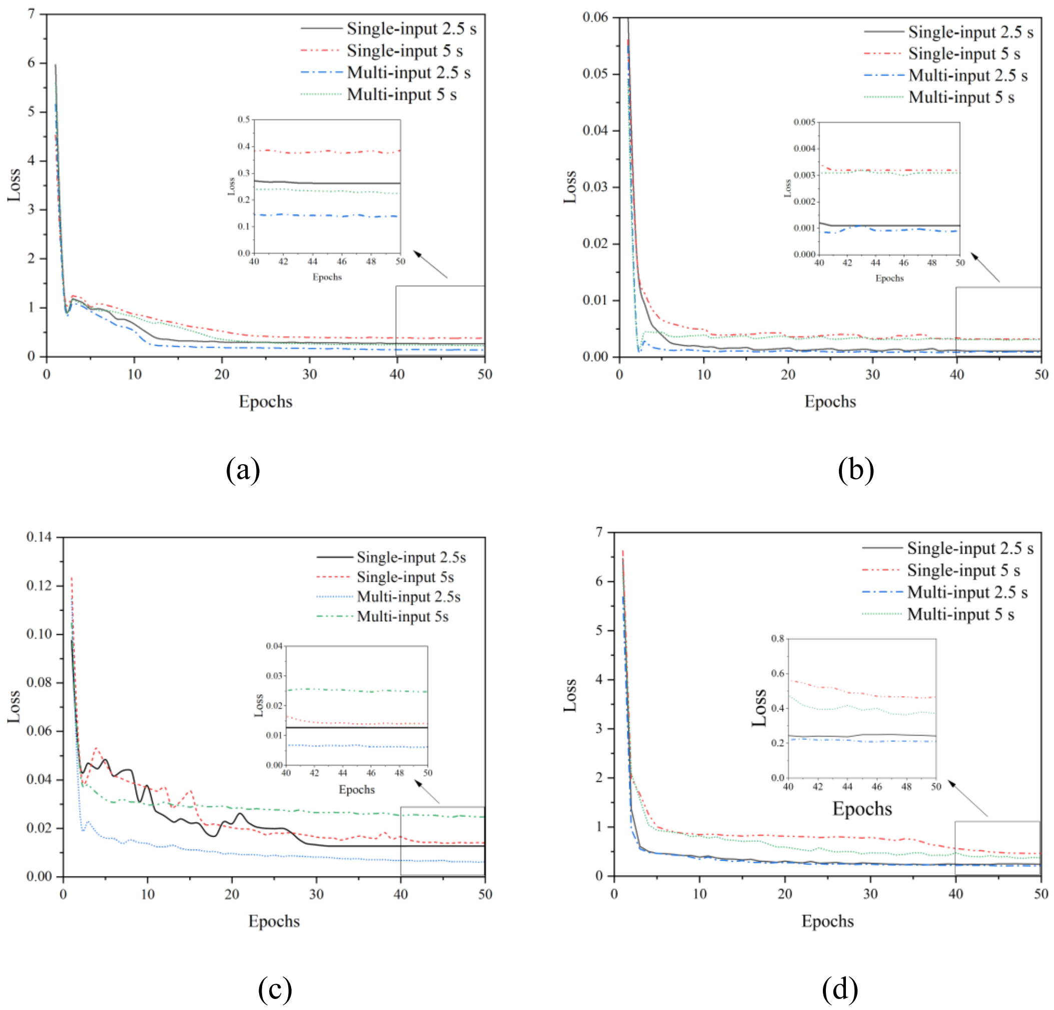

Figure 14. The curve of Loss affected by Epochs for different directions:

(a) Surge; (b) Sway; (c) Heave; (d) Pitch

At the same time, the Loss of the MI-LSTM model is found to be lower than that of the

SI-LSTM model both in 2.5 s and 5 s. It can be considered that the learning ability of the model is improved after additional factors are added to the training. The predicted results are shown in Sections 4.2 and 4.3 and compared with simulation data. It is difficult to observe their overall discretization, so a scatter plot of the prediction results in different input modes is plotted in this Section, as shown in **Figure 15.**

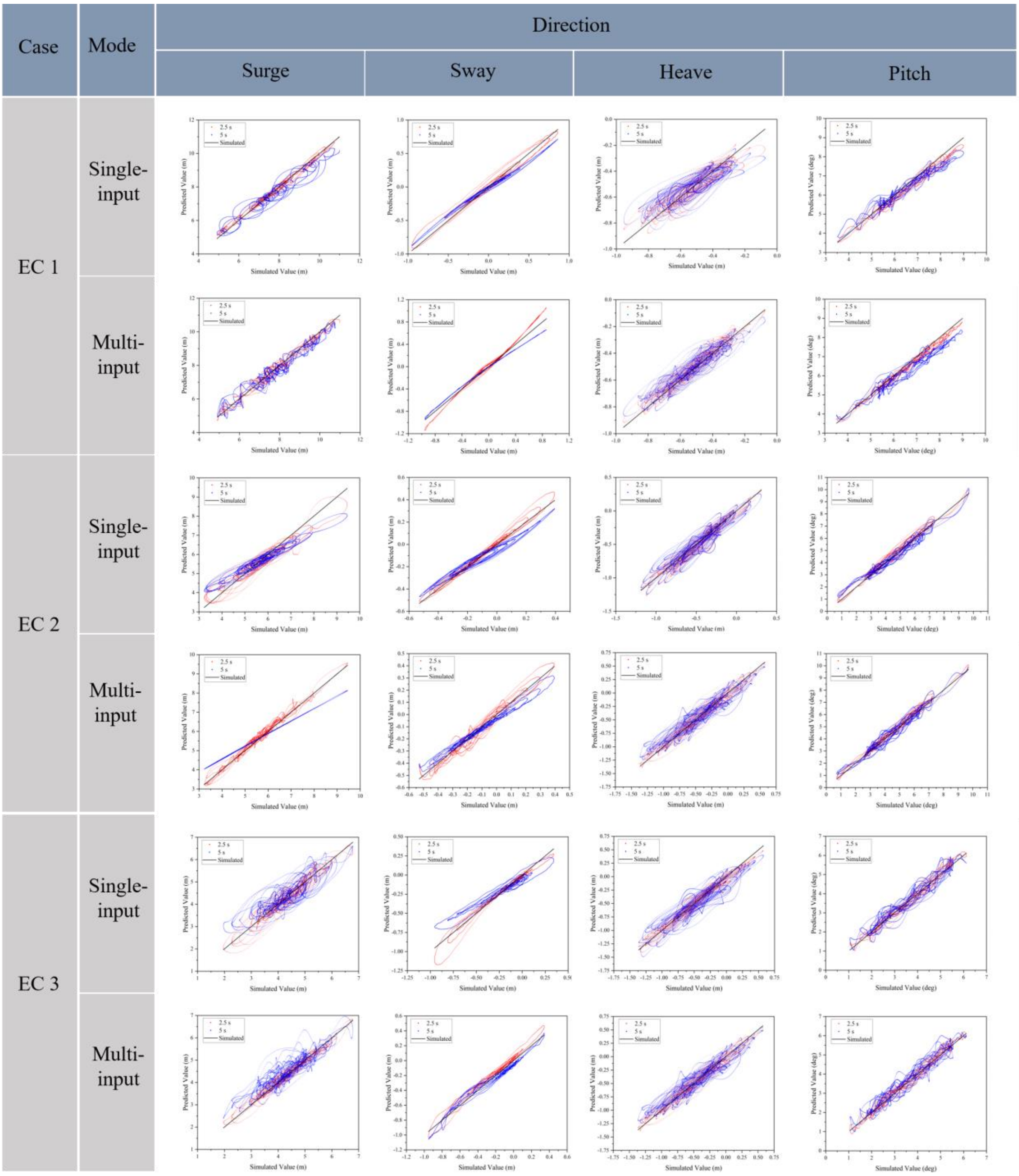

Figure 15. The discrete scatter plot of prediction results with two models

According to **Figure 15**, comparing the SI-LSTM model with the MI-LSTM model under the different cases, it can be found that after adding two additional input factors, the discrete situation of the MI-LSTM model prediction results is significantly smaller than that of the SI-LSTM model prediction results. This phenomenon is more evident in the sway and heave of EC1, surge and sway of EC2, and sway and heave of EC3. The use of the MI-LSTM model is beneficial in reducing the discrete nature of predicted results.

In addition to the impact of discrete situations, the overall accuracy of the MI-LSTM model and the single-input model is also important. The individual statistics for predicting the final result of the FOWT motion response using both models are listed in Table 3. The overall accuracy of both models is presented in Figure 16.

Table 3. The accuracy of each statistic under the different input model

Mode	Statistics	EC 1				EC 2				EC 3			
		Heave	Pitch	Surge	Sway	Heave	Pitch	Surge	Sway	Heave	Pitch	Surge	Sway
Single-input 2.5 s	Max	73.2%	95.9%	99.9%	96.7%	96.2%	92.6%	95.3%	81.2%	84.3%	98.8%	97.8%	81.0%
	Min	92.3%	99.0%	96.2%	96.2%	93.4%	92.4%	93.0%	97.1%	96.8%	96.2%	92.4%	76.9%
	Average	99.7%	97.2%	99.8%	88.6%	95.6%	92.4%	98.5%	90.6%	96.9%	93.3%	96.5%	94.9%
	STD	87.5%	93.7%	94.3%	94.0%	97.7%	98.9%	83.7%	90.6%	96.0%	92.1%	93.5%	97.7%
	Overall	**88.2%**	**96.4%**	**97.6%**	**93.9%**	**95.7%**	**94.1%**	**92.6%**	**89.9%**	**93.5%**	**95.1%**	**95.0%**	**87.6%**
Multi-input 2.5 s	Max	73.2%	98.0%	97.6%	97.1%	97.4%	96.1%	96.8%	92.5%	95.8%	98.5%	99.4%	82.9%
	Min	96.0%	97.8%	95.8%	89.6%	93.3%	93.9%	98.2%	98.7%	98.3%	93.5%	96.6%	91.9%
	Average	97.5%	98.2%	99.4%	88.6%	96.0%	98.5%	98.9%	96.6%	99.2%	98.2%	99.0%	92.4%
	STD	97.3%	95.3%	96.8%	97.9%	97.8%	98.8%	95.6%	95.5%	96.6%	98.1%	94.9%	96.6%
	Overall	**91.0%**	**97.3%**	**97.4%**	**93.3%**	**96.1%**	**96.8%**	**97.4%**	**95.8%**	**97.5%**	**97.1%**	**97.5%**	**91.0%**
Single-input 5 s	Max	73.2%	92.5%	98.7%	83.2%	82.9%	95.9%	86.1%	81.1%	69.7%	88.9%	97.4%	67.9%
	Min	89.3%	93.0%	96.7%	92.2%	91.4%	80.1%	74.9%	94.4%	90.8%	89.5%	67.2%	74.3%
	Average	98.9%	97.7%	97.8%	75.0%	93.0%	89.0%	89.8%	91.7%	92.3%	93.5%	98.3%	92.9%
	STD	75.6%	81.5%	88.3%	82.6%	93.3%	89.8%	76.2%	78.7%	90.4%	87.3%	85.3%	70.2%
	Overall	**84.3%**	**91.2%**	**95.4%**	**83.3%**	**90.1%**	**88.7%**	**81.8%**	**86.5%**	**85.8%**	**89.8%**	**87.1%**	**76.3%**
Multi-input 5 s	Max	73.2%	93.3%	98.1%	76.8%	82.5%	98.2%	87.8%	80.8%	85.3%	89.1%	97.4%	82.1%
	Min	91.3%	95.1%	98.5%	98.4%	96.0%	76.5%	85.7%	94.4%	91.0%	94.3%	78.4%	89.0%
	Average	97.7%	95.5%	98.6%	83.7%	96.9%	89.8%	88.4%	91.9%	98.0%	97.5%	96.4%	89.3%
	STD	89.7%	86.2%	91.3%	85.3%	97.0%	98.0%	90.8%	81.0%	88.8%	91.6%	87.2%	93.2%
	Overall	**88.0%**	**92.5%**	**96.7%**	**86.1%**	**93.1%**	**90.6%**	**88.2%**	**87.0%**	**90.8%**	**93.1%**	**89.8%**	**88.4%**

Based on Table 3 and Figure 16, the results at PAT of 2.5 s present better agreements than at PAT of 5 s. After adopting the MI-LSTM model, the accuracy of the prediction results in pitch and heave has been significantly improved. With the increment of PAT, the period between input and output becomes larger, so the time correlation between the two decreases and the uncertainty increases. The upper limit of learning ability decreases as the correlation between input and output information decreases. Therefore, the accuracy at PAT of 5 s is lower than that of 2.5 s.

At the same time, the overall prediction result of the MI-LSTM model is better than the SI-LSTM model. The additional input factors increase the dimension of information, which enables the MI-LSTM model to explore more relationships between different input factors and the motion response of the target output. MI-LSTM model also adds more details to the final prediction results, improving the overall accuracy of the prediction results. In other words, there is a positive correlation between mooring force, wave elevation, and the motion response of the platform.

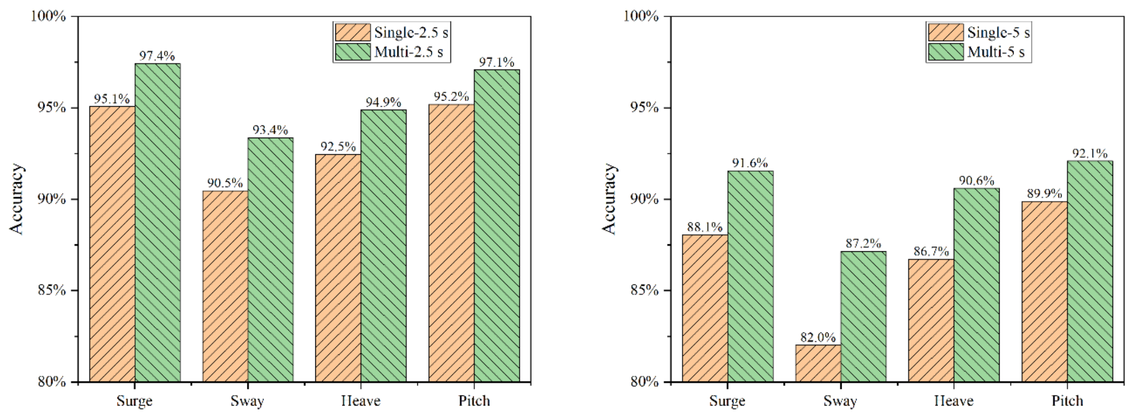

(a) (b)

Figure 16. Overall accuracy under different PATs: (a) 2.5 s; (b) 5 s

5. Second-order Hydrodynamic Effects

5.1 Prediction results under the influence of second-order hydrodynamic effects

The influence of second-order hydrodynamics is significant for the load prediction of a FOWT [30]. EC1-EC3 are again simulated considering second-order hydrodynamic effects, the simulation data is imported into the MI-LSTM model for training. The prediction results under the second-order hydrodynamic force are obtained after the training, shown in **Figures 17-19.**

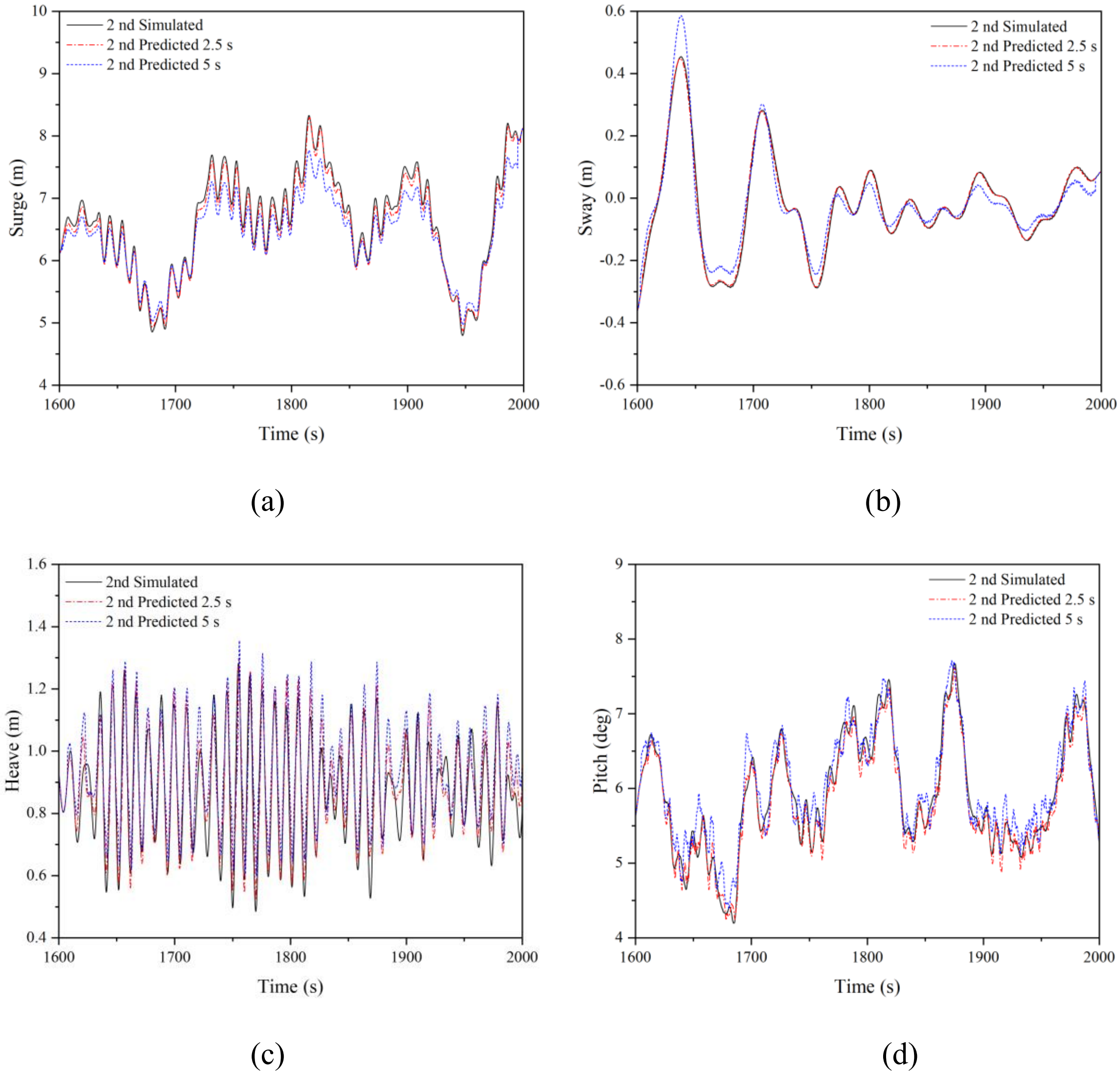

Figure 17. Simulated and predicted values of EC 1 at 2.5 s and 5 s:

(a) Surge; (b) Sway; (c) Heave; (d) Pitch

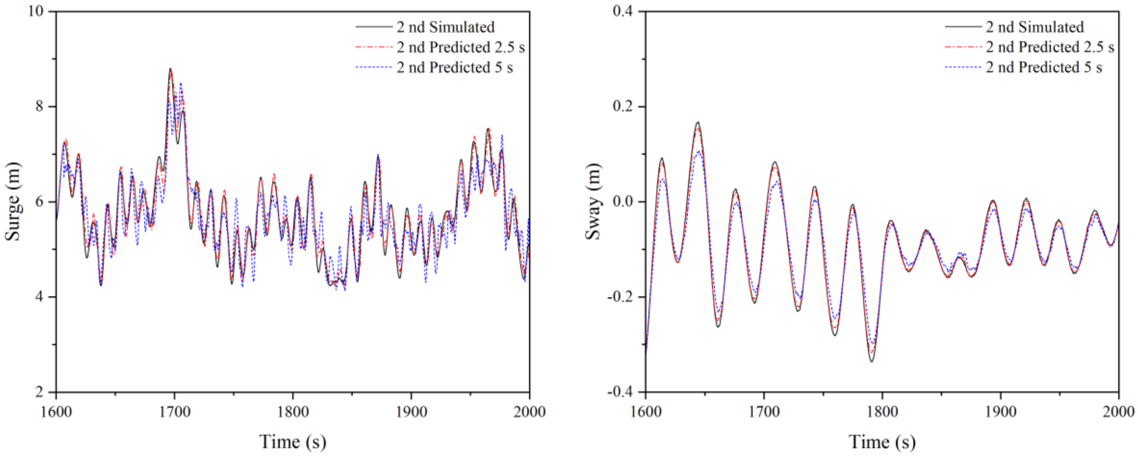

(a) (b)

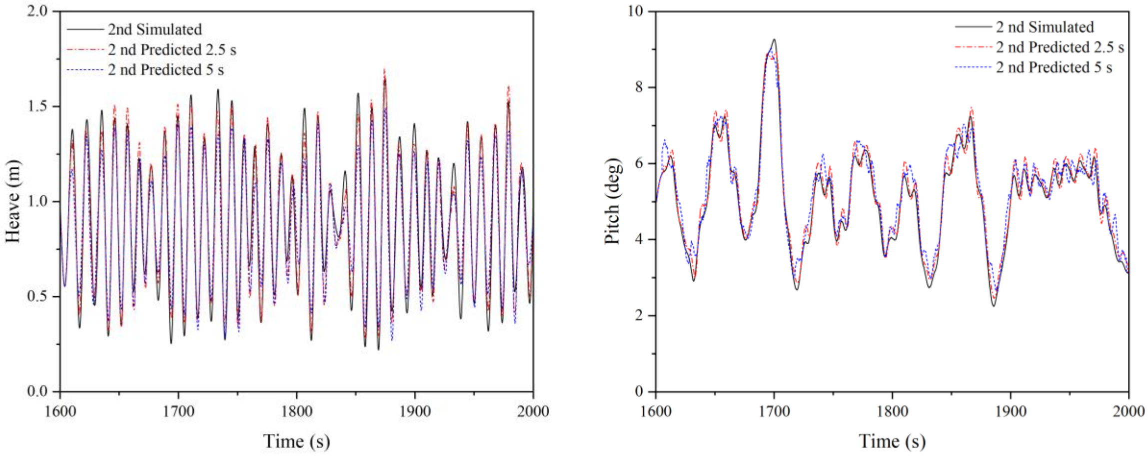

(c) (d)

Figure 18. Simulated and predicted values of EC 2 at 2.5 s and 5 s:

(a) Surge; (b) Sway; (c) Heave; (d) Pitch

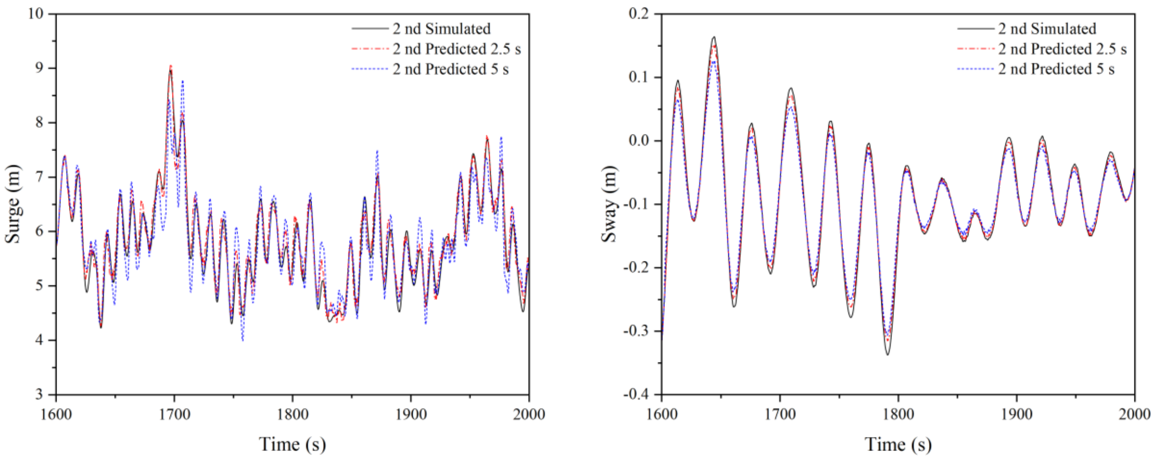

(a) (b)

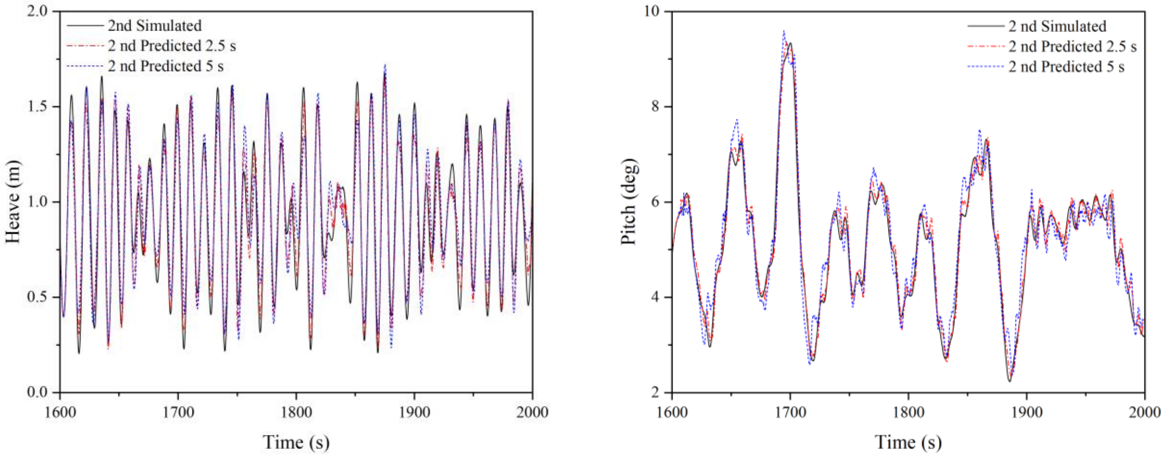

(c) (d)

Figure 19. Simulated and predicted values of EC 3 at 2.5 s and 5 s：

(a) Surge; (b) Sway; (c) Heave; (d) Pitch

Figures 17-19 show that the peak fitting in all directions at 5 s is weaker than that of 2.5 s, similar to the case when the platform model is affected by first-order hydrodynamic forces. Compared with the first-order hydrodynamic influence, the prediction results under the second-order hydrodynamics show smaller fluctuations in both surge and pitch. On the other hand, the predicted value of sway is smooth, and there is no slight fluctuation. The error of prediction results in heave mainly occurs in peaks and troughs, but it is not obvious. The statistical accuracy in each direction, as well as the overall accuracy, is further analyzed in Section 5.2.

5.2. Error Analysis

To compare the short-term prediction effect of the MI-LSTM model in both first-order hydrodynamics and second-order hydrodynamics cases, the results of the PAT of 2.5 s under EC 1 are selected for comparison, shown in **Figure 20**.

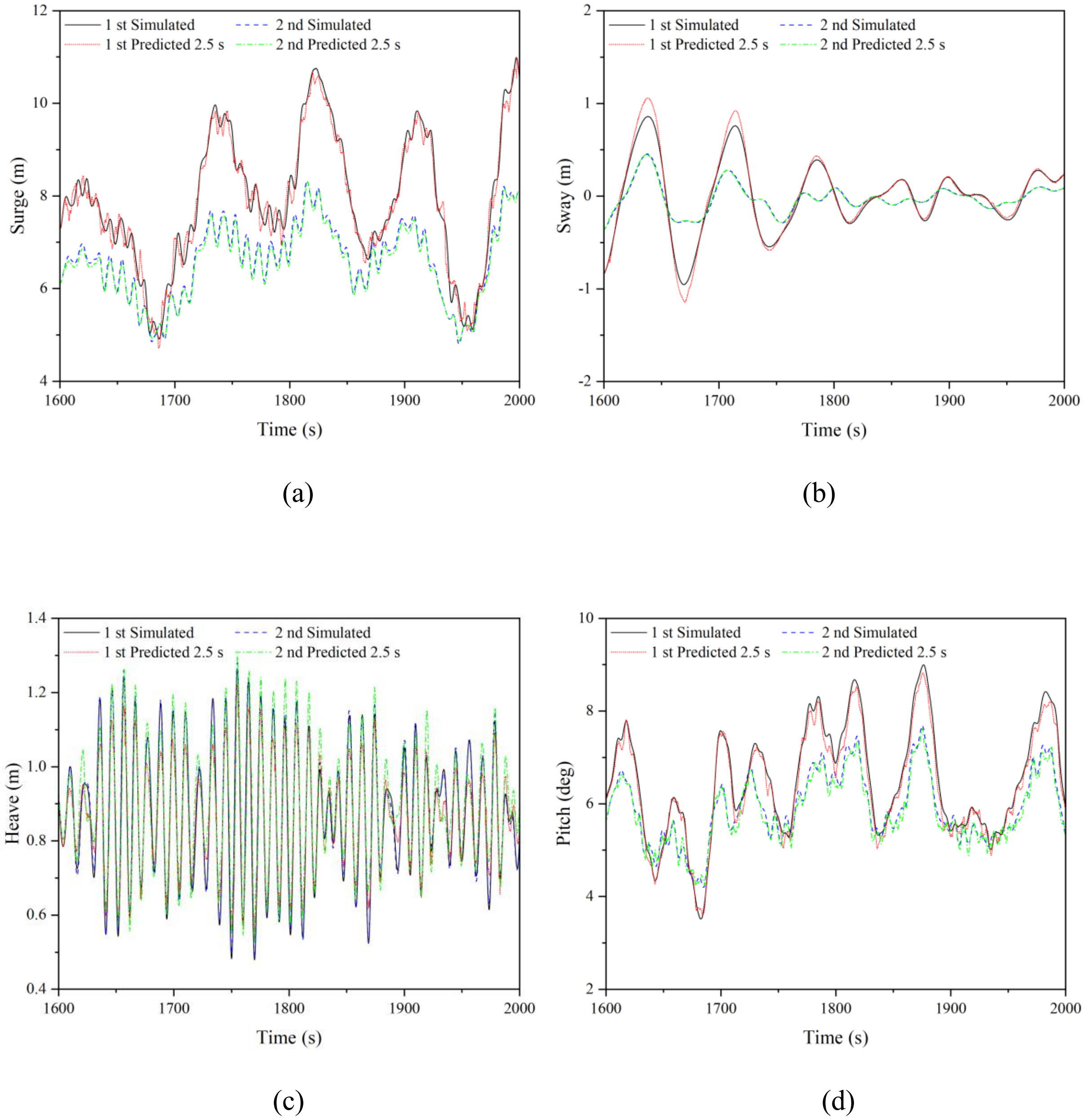

Figure 20. Comparison of 1st-order and 2nd-order hydrodynamic prediction results: (a) Surge; (b) Sway; (c)Heave; (d) Pitch

According to **Figure 20**, it is observed that the motion response exhibits a stronger nonlinear characteristic under the influence of second-order hydrodynamic forces. This phenomenon is particularly evident in the surge, pitch, and sway directions, where more nonlinear fluctuations appear at the extremes of the kinematic response in all three directions. The effect of second-order hydrodynamic forces did not have much influence in the heave direction.

At the same time, in the surge, sway and pitch directions, there are significant deviations in the predicted values at the extremes of the motion response for the first-order hydrodynamics case. While in the second-order hydrodynamics case, the MI-LSTM model has better prediction at both peak and trough values. In the heave direction, the motion response of the platform in the two cases does not differ much and does not have the nonlinear characteristics in the other three directions. Therefore, the prediction effect of the MI-LSTM model in the heave direction under the influence of second-order hydrodynamics is not significantly improved.

Under the influence of second-order hydrodynamics, this section also analyzes the individual statistics of the prediction results and calculates the overall accuracy of each direction of motion response, shown in **Table 4**.

Table 4. The accuracy of each statistic under the influence of second-order hydrodynamics

Mode	Statistics	EC 1				EC 2				EC 3			
		Heave	Pitch	Surge	Sway	Heave	Pitch	Surge	Sway	Heave	Pitch	Surge	Sway
Multi-input 2.5 s	Max	96.5%	99.4%	99.6%	98.7%	92.6%	96.3%	99.5%	92.2%	98.0%	98.9%	98.8%	91.8%
	Min	88.5%	99.2%	98.5%	99.1%	90.9%	90.7%	99.2%	97.0%	90.2%	96.2%	99.1%	94.9%
	Average	98.8%	98.8%	98.9%	96.5%	98.0%	97.6%	99.7%	99.0%	99.9%	99.0%	98.9%	99.2%
	STD	89.9%	96.2%	96.1%	98.6%	95.8%	96.5%	99.6%	94.6%	98.6%	99.2%	96.7%	92.8%
	Overall	**93.4%**	**98.4%**	**98.3%**	**98.2%**	**94.3%**	**95.3%**	**99.5%**	**95.7%**	**96.7%**	**98.3%**	**98.4%**	**94.7%**
Multi-input 5 s	Max	87.0%	99.5%	97.6%	71.0%	97.1%	97.5%	96.6%	63.4%	94.2%	97.2%	97.8%	77.1%
	Min	94.3%	95.5%	96.5%	97.5%	89.5%	82.5%	97.4%	97.0%	94.3%	93.4%	94.4%	94.9%
	Average	98.6%	98.1%	97.3%	80.7%	94.6%	96.5%	99.3%	98.2%	94.5%	98.8%	99.6%	99.0%
	STD	87.9%	92.3%	91.4%	98.1%	93.1%	92.5%	90.9%	80.4%	92.6%	98.0%	91.3%	84.1%
	Overall	**92.0%**	**96.3%**	**95.7%**	**86.8%**	**93.6%**	**92.3%**	**96.0%**	**84.8%**	**93.9%**	**96.9%**	**95.8%**	**88.8%**

According to the results given in **Table 4**, it can be seen that the accuracy of the predicted results in all directions under the influence of second-order hydrodynamics is still at a high level, overall accuracy exceeds 90% at PAT of 2.5 s and 85% at PAT of 5 s. This phenomenon verifies the conclusions of Section 4 and confirms that an increase in PAT leads to a decrease in prediction accuracy.

The overall accuracy of the 4 degrees of freedom directions calculated from **Table 4** is shown in **Figure 21**. At PAT of 2.5 s, the difference in prediction accuracy between the second-order hydrodynamics and the first-order hydrodynamics is more obvious in surge and sway. At PAT of 5 s, in the direction of surge, heave, and pitch, the prediction accuracy in the second-order hydrodynamics case is about 3% higher than that in the first-order hydrodynamics.

By comparing with the results in the first-order hydrodynamics in Section 4, it can be found that the MI-LSTM model in the second-order hydrodynamics case not only has a good ability to learn multi-factor relationships and platform response prediction but also has a higher prediction accuracy than the first-order hydrodynamics case.

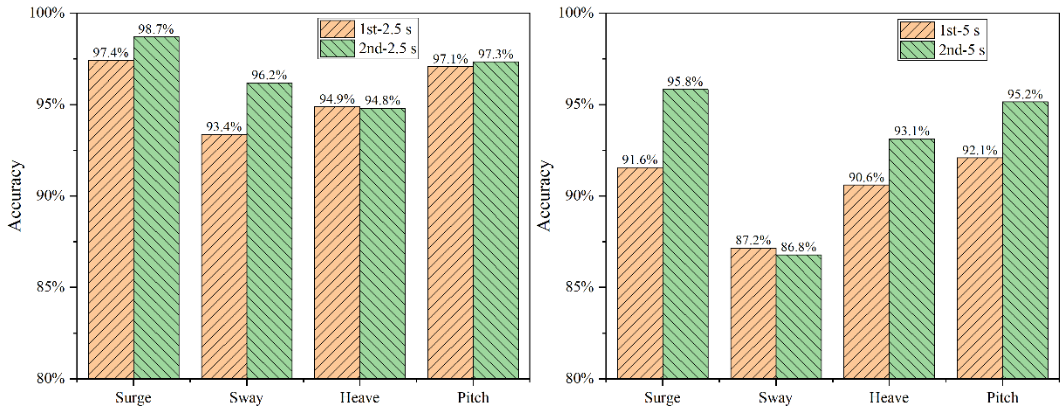

(a) (b)

Figure 21. Overall accuracy under different PATs: (a) 2.5 s; (b) 5 s

6. Comparison with the MI1D-CNN model

6.1 Predicted results with MI1D-CNN model

Currently, the mainstream deep learning methods mainly include the CNN method and the RNN method, and the MI-LSTM model established in Section 4 belongs to the RNN method. CNN methods are mostly used in image recognition and text recognition. As a representative method to deal with time series problems in CNN, a one-dimensional convolutional neural network (1D-CNN) has a certain effect on short-term prediction by adding a pooling layer.

In this section, a multi-input one-dimensional convolutional neural network (MI1D-CNN) is built to compare the CNN method with the LSTM method for the motion response prediction problem, using the same training data as in Section 4. The training of the MI1D-CNN model is completed, and the results obtained from the multi-input LSTM model are compared in Section 6.2 in terms of training time and overall accuracy. The prediction results obtained by the MI1D-CNN model are shown in **Figures 22-24**.

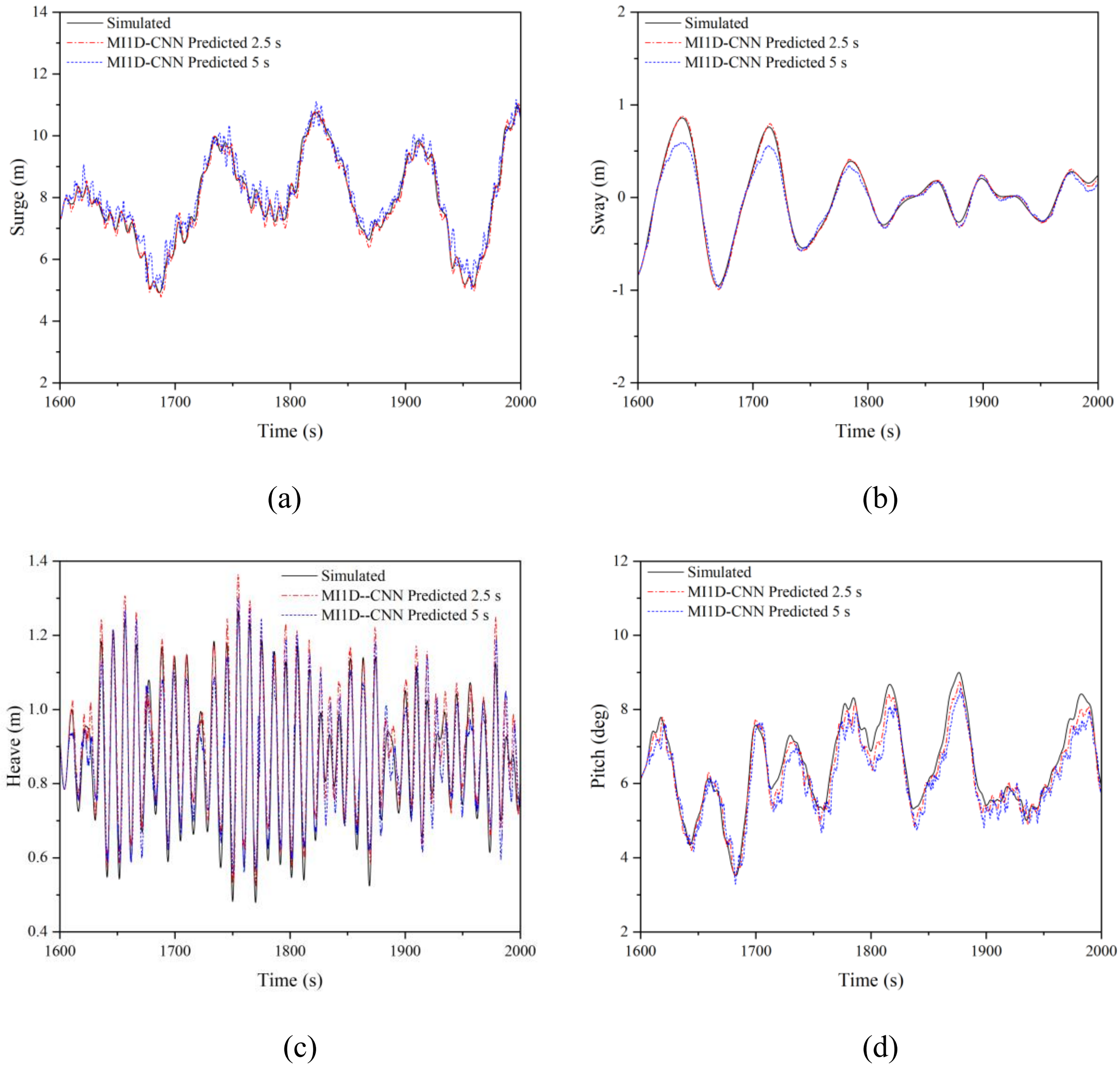

Figure 22. Simulated and predicted values of EC 1 at 2.5 s and 5 s:

(a) Surge; (b) Sway; (c) Heave; (d) Pitch

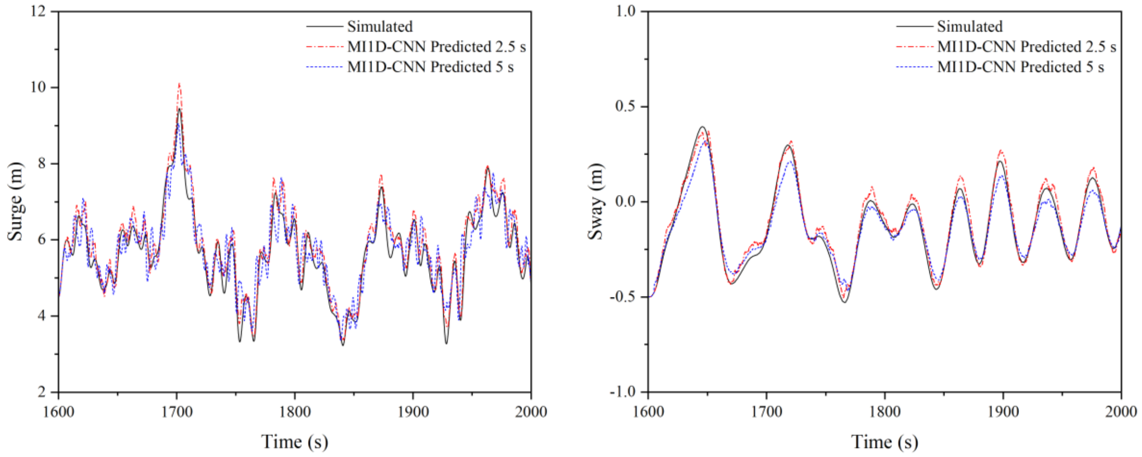

(a) (b)

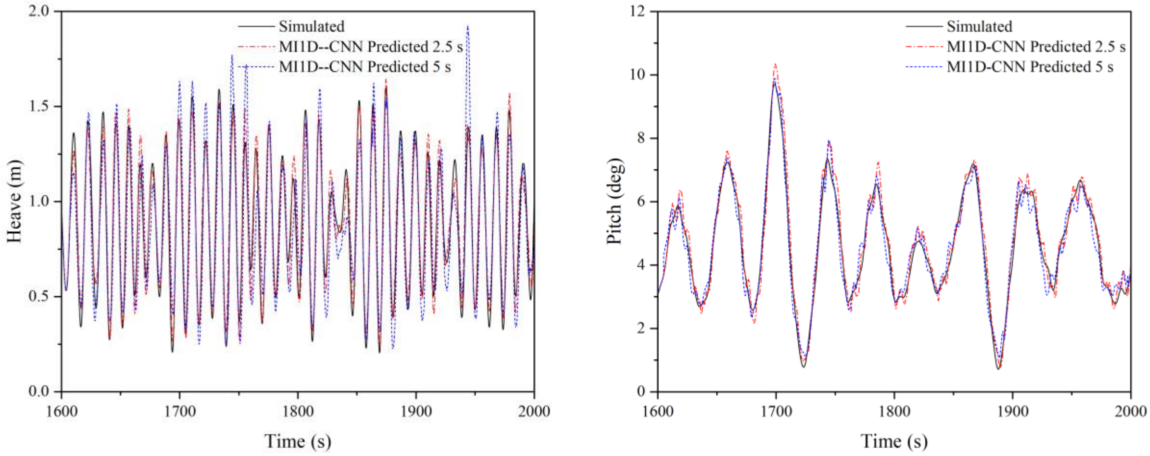

(c) (d)

Figure 23. Simulated and predicted values of EC 2 at 2.5 s and 5 s:

(a) Surge; (b) Sway; (c) Heave; (d) Pitch

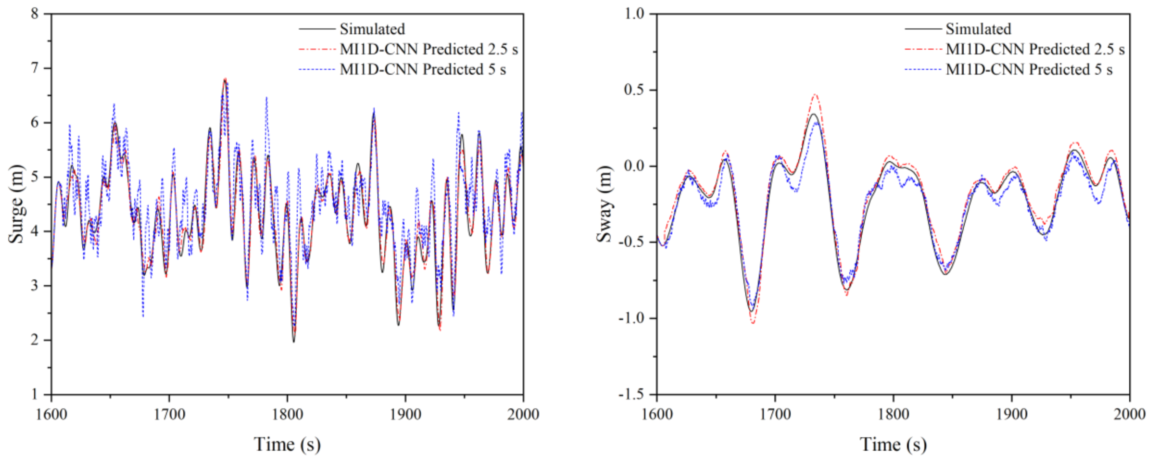

(a) (b)

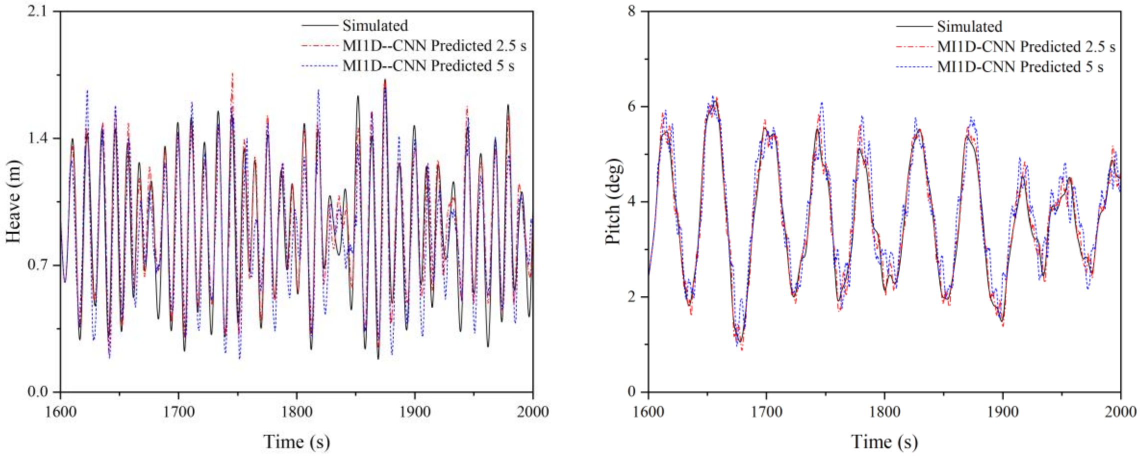

(c) (d)

Figure 24. Simulated and predicted values of EC 3 at 2.5 s and 5 s:

(a) Surge; (b) Sway; (c) Heave; (d) Pitch

According to **Figures 22-24**, and compared with **Figures 11-13** in Section 4.3, it can be found that the motion response predicted by the MI1D-CNN model produces a large number of serrations in surge and pitch of each environmental condition, especially at PAT of 2.5 s. At the same time, the prediction result at PAT of 5 s in sway does not fit well with the simulation results. To further compare the results of the MI-LSTM model with the MI1D-CNN model, it is further explained from the aspects of training time and overall accuracy in Section 6.2.

6.2 Comparison with Multi-input LSTM Model

To further observe the imitative effect between the predicted values obtained by the two models and the simulated values, EC1 is selected and the results are summarized as shown in **Figure 25**.

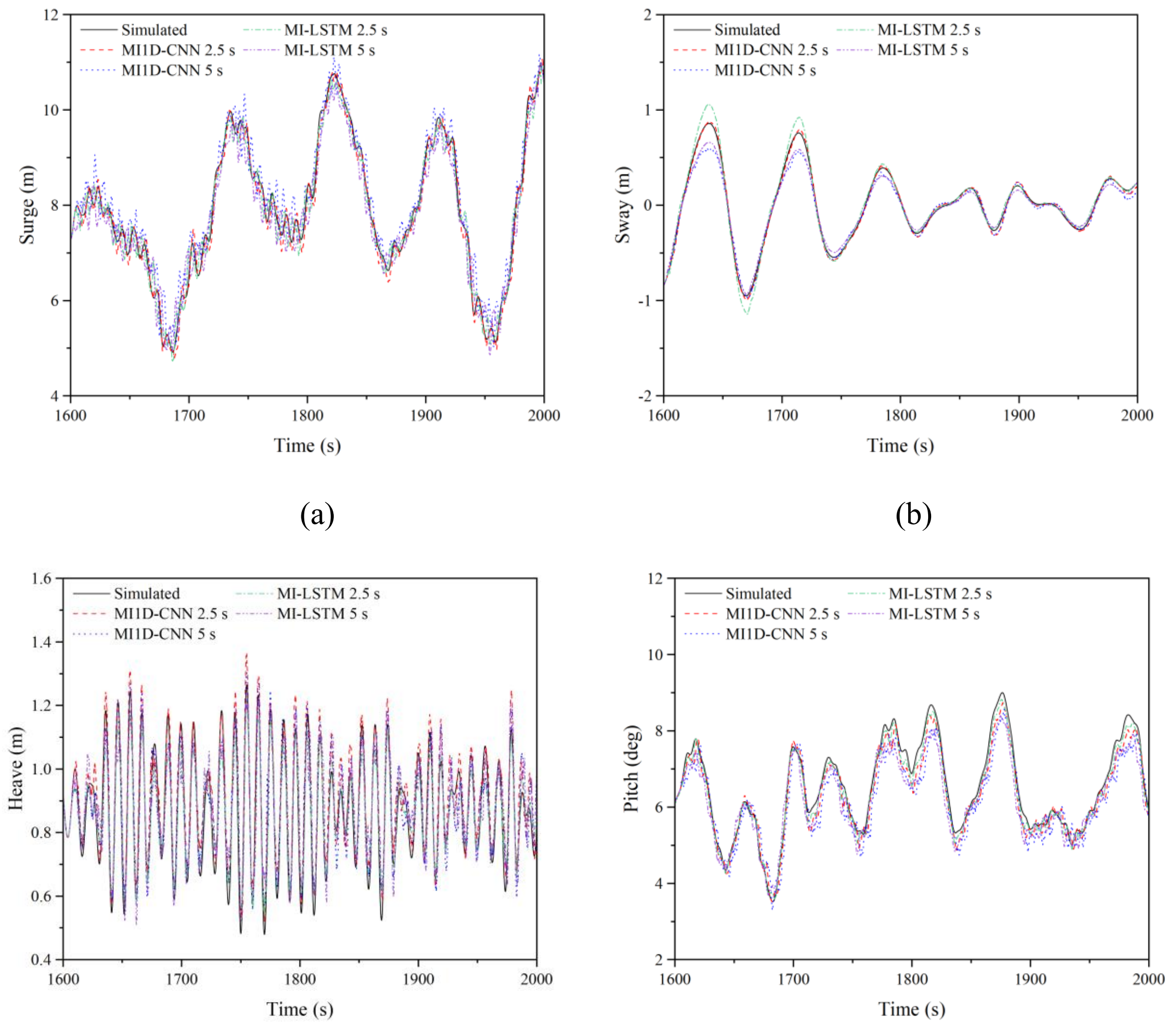

(c) (d)

Figure 25. The results of the MI1D-CNN model and the MI-LSTM model are compared: (a) Surge; (b) Sway; (c) Heave; (d) Pitch

According to **Figure 25**, from the overall imitative effect of the time series curve, the prediction results of both models fit well with the simulation results at PAT of 2.5 s. However, at PAT of 5 s, the result of the MI1D-CNN model is slightly inferior to the MI-LSTM model result, and when the PAT is at 5 s, the predicted value of the former has a large fluctuation. This volatility does not exist in the simulation value, particularly in **Figures 25(a**) and **(d)**. The time series of the platform response has a certain smoothness in sway, so both models' imitative effects are good. While the time series of the platform response itself is more volatile in heave, the imitative effects of the peak are not as good as in other directions.

To find out the difference between the MI1D-CNN model and the MI-LSTM model, the overall accuracy of the MI1D-CNN model is calculated by combining each operating condition. Then compare the overall accuracy of the MI1D-CNN model with the MI-LSTM model proposed in Section 4 and the result is shown in **Figure 26**.

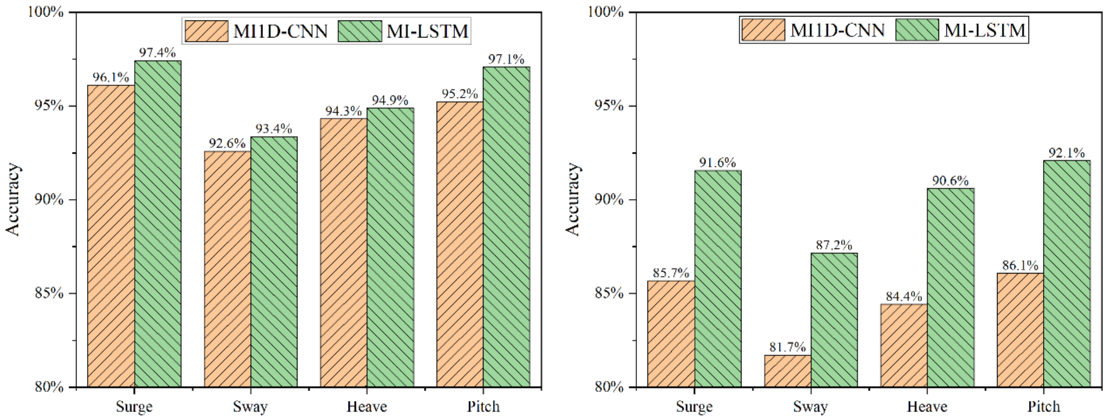

(a) (b)

Figure 26. Comparison of the overall accuracy of different models in each direction:

(a) 2.5 s; (b) 5s

According to **Figure 26**, it can be found that there is no significant difference between the results of the two models when PAT is at 2.5 s, the overall effect of the MI-LSTM model is slightly better than the MI1D-CNN model, and the accuracy of the former is 1%-2% higher than the latter in all directions. But at PAT of 5 s, the situation is very different, the MI-LSTM model performs much better than the MI1D-CNN model, and the accuracy of the former is about 5% higher than the latter in all directions.

It can be seen that when the corresponding period of the prediction platform becomes longer, the traditional CNN model is not satisfactory, while the MI-LSTM model proposed in this paper performs well. Since 1D-CNN only performs convolution operations on time series information within the length of a convolution, heritability in time series information is only reflected in a single convolutional neuron. Therefore, when PAT is small, the effect on the MI1D-CNN model and the MI-LSTM model is insignificant. However, with the increase of

PAT, the disadvantage of the MI1D-CNN model in processing temporal genetic information will become significant.

In addition, the training time of the two models is also recorded, as shown in **Table 5**. According to **Table 5**, the training time of the MI1D-CNN model is much shorter than that of the MI-LSTM model, which is related to the learning and calculation method of the model itself. The training time of the MI1D-CNN model is short, but it sacrifices a part of the accuracy, and the training time of the MI-LSTM model is relatively long, but the accuracy is greatly improved.

Table 5. Statistics on the training duration of the two models

Modes	PAT (s)	Epochs	Time (s)
MI-LSTM	2.5	50	912
	5	50	1053
MI1D-CNN	2.5	50	108
	5	50	157

In summary, balancing training time and accuracy has always been an important issue in deep learning. If the goal is ultra-short-term forecasting of the FOWT motion response and the accuracy requirement is relatively low, the MI1D-CNN model can be chosen. However, to increase the time span of motion response forecasting and maintain the prediction accuracy, MI-LSTM model is a better choice.

7. Conclusion

Based on the motion response data of the Braceless platform, the MI-LSTM prediction model is established by the RNN deep learning method and is trained for different degrees of freedom under different environmental conditions. The accuracy of prediction results under different PAT and input methods are determined and compared using statistics. Based on the analysis and discussions, the conclusion can be made as follows:

(1)Taking the previous data of platform motion response, mooring force, and wave elevation as input, after 50 rounds of training with two LSTM models, the Loss no longer decreases, resulting in accurate prediction results. The Loss of the MI-LSTM model is slightly better than the SI-LSTM model. The MI-LSTM model more comprehensively learns the relationship between multiple factors and the target output.

(2)Based on the established and trained LSTM neural network model, the prediction results of the model fit well with the simulated value. The prediction accuracy with PAT at 2.5 s is slightly higher than the accuracy with PAT at 5 s and the overall performance of the MI-LSTM model is better than the SI-LSTM model. The additional two factors can positively improve the accuracy of the final prediction result.

(3) The established MI-LSTM model is applied to the situation where the platform is affected by second-order hydrodynamics, and it is found that the model has a better predictive effect on the response of the Braceless platform affected by second-order hydrodynamics. The MI-LSTM model has a better performance for the case where the nonlinearity phenomenon is more pronounced.

(4) The MI-LSTM model established in this paper is compared with the traditional MI1D-CNN model, and the advantages and disadvantages of the two models are clarified from the aspects of training time and overall accuracy. When the PAT is small, the difference between the results of the two models is not significant, while when the PAT increases, the results obtained by the MI-LSTM model are better than those obtained by the MI1D-CNN model.

Acknowledgment

This research is funded by the National Natural Science Foundation of China (Grant No. 52071058, 51939002). This paper is also partially funded by Central Guidance on Local Science and Technology Development Fund of Shenzhen (2021Szvup018) and the Open Research Fund of Hunan Provincial Key Laboratory of Key Technology on Hydropower Development (PKLHD202003). The last author is now supported by the National Natural Science Foundation of China (Grant No. 52201379).

References

[1] Gao W, Li C, Ye Z. The current situation and latest research of deep-sea floating wind turbine. Engineering Sciences 2014; 16(2): 79-87.

[2] Ren, ZR, Zhou HY, Li BB, Hu ZZ, Yu MH, Shi W. Localization and topological observability analysis of a moored floating structure using mooring line tension measurements, Ocean Engineering 2022; 266P5: 112706. https://doi.org/10.1016/j.energy.2022. 112706

[3] Zeng YX, Shi W, Michailides C, Ren ZR, Li X. Turbulence model effects on the hydrodynamic response of an oscillating water column (OWC) with use of a computational fluid dynamics model. Energy 2022; 261:124926. https://doi.org/10.1016/j.energy.2022.124926

[4] Zhang LX, Shi W, Zeng YX, Michailides C, Zheng SM, Li Y. Experimental Investigation on the hydrodynamic effects of Heave Plates for application of floating offshore wind turbine. Ocean Engineering 2023; 267C:113103. https://doi.org/10.1016/j.oceaneng.2022.113103

[5] Shi W, Zhang L, Karimirad M, Michailides C, Jiang Z, Li X. Combined effects of aerodynamic and second-order hydrodynamic loads for three semisubmersible floating wind turbines in different water depths. Applied Ocean Research 2023; 130: 103416 https://doi.org/10.1016/j.apor.2022.103416

[6] Zhang Y, Shi W, Li DS, Li X, Duan YF, Verma, AS. A novel framework for modeling floating offshore wind turbines based on the vector form intrinsic finite element (VFIFE) method, Ocean Engineering 2022; 262:112221. https://doi.org/10.1016/j.oceaneng.2022.112221

[7] Stetco A, Dinmohammadi F, Zhao X, Robu V, Flynn D, Barnes, M. Machine learning methods for wind turbine condition monitoring: a review. Renewable Energy 2019; 133: 620-635. https://doi.org/10.1016/j.renene.2018.10.047.

[8] Huang LF. Research On Online Prediction of Nonstationary Nonlinear Ship Motion in Ocean Waves. Harbin Engineering University, 2016.

[9] Li HB, Xiao LF, Wei HD. Research on Online Prediction of Floating Offshore Platform Motions based on LSTM Network. Journal of Ship Mechanics 2021; 25:576-585. https://doi.org/10.3969/j.issn.1007-7294.2021.05.006.

[10] Bahdanau D, Cho K, Bengio Y. Neural machine translation by jointly learning to align and translate. Computer Science 2014; 1: 1409.0473. https://doi.org/10.48550/arXiv.1409.0473.

[11] Wang ZM, Qiao DS, Yan J, Tang GQ. A new approach to predict dynamic mooring tension using LSTM neural network based on responses of floating structure. Ocean Engineering 2022;249: 110905. https://doi.org/10.1016/j.oceaneng.2022.110905

[12] Khan A, Bil C, Marion KE. Ship motion prediction for launch and recovery of air vehicles. Oceans 2005:1640198. https://doi.org/10.1109/OCEANS.2005.1640198.

[13] Gu M, Liu CD, Zhang JF. Extreme short-term prediction of ship motion based on chaotic theory and RBF neural network. Journal of Ship Mechanics 2013; 17(10): 1147-1152. https://doi.org/10.3969/j.issn.1007-7294.2013.10.007.

[14] Liu Y, Duan W, Huang L, Duan S. The input vector space optimization for LSTM deep learning model in real-time prediction of ship motions. Ocean Engineering 2020; 213: 107681. https://doi.org/10.1016/j.oceaneng.2020.107681.

[15] Pena B, Huang L. Wave-GAN: A deep learning approach for the prediction of nonlinear regular wave loads and run-up on a fixed cylinder. Coastal Engineering (Amsterdam) 2021; 167: 103902. https://doi.org/10.1016/j.coastaleng.2021.103902.

[16] Lian LK, Zhao YP, Bi CW, Xu ZJ, Du H. Research on Damage Detection Method of Flat Fishing Net Based on Digital Twin Technology. Fishery Sciences 2022; 43: 19663. https://doi.org/10.19663/ j. issn.2095-9869.20210825001.

[17] Bjørni F, Lien S, Midtgarden T, Kulia G. Prediction of dynamic mooring responses of a floating wind turbine using an artificial neural network. IOP Conference Series. Materials Science and Engineering 2021; 1201(1): 12023. https://doi.org/10.1088/1757-899X/1201/1/012023.

[18] Zhang F, Guo Z, Sun, X. Short-term wind power prediction based on EMD-LSTM combined model. IOP Conference Series: Earth and Environmental Science 2020; 514(4): 042003. https://doi.org/10.1088/1755-1315/514/4/042003.

[19] Sutskever I, Vinyals O, Le Quoc V. Sequence to sequence learning with neural networks. Advances in neural information processing systems 2014; 27.

[20] Cho K, Van Merriënboer B, Gulcehre C. Learning phrase representations using RNN encoder-decoder for statistical machine translation. Computer Science 2014;1406.1078. https://arxiv.org/abs/1406.1078

[21] Vinyals O, Le Q. A Neural Conversational Model. Computer Science 2015; 1506.05869. https://arxiv.org/abs/1506.05869

[22] Liu Y, Li D. Research on User Gender Prediction of Chinese Microblog Based on Short Text Analysis. IEEE 2018: 775-779. https://doi.org/10.1109/ICIVC.2018.8492759

[23] Hochreiter S, Schmidhuber J. Long short-term memory. Neural Computation 1997; 9(8): 1735-1780. https://doi.org/10.1162/neco.1997.9.8.1735

[24] Graves A. Supervised sequence labelling with recurrent neural networks. Studies in Computational Intelligence, 2013; 385.

[25] Hurst HE. Long-term storage capacity of reservoirs. Transactions of the American society of civil engineers, 1951, 116(1): 770-799. https://doi.org/10.1061/TACEAT.0006518

[26] Graves A. Generating sequences with recurrent neural networks. Computer Science 2013. https://doi.org/10.48550/arXiv.1308.0850

[27] Kingma D, Ba J. Adam: a method for stochastic optimization. Computer Science 2014. https://doi.org/10.48550/arXiv.1412.6980

[28] Srivastava N, Hinton G, Krizhevsky A, Sutskever I, Salakhutdinov R. Dropout: a simple way to prevent neural networks from overfitting. Journal of Machine Learning Research 2014; 15(1): 1929-1958.

[29] Hinton G, Srivastava N, Krizhevsky A, Sutskever I. Improving neural networks by preventing co-adaptation of feature detectors. Computer Science 2012. https://doi.org/10.48550/arXiv.1207.0580

[30] Zhang LX, Shi W, Karimirad M, Michailides C, Jiang ZY. Second-order Hydrodynamic Effects on the Response of Three Semisubmersible Floating Offshore Wind Turbines. Ocean Engineering 2020; 207.C: 107371. Web. https://doi.org/10.1016/j.oceaneng.2020.107371

Short-term Motion Prediction of floating offshore wind turbine Based on Muti-input LSTM Neural Network

Wei Shi[1,2,3], Lehan Hu[1], Zaibin Lin[4], Lixian Zhang[1], Jun Wu[5], Wei Chai[6*]

[1]DeepWater Engineering Research Centre, Dalian University of Technology, China;

[2] State Key Laboratory of Coastal and Offshore Engineering, Dalian University of Technology, Dalian, China;

[3] Research Institute of Dalian University of Technology in Shenzhen, Shenzhen, China;

[4]School of Engineering, University of Aberdeen, UK

[5] School of Naval Architecture and Ocean Engineering, Huazhong University of Science and Technology, Wuhan, China

[6] School of Naval Architecture, Ocean and Energy Power Engineering, Wuhan University of Technology, Wuhan 430063, China;

* Corresponding author: Prof. Wei Chai, Email: chaiwei@whut.edu.cn

Abstract: The motion response of an offshore floating wind turbine (FOWT) platform is closely related to the control operation regarding the safety of a wind turbine. It is affected by various factors such as sea state environments and mooring systems. In practice, how to predict the motion response of the wind turbine platform in the short term has always been a concern of engineering practice. At present, the development of deep learning technology has brought some potential solutions to this problem. In this paper, a Multi-Input Long-Short Term Memory (MI-LSTM) neural network method is proposed to predict the short-term motion response of a floating offshore wind turbine platform. Specifically, the numerical simulation of the 5MW Braceless platform is carried out under different environmental conditions, and the data of

platform motion response, wave elevation, and mooring force are selected as input variables. Then the training and test groups are established after post-processing data. Subsequently, a Single-Input LSTM (SI-LSTM) model and a Multi-Input LSTM (MI-LSTM) model are established to learn the input data. After comparing the overall accuracy of the results, it is found that the additional mooring force and wave elevation positively affects the platform response prediction results. From the aspects of discreteness and overall accuracy, it is verified that the established MI-LSTM model is also applicable, considering the influence of second-order hydrodynamics. Lastly, compared with the prediction results obtained by the multi-input one-dimensional convolutional neural network (MI1D-CNN), the advantages of the two different models are expounded from the perspectives of training time and accuracy, which provides ideas for the optimization of the FOWT motion response prediction model. This study sheds insights on the short-term motion response forecast and platform positioning of a FOWT. Short-term forecasts of a FOWT can be achieved under various sea conditions by combining the global positioning system.

Keywords: Floating offshore wind turbine; deep learning; response prediction; multi-input LSTM model; second-order hydrodynamic

1. Introduction

With the rapid development of the global economy, energy has become a critical factor in determining social and economic development. To meet the Net Zero target by utilizing sustainable energy, the vigorous growth of renewable energy has become an essential part of the development strategy worldwide. Due to its high energy conversion ability, offshore wind power has been gradually installed in various countries recently. Different foundations of floating offshore wind turbines have been proposed, including spar, tension leg platform (TLP) shape, semi-submersible, and barge [1]-[3]. Substantial research has been carried out in terms of hydrodynamics, mooring systems, stability, performance, and survivability of a FOWT [4]-

[9].

Compared with the onshore wind turbine structure, a FOWT encounters a more complex ocean environment. The motion response of a FOWT occurs in six degrees of freedom (6DOF) and leads to significant challenges in design and assessment [10]. Therefore, it is of great significance to propose an accurate prediction method for the motion response of the FOWT to guide the design and assess structural safety. In the deep learning model, motion response prediction is generally based on the historical data of motion response and many other results from numerical and experimental measurements. In general, deep learning technology is applied to predict the motion response of structures in the next few seconds [11]. According to the length of the forecast time, motion response prediction can be categorized as short-term and safe-period motion prediction. Short-term prediction plays a vital role in improving dynamic positioning control performance, and it provides early warning in extreme sea conditions to reduce platform damage to a certain extent. A short-term forecast's prediction advanced time (PAT) is generally a few seconds, and it requires high forecast accuracy [12].

In recent years, the application of deep learning technology in offshore structures has gradually expanded. The research is mainly carried out by the convolutional neural network (CNN) and the recurrent neural network (RNN) methods [13]-[21]. Wang et al. [14] proposed the Low-frequency adds wave-frequency responses (LAWR) method to predict the mooring line tension of a semi-submersible platform. Combined with the LSTM method, accurate results are obtained to predict mooring line tension under different cases. Pena et al. [18] proposed the Wave-Generative Adversarial Network (Wave-GAN) technology, combined with CNN convolutional neural network and CFD method, to predict the load of nonlinear waves on fixed structural columns. Pena et al. [18] concluded the maximum error between the Wave-GAN predicted value and CFD simulated value of 1.5%-2% by adjusting several parameters, and the mean absolute error (MAE) of the test group is about 0.014. Lian et al. [19] constructed the digital twin of mesh clothing and established the deep neural network (DNN) to predict whether the mesh clothing is damaged. The average accuracy of the final identification model is 94.3%. Bjørni et al. [20] predicted the mooring line tension in the next 30 s by making use of the platform motion response in the first 60 s as input and constructed a three-layer deep neural network with bias term. It is concluded that the average error of anchor chain tension is 0.46% through cross-sectional comparisons. According to the combined prediction method of the Extreme Learning Machine (ELM), the Empirical Mode Decomposition (EMD), and LSTM neural network, Zhang et al. [21] proved that the combined prediction method presented higher prediction accuracy than the single LSTM model and ELM-LSTM model. However, when considering the influence of environmental factors and mooring force, there is limited research on predicting the motion response of a FOWT. At the same time, in practice, it needs to assess the motion response of a FOWT under the influence of various complex factors and consider the impact of second-order hydrodynamic force. Moreover, the amount of research on the motion response prediction of a FOWT under the effect of the second-order hydrodynamic force is also limited.

To investigate the short-term motion prediction of a FOWT, the MI-LSTM Neural Network model is used. This paper is organized as follows: Section 2 introduces the basic principles of the RNN. The architecture and differences between the established SI-LSTM model and the MI-LSTM model are explained in detail. The hyperparameters of the model and the selection of the training and test groups are also given in this section. Then, in Section 3, the structure size of the 5 MW Braceless platform model is shown. A detailed comparison is made between the prediction results of the SI-LSTM and MI-LSTM models under different environmental conditions in Section 4. This proves the positive excitation of the increased input factor numbers on the prediction results and illustrates the advantages and benefits of the MI-LSTM model. In Section 5, the applicability of the proposed model is demonstrated when the second-order hydrodynamic force is considered. Given that there are few comparisons between the RNN model and CNN model regarding time domain problems, in Section 6, by comparing the prediction results of the proposed model with the multi-input one-dimensional convolutional neural network (MI1D-CNN) model, the advantages of the two models are illustrated from the perspectives of overall accuracy and training time. Finally, the conclusions and recommendations are made for the future optimization of the platform response prediction model.

2. Long-Short Term Memory (LSTM) Neural Network

2.1. Recurrent Neural Network (RNN)

Recurrent neural network (RNN) is gradually emerging in the interdisciplinary field as a typical representative of deep learning technology. RNN takes time series data as input and performs recursion in the evolution direction of the sequence, where all nodes (cyclic units) are linked in a chain [22]. RNN has memorization, parameter sharing, and turning completeness [23]-[25], so it has clear advantages in learning the nonlinear features in sequences. RNNs are widely used in natural language processing, such as speech recognition, language modeling, and time series prediction. RNN performs outstandingly in solving scheduling problems, and motion response prediction is the typical time domain problem. Therefore, in this paper, RNN is selected for model architecture.

Since the motion of the platform at time *t* is affected by the motion at the previous time $t-1$, meanwhile, the motion at current time *t* will also have an impact at forward time $t+1$, platform motion response is a continuous process with time dependence. Considering this characteristic, the traditional deep neural network (DNN) cannot convey information precisely in the time sequence, but the RNN is developed to overcome this problem. Training input data from a FOWT system to predict the motion response in the next few seconds can be viewed as an adaptive function mapping. The input is the previous time series information of different input factors, and the output is the motion response in the future. Hence, the trained deep learning model can achieve prediction in a short time.

The timeline expansion of the RNN is shown in **Figure 1**, where x is the network input layer, s is the network node hiding layer, and o is the network node output layer. After the network receives the input x_t at time t, the value of the hidden layer is s_t and the output value is o_t. The value of s_t depends not only on x_t, but also on s_{t-1}. In other words, s inherits the information from each node.

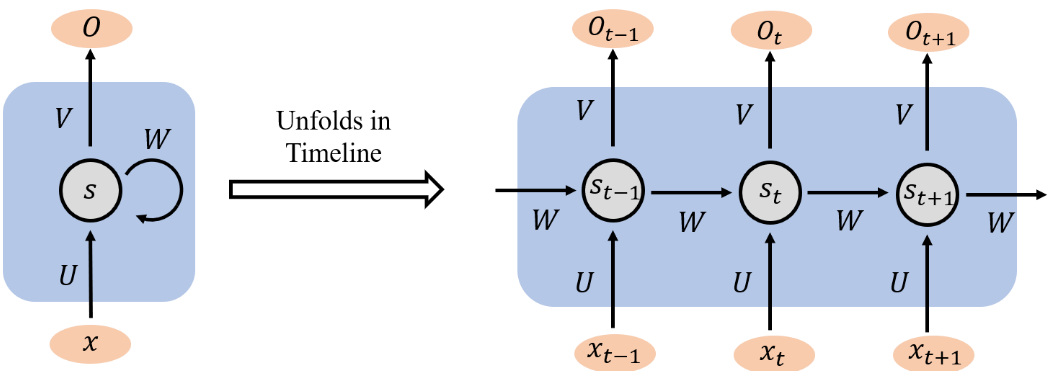

Figure 1. An unfolded RNN network

The calculation method of the RNN network is shown in Equations 1-2:

$$o_t = \boldsymbol{g}(\mathbf{V} \cdot s_t) \tag{1}$$

$$s_t = \boldsymbol{f}(\mathbf{U} \cdot x_t + \mathbf{W} \cdot s_{t-1}) \tag{2}$$

where **V** is the weight matrix of the output layer, ***g*** is the activation function for the output layer, **U** is the weight matrix of the input layer *x*, and **W** is the weight matrix of the last value, which is the input of the present time, and ***f*** is the activation function for the hidden layer. Common activation functions, such as sigmoid, tanh, Rectified Linear Unit (ReLU), and linear activation function, can be selected according to data characteristics and experimental effects. The sigmoid activation function is generally selected for hidden layer activation function ***f***, while the linear activation function is generally chosen for output layer activation function ***g***. Equation 1 is the calculation formula of the output layer. The output layer is fully connected, indicating that every node in the output layer is connected to every node in the hidden layer. Equation 2 is the calculation formula of the hidden layer.

2.2. Long-Short Term Memory (LSTM) Network

LSTM is first proposed by Hochreiter and Schmidhuber [25]. Compared with traditional RNN, the LSTM network has improved the gradient explosion and gradient extinction. It has been one of the most popular RNN models and is widely applied in many fields, such as speech recognition, image description, and natural language processing. The internal structure of the LSTM node is shown in **Figure 2** [27].

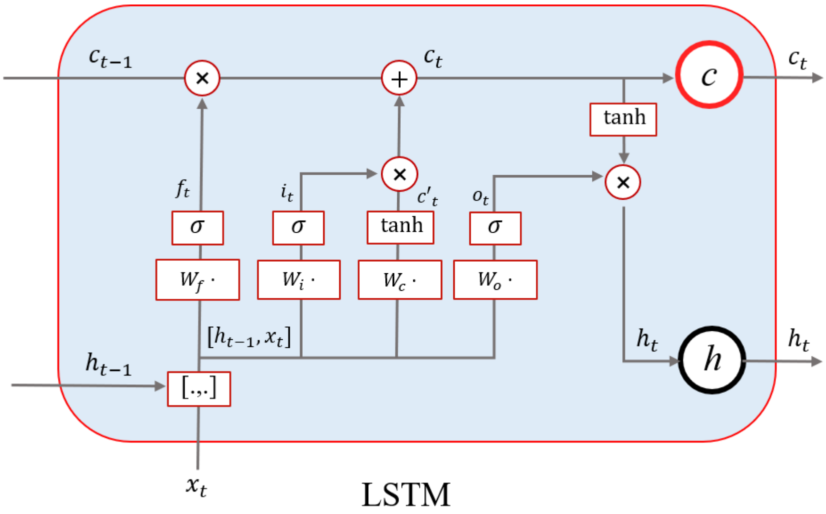

Figure 2. LSTM node unit internal structure

At time t, the LSTM network has three inputs: current time input value x_t, LSTM output value h_{t-1} at the last time, and the unit state c_{t-1} at the previous time. The output of LSTM has two parts: the output value of LSTM at the current time h_t, and the unit state at the current time c_t. x, h, and c are vectors. In addition, LSTM uses the concept of a Gate to control the state of the unit [27]. Gate is a full connection layer that controls information transmission between input and output. Its input is a vector of time series information, and its output is a vector of real numbers between 0 and 1. The gate can be expressed as:

$$G(x) = \boldsymbol{\sigma}(\boldsymbol{W} \cdot \boldsymbol{x} + \mathbf{b}) \tag{3}$$

where $\boldsymbol{W}$ is the weight matrix of the gate, $\mathbf{b}$ is the bias term, and $\boldsymbol{\sigma}$ is the generally sigmoid activation function.

The output vector of the gate is multiplied by the element and the vector is controlled to achieve the gate effect. The gated output is a vector of real numbers between 0 and 1. When the gated output is 0, any vectors multiplied by the output will get the 0 vectors, indicating that no information can pass through. When the gated output is 1, no changes are applied by multiplying, indicating that any information can pass through. Because $\boldsymbol{\sigma}$ has a range of (0,1), the gate is an intermediate state.

LSTM relies on two gates to control the content of the cell state: (1) one is the forget gate that determines the amount of the cell state c_{t-1} at the last moment. c_{t-1} is used to retain the current moment c_t; (2) one is the input gate that determines the amount of the current network input x_t, which is saved to the unit state c_t. Meanwhile, LSTM uses an output gate to control the amount of unit state c_t that is generated from the current output value h_t. The governing equations of each gate are given as follows:

$$f_t = \boldsymbol{\sigma}(\mathbf{W_f} \cdot [\boldsymbol{h_{t-1}}, \boldsymbol{x_t}] + \mathbf{b_f}) \tag{4}$$

$$i_t = \boldsymbol{\sigma}(\mathbf{W_i} \cdot [\boldsymbol{h_{t-1}}, \boldsymbol{x_t}] + \mathbf{b_i}) \tag{5}$$

$$c_t = f_t \cdot c_{t-1} + i_c \cdot tanh(\mathbf{W_C} \cdot [\boldsymbol{h_{t-1}}, \boldsymbol{x_t}] + \mathbf{b_c}) \tag{6}$$

$$o_t = \boldsymbol{\sigma}(\mathbf{W_o} \cdot [\boldsymbol{h_{t-1}}, \boldsymbol{x_t}] + \mathbf{b_o}) \tag{7}$$

$$h_t = o_t \cdot tanh(\boldsymbol{c_t}) \tag{8}$$

where f_t is the forgetting gate equation, $\mathbf{W_f}$ is the weight matrix of the forgetting gate, $[h_{t-1,} x_t]$ is joining two vectors into a longer vector, $\mathbf{b_f}$ is the biased term of the forgetting gate, i_t is the input gate equation, $\mathbf{W_i}$ is the weight matrix of the input gate, $\mathbf{b_i}$ is the offset term of the input gate, c_t is the current moment element state equation, o_t is the output gate control equation, h_t is the final output equation determined by the output gate and unit state.

The unique Gate structure in the LSTM model effectively improves the phenomenon of gradient explosion and gradient disappearance. the activation function of the gate structure in the LSTM model is the sigmoid function, and the Sigmoid function controls the value of the forgetting gate between 0 and 1. When the output of the gate is 1, the forgetting gate is saturated, at this time the long-range information gradient does not disappear, and the gradient can be well passed in the LSTM, largely mitigating the probability of gradient disappearance occurring; when the output of the gate is 0, at this time the model is blocking the gradient flow and forgetting the previous information, indicating that the information of the previous moment does not affect on the current moment. Through the gate structure and sigmoid activation function, the LSTM model can effectively solve the gradient disappearance and gradient explosion problems.

Existing LSTM network prediction modes mainly fall into the following four types [28]: point-to-point, point-to-sequence, sequence-to-point, and sequence-to-sequence, as shown in **Figure 3**:

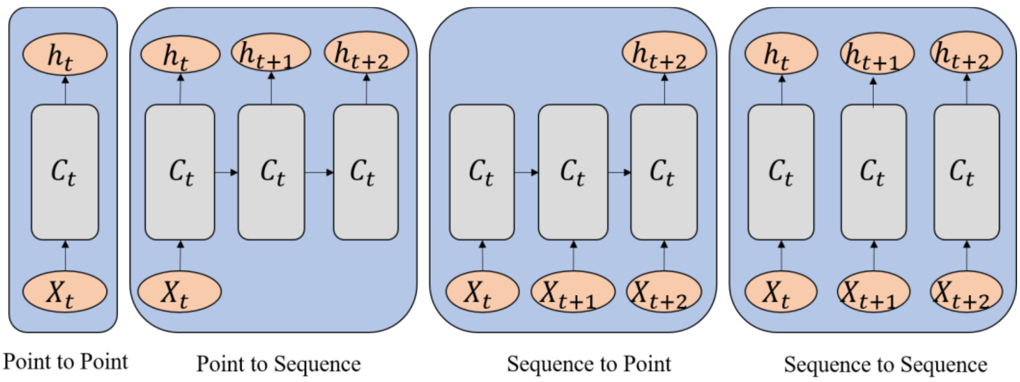

Figure 3. LSTM network prediction modes

The LSTM network in this paper is set up by using sequence-to-point mode for a prediction model, which uses forecasting point response from previous time series after the selected data input mode is adopted in the form of the sliding window. Each window length has 200 time points and the 10 s surge motion. The sliding window form is shown in **Figure 4**, where the mapping relationship between the data input and output is presented when the forecast time is 5 s. Therefore, the response at $t + 5$ is predicted based on the response from t-10 to t.

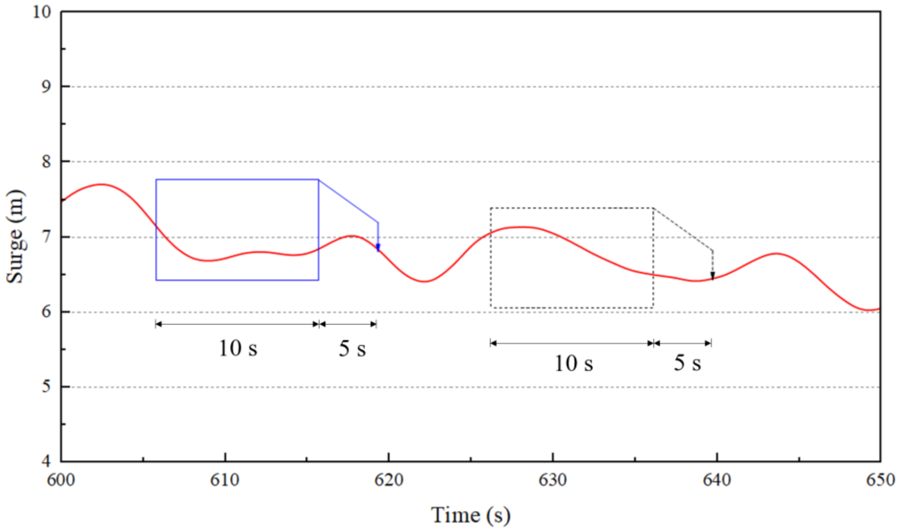

Figure 4. Sliding windows for data input and output

2.3. LSTM Model Structure

The LSTM network model established in this paper has three hidden layers and one fully connected output layer, shown in **Figure 5**. The data sampling frequency is 20 Hz. The input time step of the LSTM network contains 200 time series points with a motion response of 10s. The batch size is set to 256 sample sets, which are also the input for training and updating internal parameters. The number of neurons is set to 200. These two parameters are hyperparameters and can be adjusted according to the performance of the actual test.

Input layer: input time series with a window of 200 data points, representing the motion response of 10s. The input dimension of the single-input model is 1, and that of the multi-input model is 3.

Hidden layer: The hidden layer has 200 nodes.

Output layer: The output layer is dense, the activation function is linear, and the output result is the motion response at the target time.

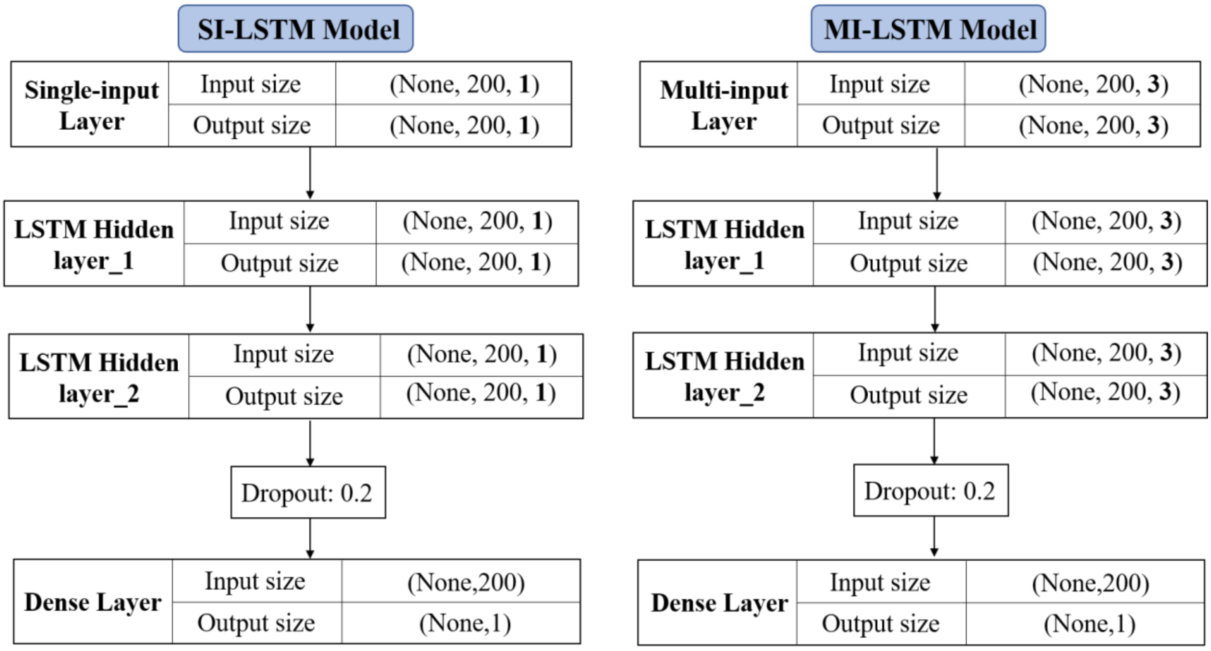

Figure 5. LSTM network model structure and data transfer format

The Adam algorithm is configured for the LSTM network [30]. Adam algorithm is an advanced Stochastic Gradient Descent (SGD) algorithm, which introduces an adaptive learning rate for each parameter. The adaptive learning method and the Momentum method are combined. The learning rate is dynamically adjusted by the first and second moment estimation of the gradient. The gradient descent process is relatively stable and suitable for most non-convex optimization problems in large data sets and high-dimensional space.

Simultaneously, the Dropout layer is added after the input layer and the hidden layer to prevent overfitting [31-[32], and the Dropout_1 and Dropout_2 are set to 0.2. Overfitting may occur due to a large number of unknown network parameters or training times. The principle of dropout is that during the neural network training, some neurons are randomly discarded and not used for training at this round to avoid overfitting and accelerate loss convergence.

In this paper, the LSTM neural network is constructed, and the input data consists of three parts, including time series of previous motion response, mooring force, and wave elevation. And the current motion response is set as the output data. The process of using the LSTM neural network model to predict the motion response is shown in **Figure 6.** The process of predicting motion response by LSTM neural network.

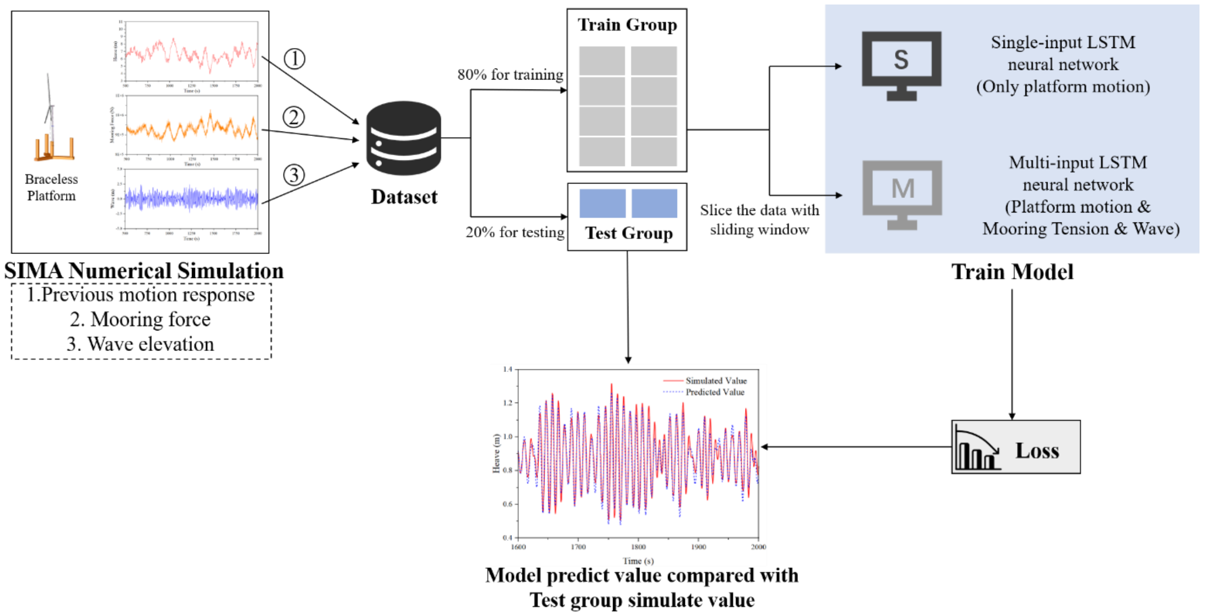

Figure 6. The process of predicting motion response by LSTM neural network

3. Braceless Platform model

The 5 MW Braceless model is established by SIMA, and the time domain response is obtained by numerical simulation. SIMA is developed for the analysis of flexible marine riser systems, but it is also suited for any slender structures, such as mooring lines, umbilicals, steel pipelines, and conventional risers. The data used in training in this paper came from the FOWT model of a 5 MW Braceless semi-submersible platform in the water depth of 100 m. The Braceless platform consists of one central column, three side columns, and three pontoons, shown in **Figure 7**.

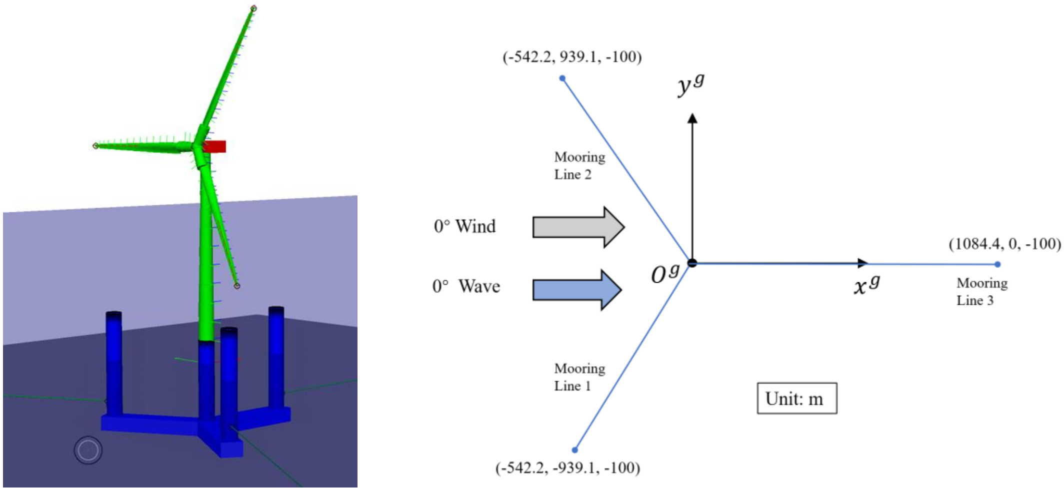

Figure 7. Schematic of 5-MW Braceless platform

Three side columns are evenly distributed around the central column at 120°. They are connected to the bottom of the central column by a floating buoy to form a Braceless semi-submersible platform. The three-point mooring system is adopted, and the anchor chain is set at the bottom of the side column. 0° wave-wind misalignment is considered in the simulation. The main parameters of the Braceless platform are shown in **Table 1.** Parameters of the 5 MW Braceless Platform:

Table 1. Parameters of the 5 MW Braceless Platform

Parameter	Value
Central column diameter (m)	6.5
Side column diameter (m)	6.5
Buoy height (m)	6
Buoy bottom width (m)	9
Buoy short radius (m)	41
Buoy long radius (m)	45.5
Depth of the draft (m)	30
Displacement (t)	10555
Steel weight (t)	1804

Equivalent thickness (m)	0.03

Based on the data given in Ref. [33], site 5 in Norway was selected as a representative site for the simulation. In the following cases, the water depth is 100 m. The average wind speed V_t, effective wave height H_S, and spectrum peak period T_p at the selected cabin height are listed. The JONSWAP spectrum is used to describe random ocean waves, and the JONSWAP spectrum is shown in Equations 9-1 to 9-3. The Kaimal wind speed spectrum is used to describe the offshore wind conditions.

$$S_{(f)} = \alpha \frac{{H_S}^2}{{T_p}^4 f^5} exp\left[-\frac{5}{4}(T_p f)^{-4}\right] \gamma^{exp\left[-\frac{(T_p f-1)}{2\sigma^2}\right]} \quad (9\text{-}1)$$

where f is the wave frequency, γ is the shape parameter, and σ and α are shown below,

$$\sigma = \begin{cases} 0.09 \;\; f \geq f_p \\ 0.07 \; f < f_p \end{cases} \quad (9\text{-}2)$$

$$\alpha = \frac{0.0624}{0.230+0.0336\gamma-0.185/(1.9+\gamma)} \quad (9\text{-}3)$$

Table 2. Environment matrix

Case	Vt (m/s)	γ	Hs (m)	Tp (s)
EC 1	9.8	3.3	2.9	9.98
EC 2	14.8	3.3	4.5	11.81
EC 3	16	3.3	5.3	12.81

4. Single-input and Multi-input

4.1. Data Partitioning and Error Measurement

The sampling frequency of the Braceless platform simulation test is 20 Hz. The total sampling length of motion response (surge, pitch, and sway) is 2000 s. The collected time series

contains 40000 data points. In the training model, the first 32000 points of response data are the training groups and the last 8000 points of response data are the test groups. Three test cases (EC1, EC2, and EC3) are selected, and each test case contained 2000 s surge, pitch, and sway motion data.

The training group data is used to train and obtain the neural network model. The relationship between training Epochs and Loss is observed through the Loss function. Then the test group data is imported into the trained neural network model to verify the accuracy and performance of the trained model.

The Loss function adopted in this paper is the Mean Squared Error (MSE), which is the averaged squared difference between the predicted value and the measured value as shown in Equation 10:

$$MSE = \frac{\Sigma(y_t' - y_t)^2}{n} \tag{10}$$

where $y_t{}'$ is the predicted value of the motion response at time t, y_t is the measured value of the motion response at time t, and n is the total number of predicted values 8000 in this study.

4.2. Single-input Predicted Results

Single-input LSTM (SI-LSTM) model is used to train the motion response data in the training group in terms of the heave, surge, sway, and pitch. The training input of the model is only based on the previous motions. The output of the model is compared and analyzed with the data of the test group. The predicted advance time is set as 2.5 s and 5 s respectively. The actual and predicted values are shown in **Figures 8-10**.

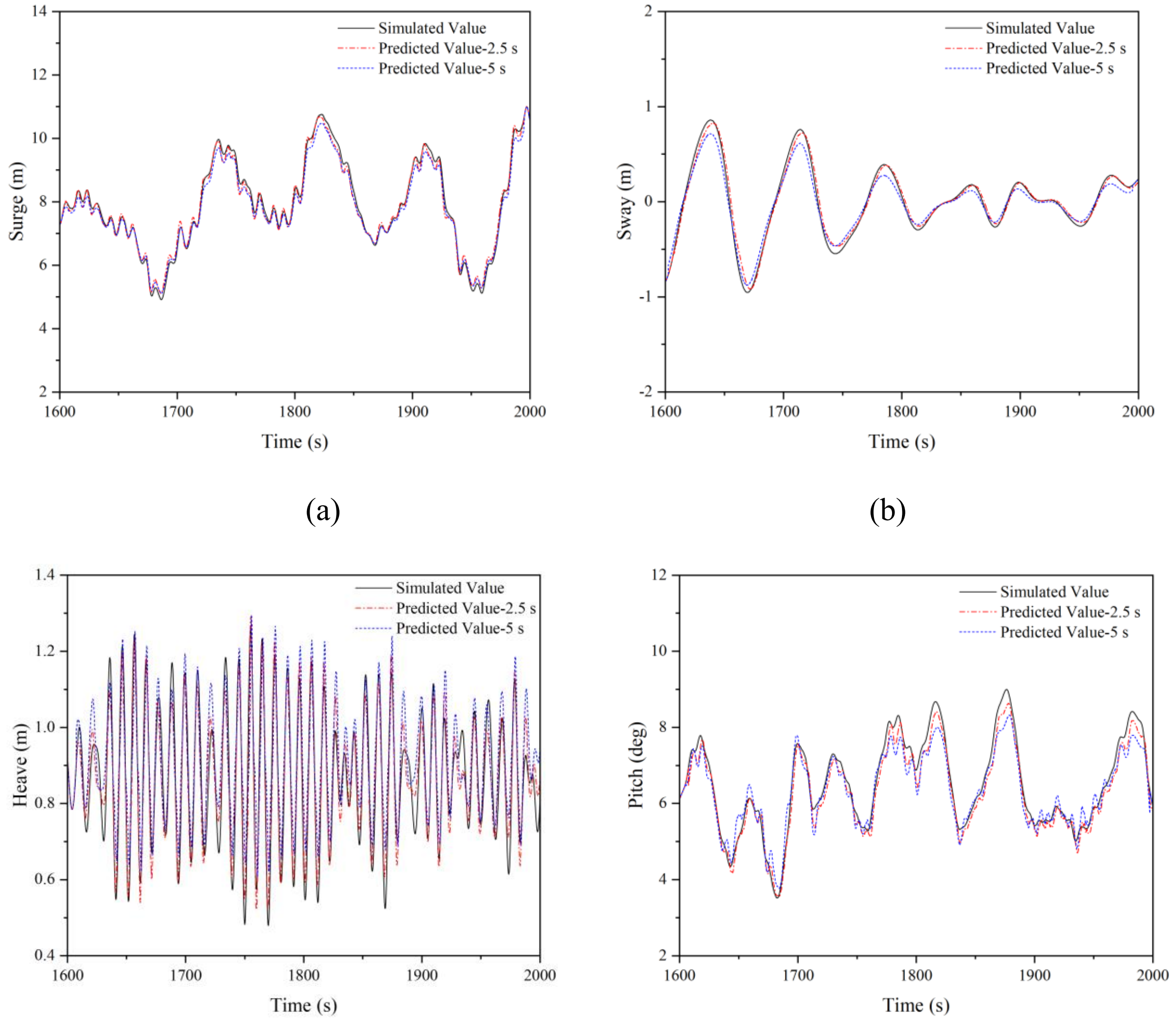

(a) (b)

(c) (d)

Figure 8. Simulated and predicted values of EC 1 at 2.5 s and 5 s:

(a) Surge; (b) Sway; (c) Heave; (d) Pitch

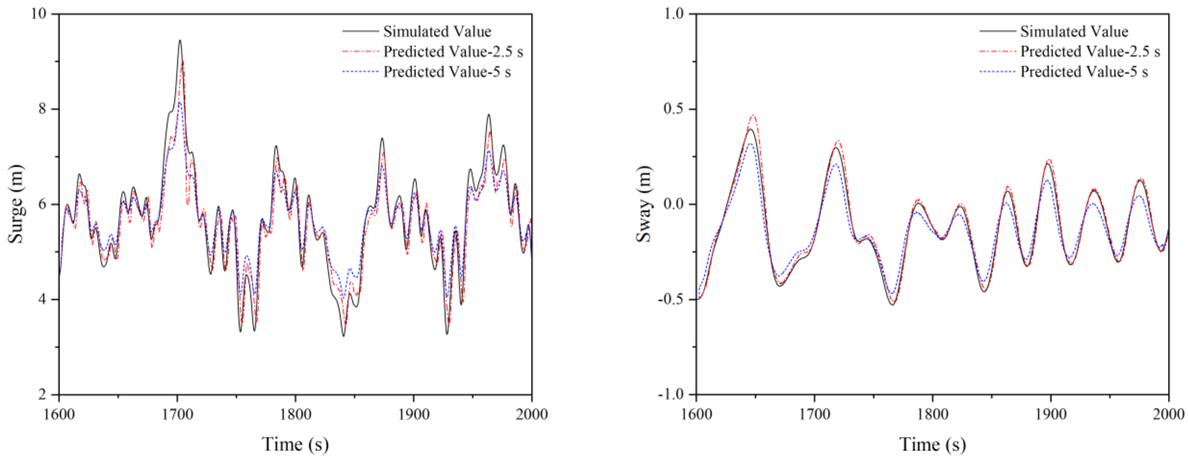

(a) (b)

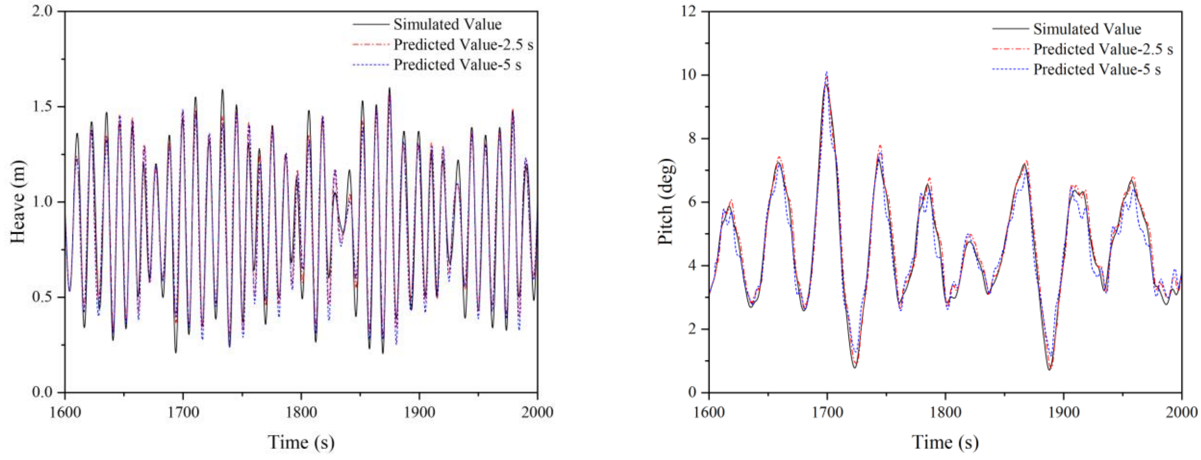

(c) (d)

Figure 9. Simulated and predicted values of EC 2 at 2.5 s and 5 s:

(a) Surge; (b) Sway; (c) Heave; (d) Pitch

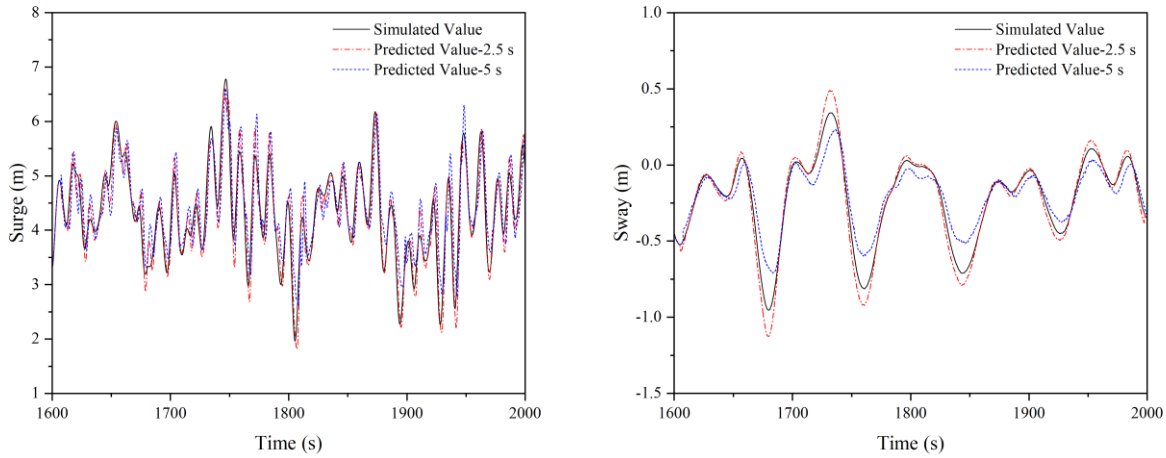

(a) (b)

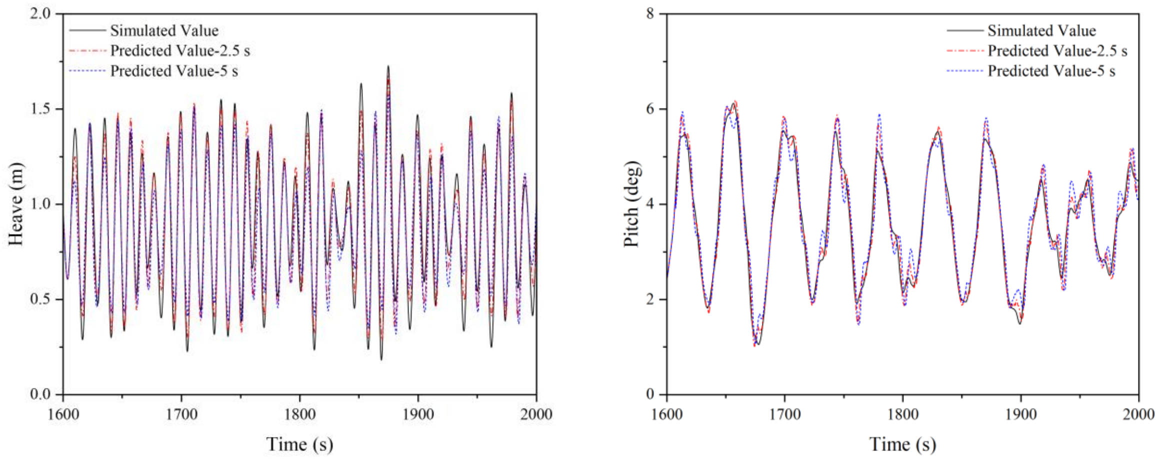

(c) (d)

Figure 10. Simulated and predicted values of EC 3 at 2.5 s and 5 s:
(a) Surge; (b) Sway; (c) Heave; (d) Pitch

It can be seen from **Figures 8-10** that when the previous motion response is used as the single input, the predicted value at PAT of 2.5 s is closer to the simulated value. Due to the large amplitude of motion in the surge, the predicted results in **Figure 8(a)** agree well with the simulation results, apart from the minor discrepancy at the peak of the surge in **Figures 9-10(a)**. Due to the small amplitude in sway, the predicted results under the two PATs generally agree with simulated results compared to the agreement between predicted and simulated surge. Similarly, there is also a minor discrepancy at the peak. The amplitude of heave motion is the smallest among the three motions, but it contains higher frequency components. The predicted heave motion in three test cases in **Figures 8-10** presents better agreement with simulated results at PAT of 2.5 s, but a minor discrepancy can be noted at the peak and trough at PAT of 5 s. The peak value of pitch in **Figures 8-10(d)** is also large, but there is higher-order fluctuation at the peak and trough due to the nonlinear motion induced by wind and waves. Single-input LSTM model learned the nonlinear features from the training data group, so the predicted value agrees well with the simulated results.

In summary, compared with the simulated values, the predicted values in all motions have very minor discrepancies at peak and trough, but a fairly good agreement has been presented. The discrepancy at peak and trough can be attributed to the limited input factors to train the neural network. To unravel this, the multi-input network structure is investigated in detail in Section 4.3.

4.3. Muti-input Predicted Results

A multi-input model is trained to explore the effects of multiple factors as input conditions on the predicted results. Unlike the single-input model, the training input of the multi-input LSTM (MI-LSTM) model is based on the previous motions, mooring forces, and wave

elevation. The output of the model is compared and analyzed with the data of the test group. The predicted advance time is set as 2.5 s and 5 s respectively. The test and predicted results are shown in **Figures 11-13**:

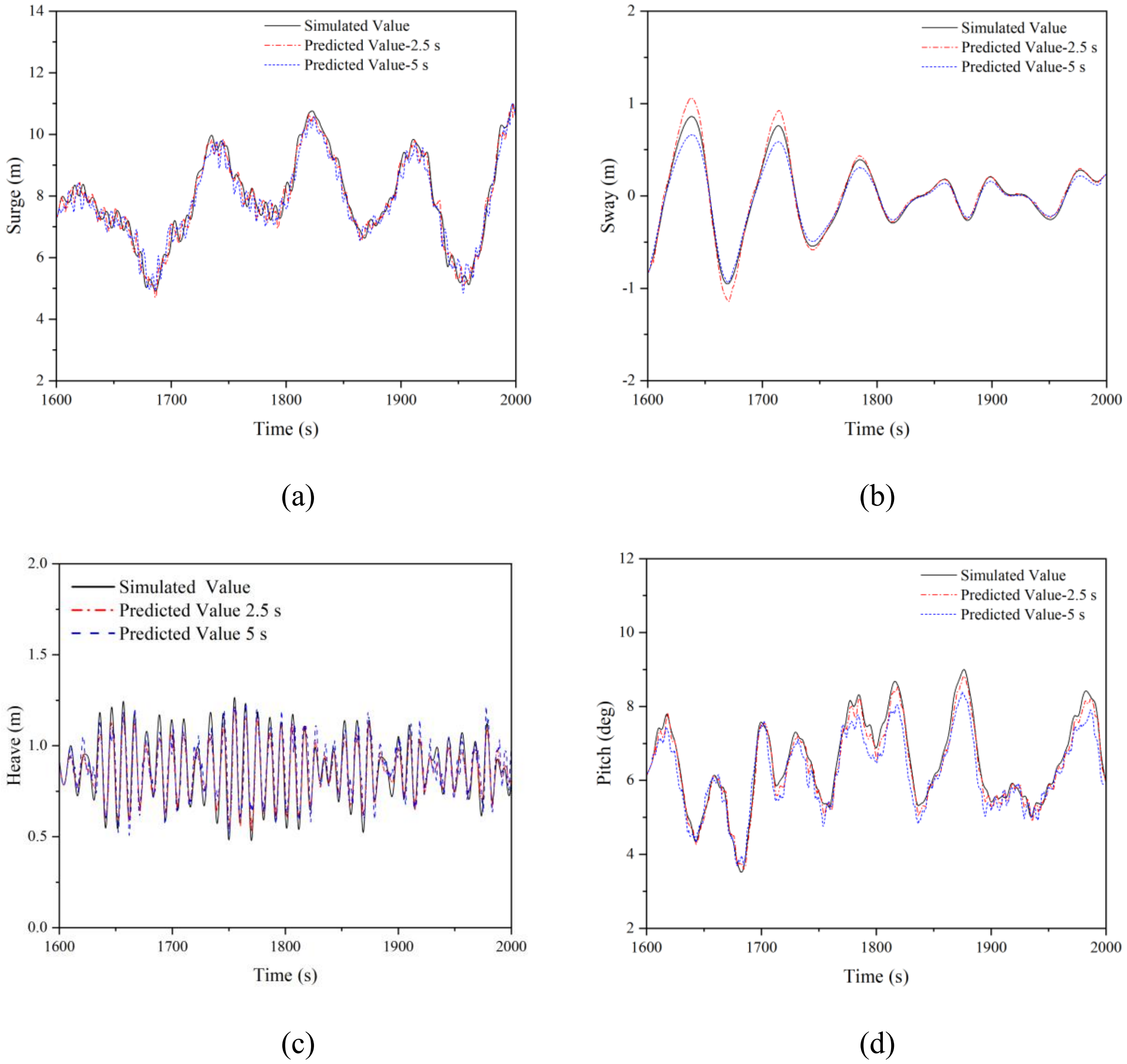

Figure 11. Simulated and predicted values of EC 1 at 2.5 s and 5 s:

(a) Surge; (b) Sway; (c) Heave; (d) Pitch

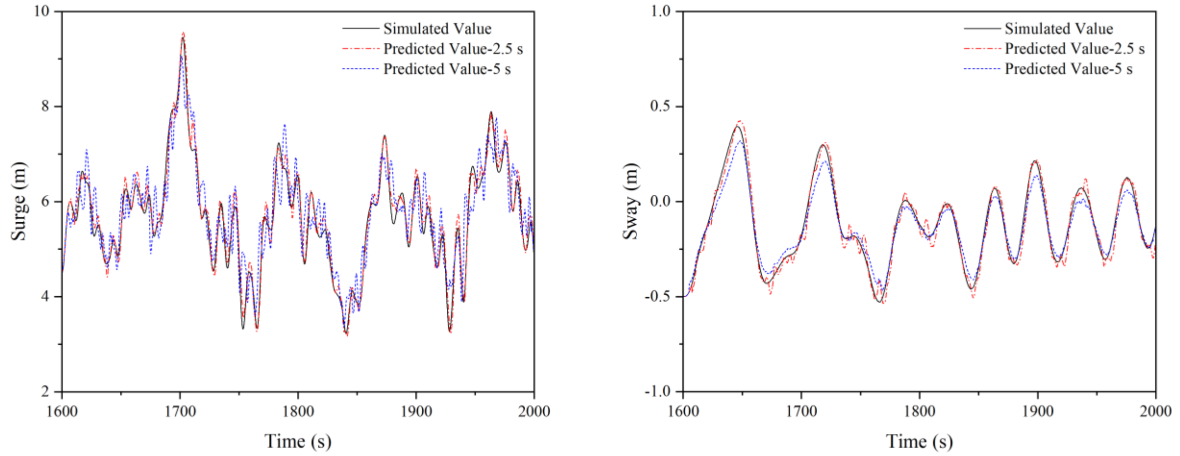

(a) (b)

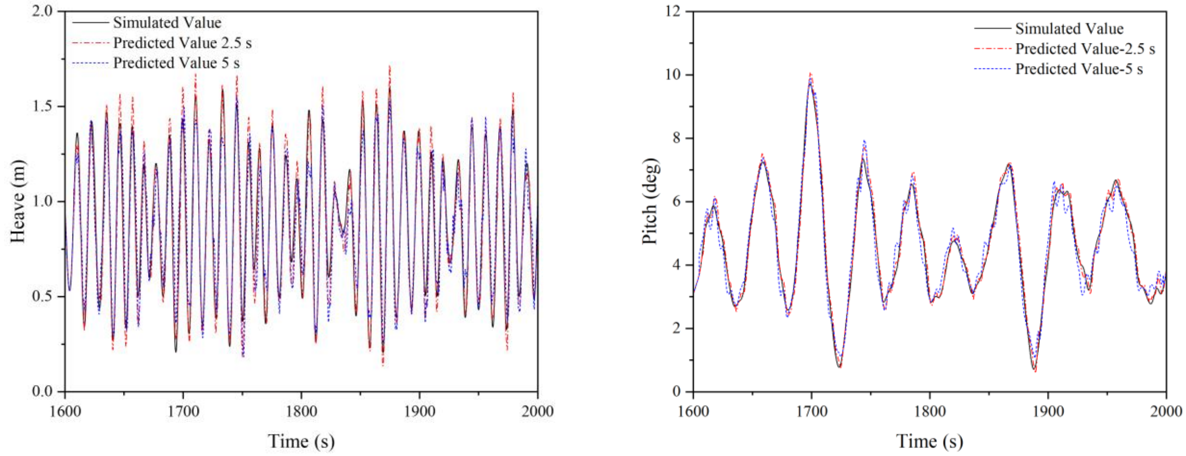

(c) (d)

Figure 12. Simulated and predicted values of EC 2 at 2.5 s and 5 s:

(a) Surge; (b) Sway; (c) Heave; (d) Pitch

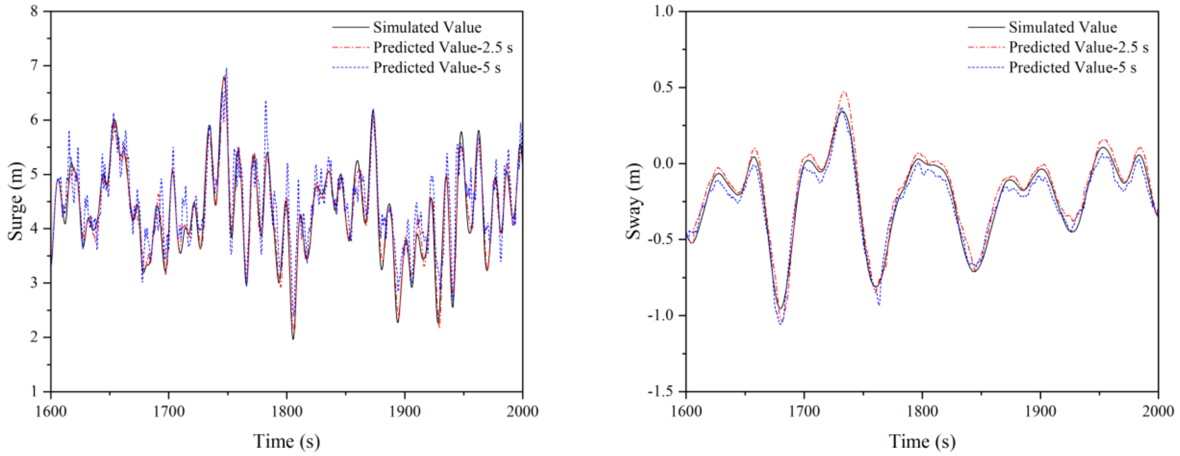

(a) (b)

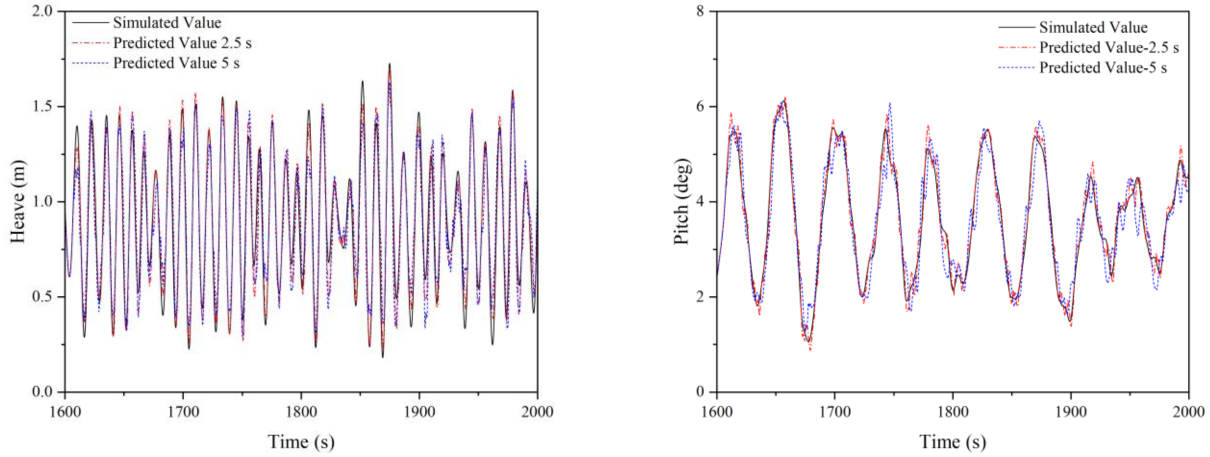

(c) (d)

Figure 13. Simulated and predicted values of EC 3 at 2.5 s and 5 s:

(a) Surge; (b) Sway; (c) Heave; (d) Pitch

When the model input factors become multiple, i.e., adding mooring force and wave elevation, a better agreement between the predicted value and the simulated value is obtained compared with the single input case. Improved agreement of surge prediction at peak in **Figure 12(a)** is presented compared to **Figure 9(a)**. But in the case of multiple inputs, the fluctuations can also be noticed from the predicted surge. Sway and heave are not significantly improved due to their less sensitivity to mooring force. With the additional input factors, the accuracy of the predicted pitch has been improved significantly as pitch motion is sensitive to mooring forces, comparing **Figure 9(d)** and **12(d)**. It can be found that in the period 1900s-2000s, the discrepancy of the single-input model can be found, while the multi-input model presented better performance with additional input data sets. Similar to the pitch, better agreements have been achieved for the predicted surge.

In a word, after adding the additional input factors to train the multi-input model, better performance in predicting the FOWT motion response has been demonstrated. However, the saw-tooth effect of the MI-LSTM model is more obvious, caused by the deep learning of the additional input information. The saw tooth effect is further analyzed after analyzing the scatterplot of discrete situations in Section 4.4.

4.4 Error Analysis

In this study, the number of Epochs is set to 50 rounds. It is shown in **Figure 14** the trend of the Loss function changing with the Epochs is generated and recorded during the training. It can be noted that with the increment of Epochs, Loss decreases rapidly in the beginning. Then after the rapid decrease stage, Loss finally tended to be stable. After the Epochs reaches 50, Loss remains unchanged. It can be concluded that the network training effect will not be further improved after 50 rounds and a neural network model with good accuracy is generated. The model has completed learning about the relationship between the input and output data.

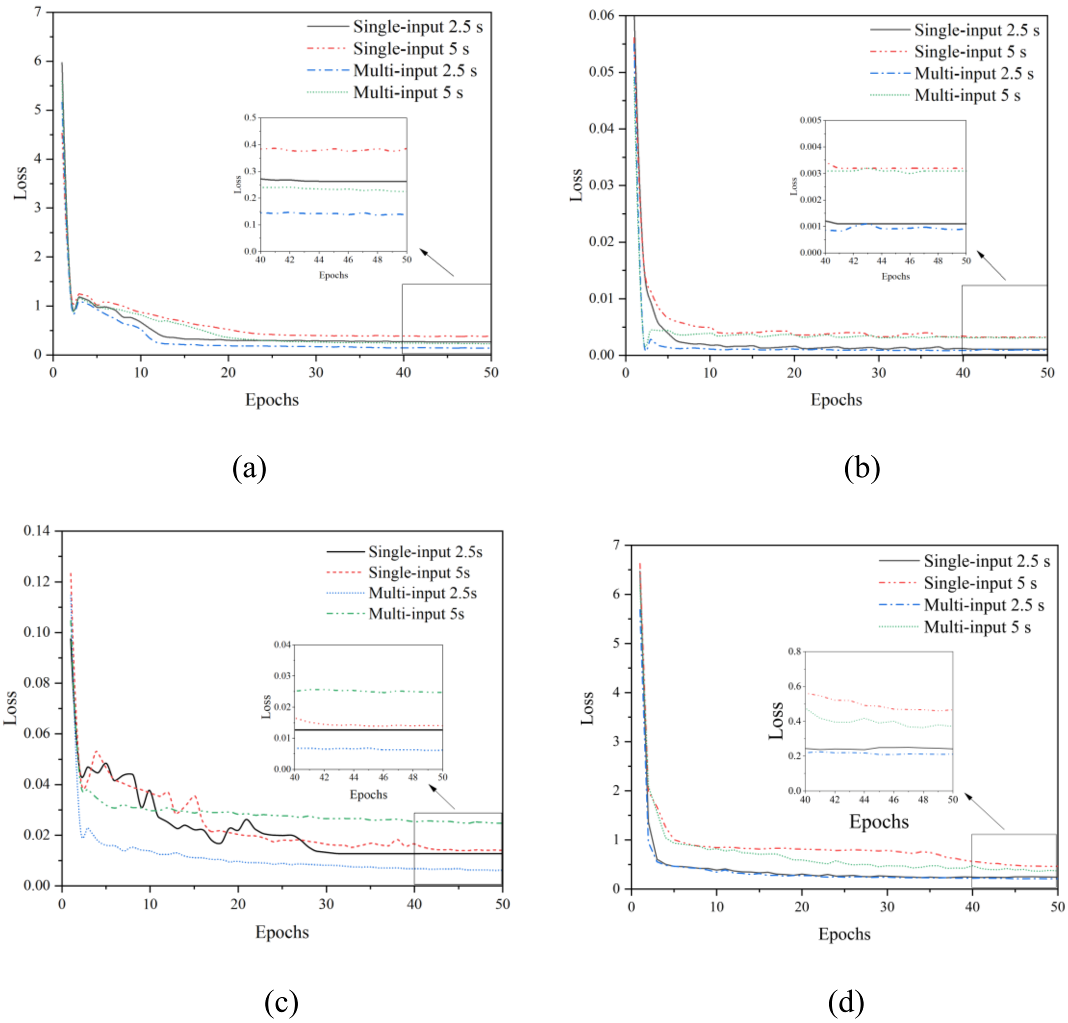

Figure 14. The curve of Loss affected by Epochs for different directions:

(a) Surge; (b) Sway; (c) Heave; (d) Pitch

At the same time, the Loss of the MI-LSTM model is found to be lower than that of the

SI-LSTM model both in 2.5 s and 5 s. It can be considered that the learning ability of the model is improved after additional factors are added to the training. The predicted results are shown in sections 4.2 and 4.3 and compared with simulation data. It is difficult to observe their overall discretization, so a scatter plot of the prediction results in different input modes is plotted in this section, as shown in **Figure 15.**

According to **Figure 15**, comparing the SI-LSTM model with the MI-LSTM model under the different cases, it can be found that after adding two additional input factors, the discrete situation of the MI-LSTM model prediction results is significantly smaller than that of the SI-LSTM model prediction results. This phenomenon is more evident in the sway and heave of EC1, surge and sway of EC2, and sway and heave of EC3. The use of the MI-LSTM model is beneficial in reducing the discrete nature of predicted results.

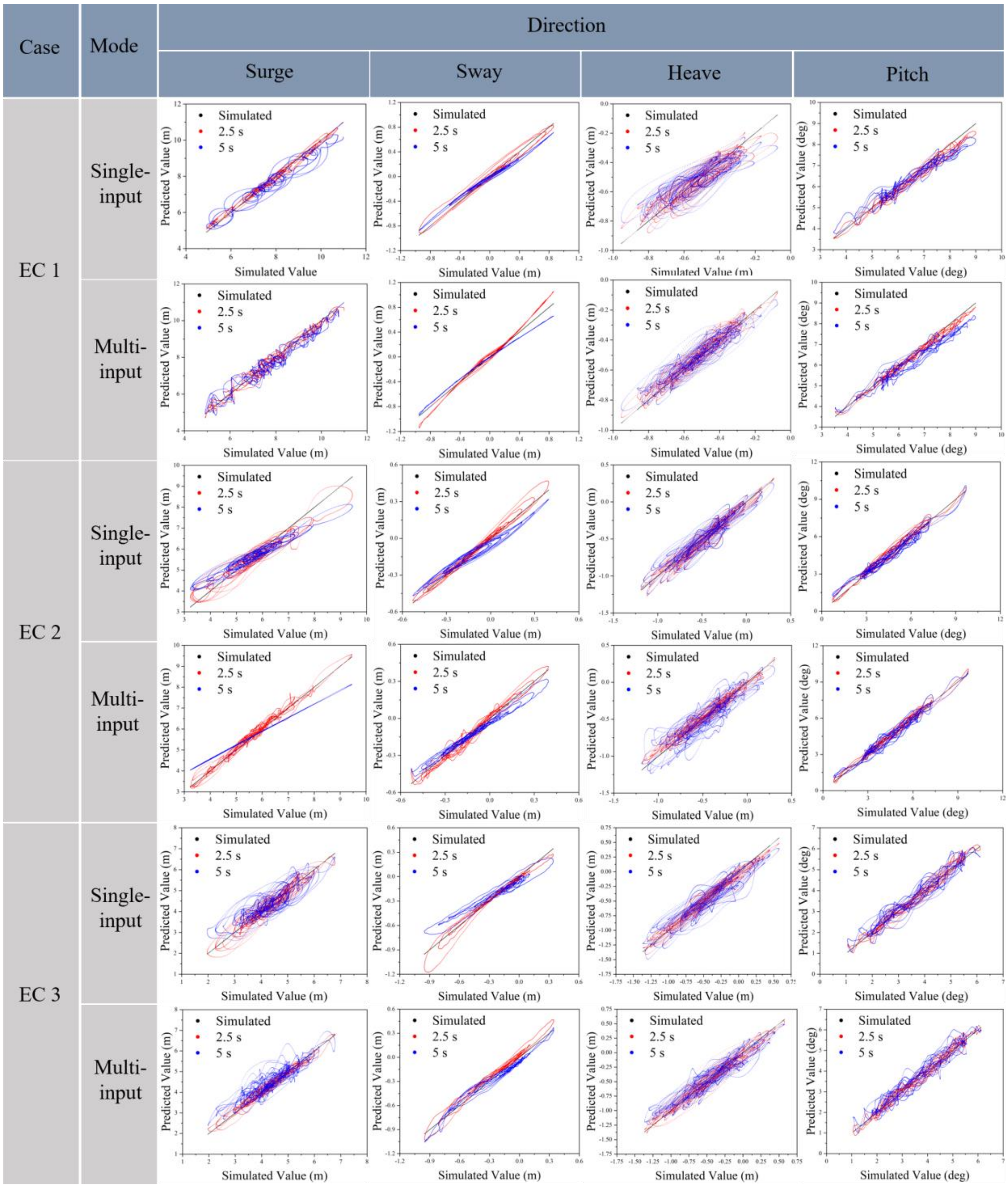

Figure 15. The discrete scatter plot of prediction results with two models

Comparing the prediction results of the SI-LSTM model with the MI-LSTM model on the same image, the comparison results for EC 1 are shown in **Figure 16**. From the figure, one can find that the prediction results of both SI-LSTM model and MI-LSTM model have high accuracy. For the surge motion, both models have the best results and have a good fit in both peak and trough positions as well. For the sway motion, the MI-LSTM model predicts a certain absolute value bias at the response extremes, while the SI-LSTM model predicts a certain absolute value bias at the response extremes. For the heave motion, since the SI-LSTM model does not take into account the effect of wave elevation, and the response in the heave direction happens to be most affected by the wave, the accuracy of the SI-LSTM model in this direction is not as good as that of the MI-LSTM model. For the pitch motion, the results of both models are similar to those of the surge direction, but the predicted values are smaller at the peak, which is more obvious in the SI-LSTM model.

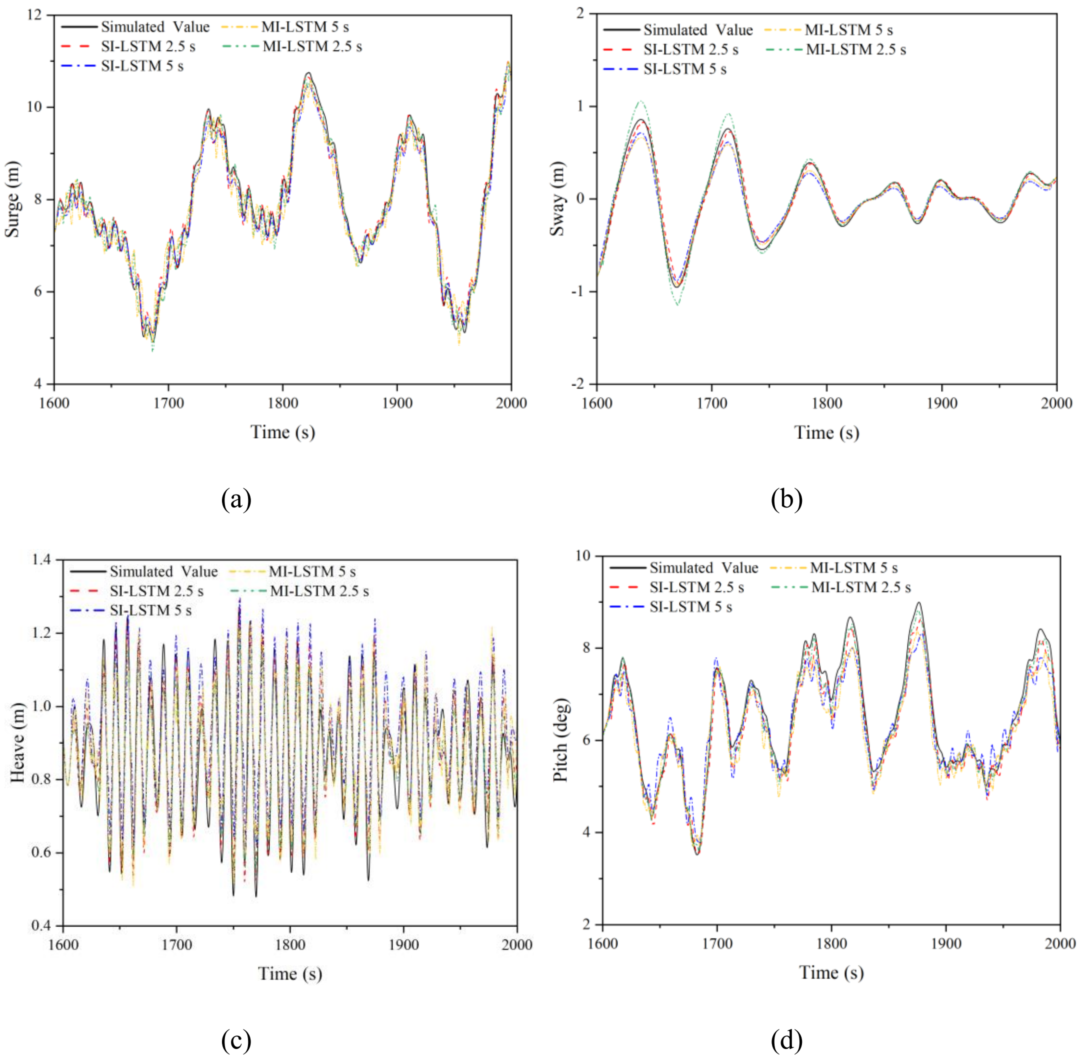

Figure 16. Comparison of 1st-order and 2nd-order hydrodynamic prediction results:

(a) Surge; (b) Sway; (c)Heave; (d) Pitch

In addition to the impact of discrete situations, the overall accuracy of the MI-LSTM model and the single-input model is also important. The individual statistics for predicting the final result of the FOWT motion response using both models are listed in Table 3. The overall accuracy of both models is presented in **Figure 17**.

Based on Table 3 and Figure 16, the results at PAT of 2.5 s present better agreements than at PAT of 5 s. After adopting the MI-LSTM model, the accuracy of the prediction results in pitch and heave has been significantly improved. With the increment of PAT, the period between input and output becomes larger, so the time correlation between the two decreases and the uncertainty increases. The upper limit of learning ability decreases as the correlation between input and output information decreases. Therefore, the accuracy at PAT of 5 s is lower than that of 2.5 s.

Mode	Statistics	EC 1				EC 2				EC 3			
		Heave	Pitch	Surge	Sway	Heave	Pitch	Surge	Sway	Heave	Pitch	Surge	Sway
Single-input 2.5 s	Max	73.2%	95.9%	99.9%	96.7%	96.2%	92.6%	95.3%	81.2%	84.3%	98.8%	97.8%	81.0%
	Min	92.3%	99.0%	96.2%	96.2%	93.4%	92.4%	93.0%	97.1%	96.8%	96.2%	92.4%	76.9%
	Average	99.7%	97.2%	99.8%	88.6%	95.6%	92.4%	98.5%	90.6%	96.9%	93.3%	96.5%	94.9%
	STD	87.5%	93.7%	94.3%	94.0%	97.7%	98.9%	83.7%	90.6%	96.0%	92.1%	93.5%	97.7%
	Overall	**88.2%**	**96.4%**	**97.6%**	**93.9%**	**95.7%**	**94.1%**	**92.6%**	**89.9%**	**93.5%**	**95.1%**	**95.0%**	**87.6%**
Multi-input 2.5 s	Max	73.2%	98.0%	97.6%	97.1%	97.4%	96.1%	96.8%	92.5%	95.8%	98.5%	99.4%	82.9%
	Min	96.0%	97.8%	95.8%	89.6%	93.3%	93.9%	98.2%	98.7%	98.3%	93.5%	96.6%	91.9%
	Average	97.5%	98.2%	99.4%	88.6%	96.0%	98.5%	98.9%	96.6%	99.2%	98.2%	99.0%	92.4%
	STD	97.3%	95.3%	96.8%	97.9%	97.8%	98.8%	95.6%	95.5%	96.6%	98.1%	94.9%	96.6%
	Overall	**91.0%**	**97.3%**	**97.4%**	**93.3%**	**96.1%**	**96.8%**	**97.4%**	**95.8%**	**97.5%**	**97.1%**	**97.5%**	**91.0%**
Single-input 5 s	Max	73.2%	92.5%	98.7%	83.2%	82.9%	95.9%	86.1%	81.1%	69.7%	88.9%	97.4%	67.9%
	Min	89.3%	93.0%	96.7%	92.2%	91.4%	80.1%	74.9%	94.4%	90.8%	89.5%	67.2%	74.3%
	Average	98.9%	97.7%	97.8%	75.0%	93.0%	89.0%	89.8%	91.7%	92.3%	93.5%	98.3%	92.9%
	STD	75.6%	81.5%	88.3%	82.6%	93.3%	89.8%	76.2%	78.7%	90.4%	87.3%	85.3%	70.2%
	Overall	**84.3%**	**91.2%**	**95.4%**	**83.3%**	**90.1%**	**88.7%**	**81.8%**	**86.5%**	**85.8%**	**89.8%**	**87.1%**	**76.3%**
Multi-input 5 s	Max	73.2%	93.3%	98.1%	76.8%	82.5%	98.2%	87.8%	80.8%	85.3%	89.1%	97.4%	82.1%
	Min	91.3%	95.1%	98.5%	98.4%	96.0%	76.5%	85.7%	94.4%	91.0%	94.3%	78.4%	89.0%
	Average	97.7%	95.5%	98.6%	83.7%	96.9%	89.8%	88.4%	91.9%	98.0%	97.5%	96.4%	89.3%
	STD	89.7%	86.2%	91.3%	85.3%	97.0%	98.0%	90.8%	81.0%	88.8%	91.6%	87.2%	93.2%
	Overall	**88.0%**	**92.5%**	**96.7%**	**86.1%**	**93.1%**	**90.6%**	**88.2%**	**87.0%**	**90.8%**	**93.1%**	**89.8%**	**88.4%**

Table 3. The accuracy of each statistic under the different input model

At the same time, the overall prediction result of the MI-LSTM model is better than the SI-LSTM model. The additional input factors increase the dimension of information, which enables the MI-LSTM model to explore more relationships between different input factors and the motion response of the target output. MI-LSTM model also adds more details to the final prediction results, improving the overall accuracy of the prediction results. In other words, there is a positive correlation between mooring force, wave elevation, and the motion response of the platform.

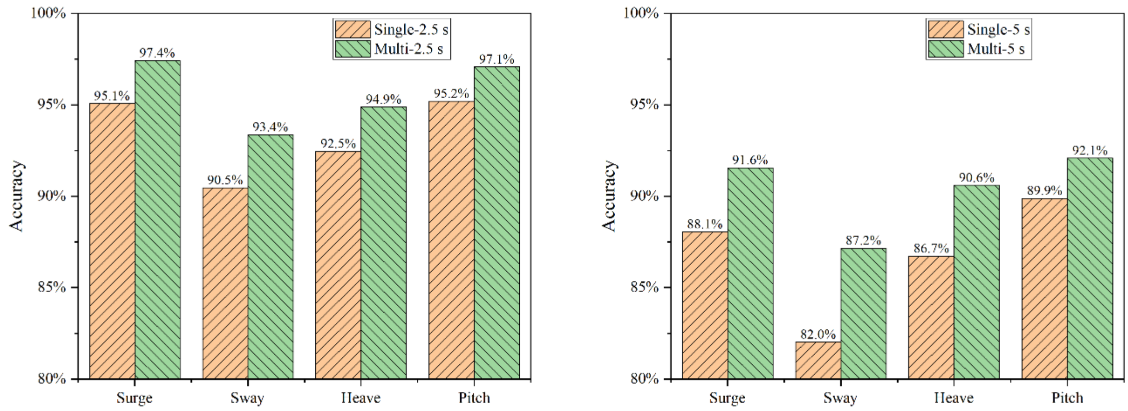

(a) (b)

Figure 17. Overall accuracy under different PATs: (a) 2.5 s; (b) 5 s

5. Second-order Hydrodynamic Effects

5.1 Prediction results under the influence of second-order hydrodynamic effects

The influence of second-order hydrodynamics is significant for the load prediction of a FOWT [34]. EC1-EC3 are again simulated considering second-order hydrodynamic effects, the simulation data is imported into the MI-LSTM model for training. The prediction results under the second-order hydrodynamic force are obtained after the training, shown in **Figures 18-20.**

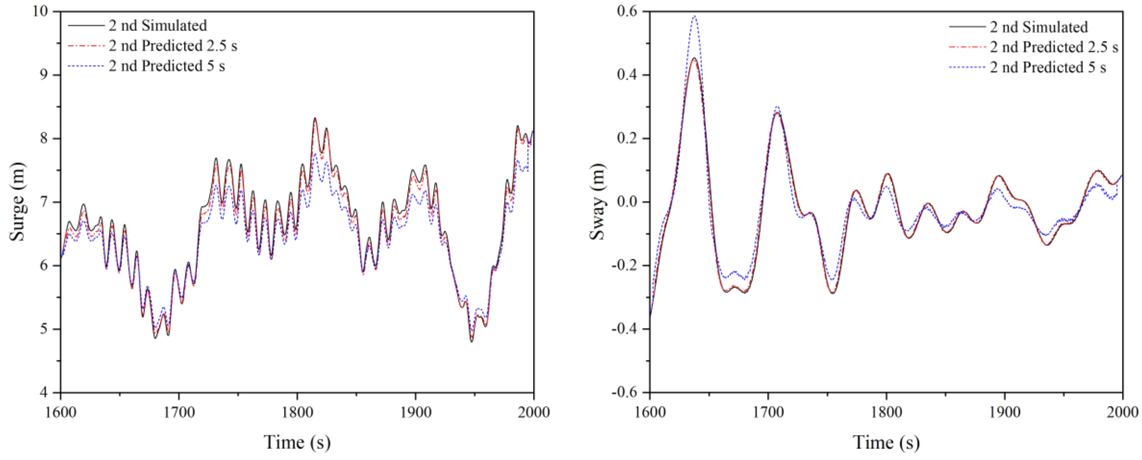

(a) (b)

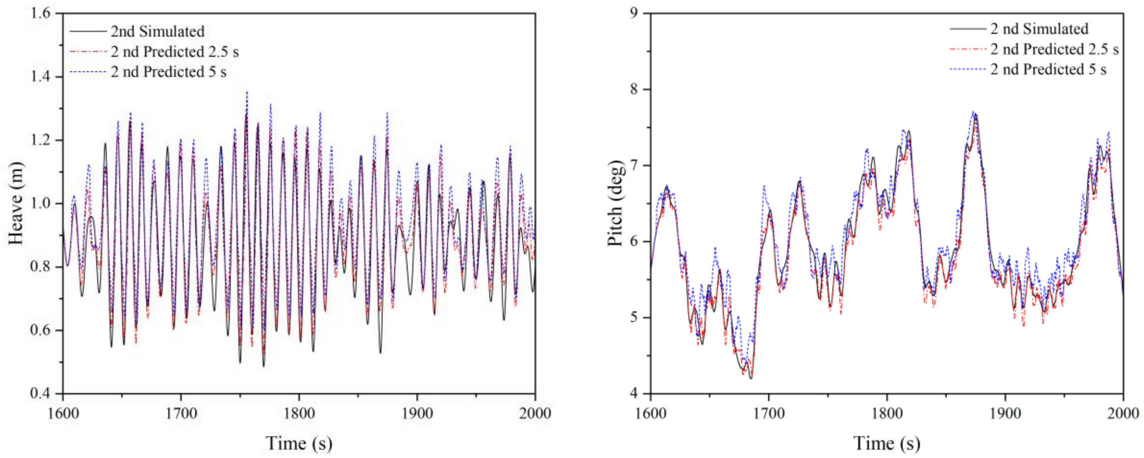

(c) (d)

Figure 18. Simulated and predicted values of EC 1 at 2.5 s and 5 s:

(a) Surge; (b) Sway; (c) Heave; (d) Pitch

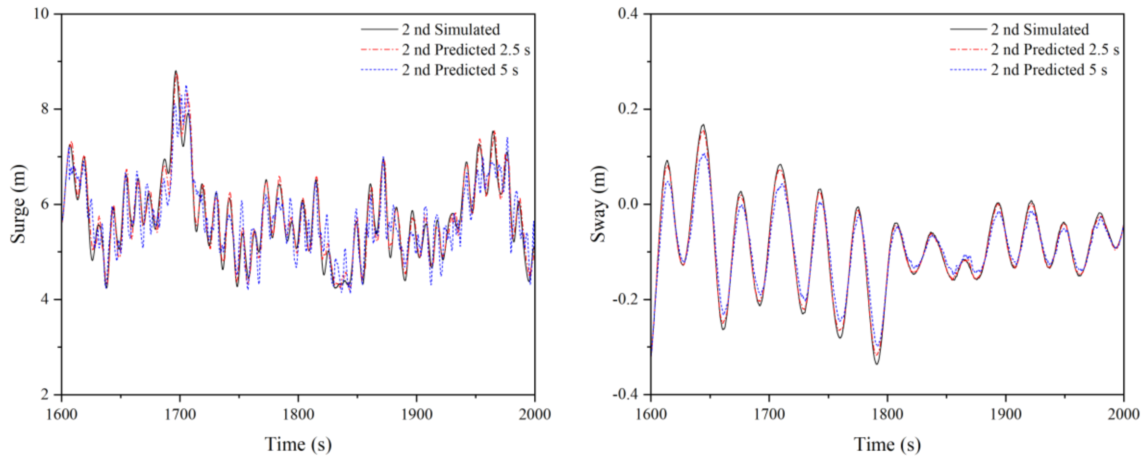

(a) (b)

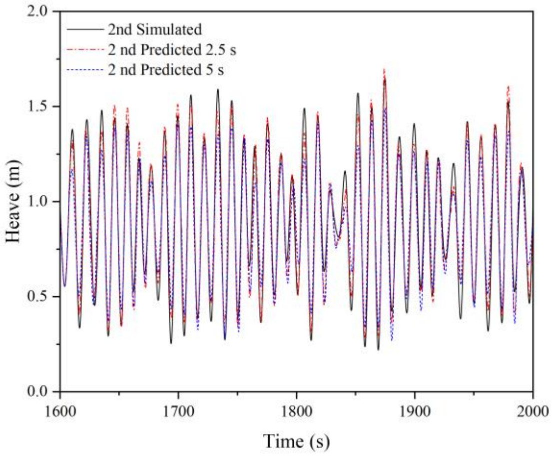

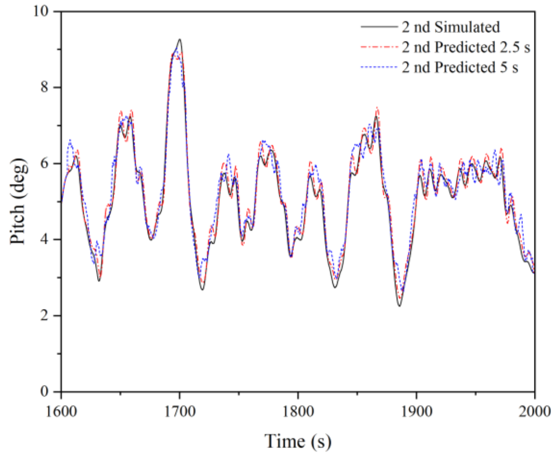

(c) (d)

Figure 19. Simulated and predicted values of EC 2 at 2.5 s and 5 s:

(a) Surge; (b) Sway; (c) Heave; (d) Pitch

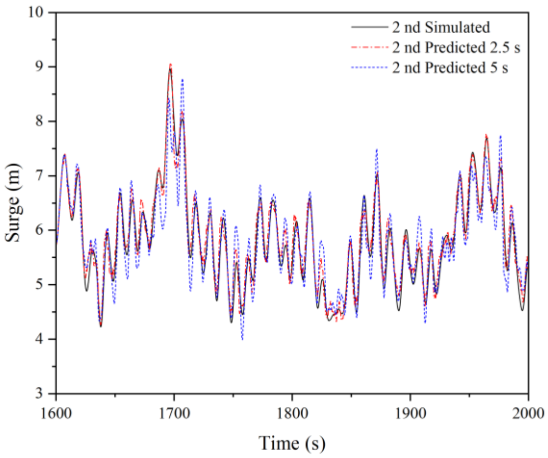

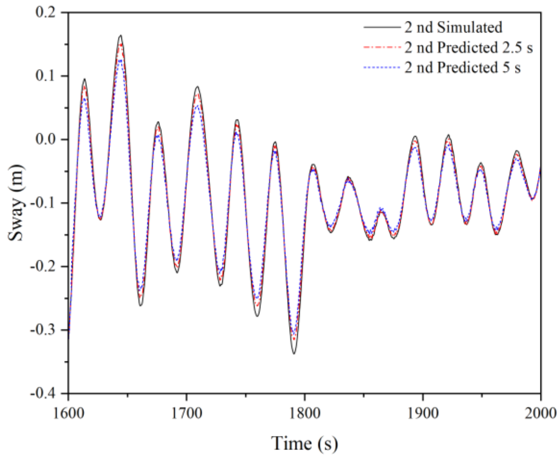

(a) (b)

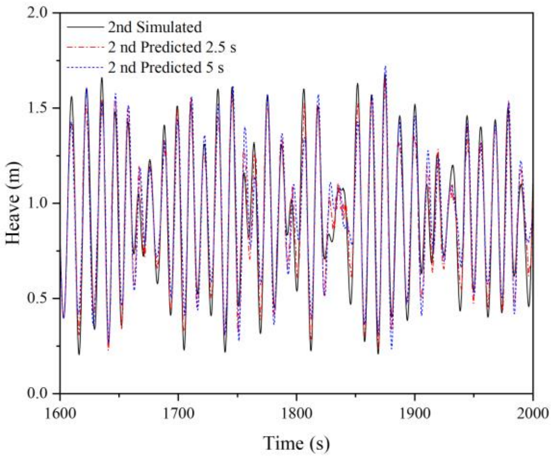

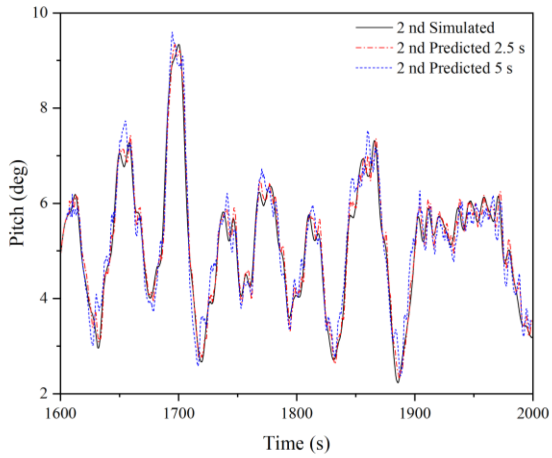

(c) (d)

Figure 20. Simulated and predicted values of EC 3 at 2.5 s and 5 s:

(a) Surge; (b) Sway; (c) Heave; (d) Pitch

Figures 18-20 show that the peak fitting in all directions at 5 s is weaker than that of 2.5 s, similar to the case when the platform model is affected by first-order hydrodynamic forces. Compared with the first-order hydrodynamic influence, the prediction results under the second-order hydrodynamics show smaller fluctuations in both surge and pitch. On the other hand, the predicted value of sway is smooth, and there is no slight fluctuation. The error of prediction results in heave mainly occurs in peaks and troughs, but it is not obvious. The statistical accuracy in each direction, as well as the overall accuracy, is further analyzed in section 5.2.

5.2. Error Analysis

To compare the short-term prediction effect of the MI-LSTM model in both first-order hydrodynamics and second-order hydrodynamics cases, the results of the PAT of 2.5 s under EC 1 are selected for comparison, shown in **Figure 21**.

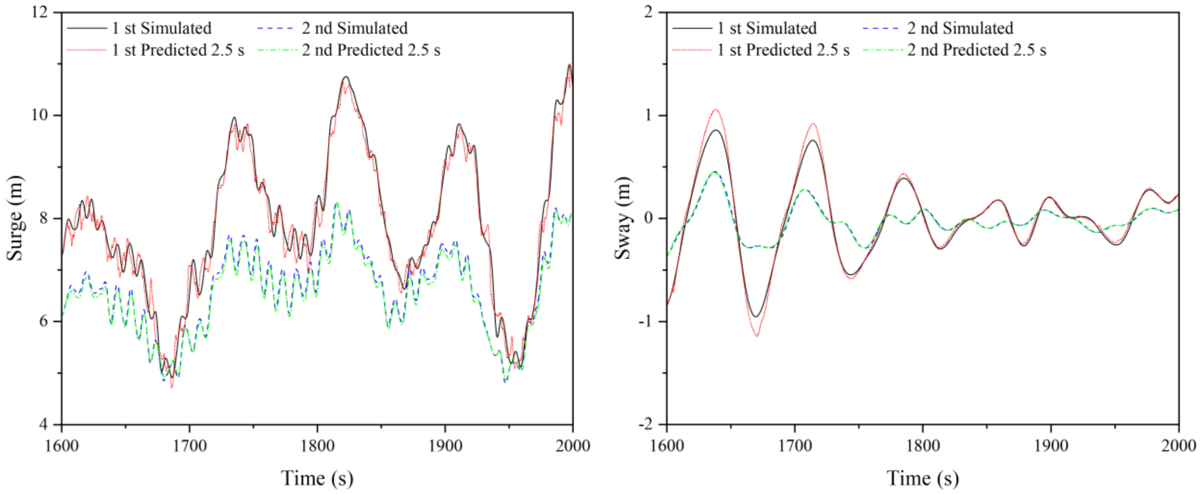

(a) (b)

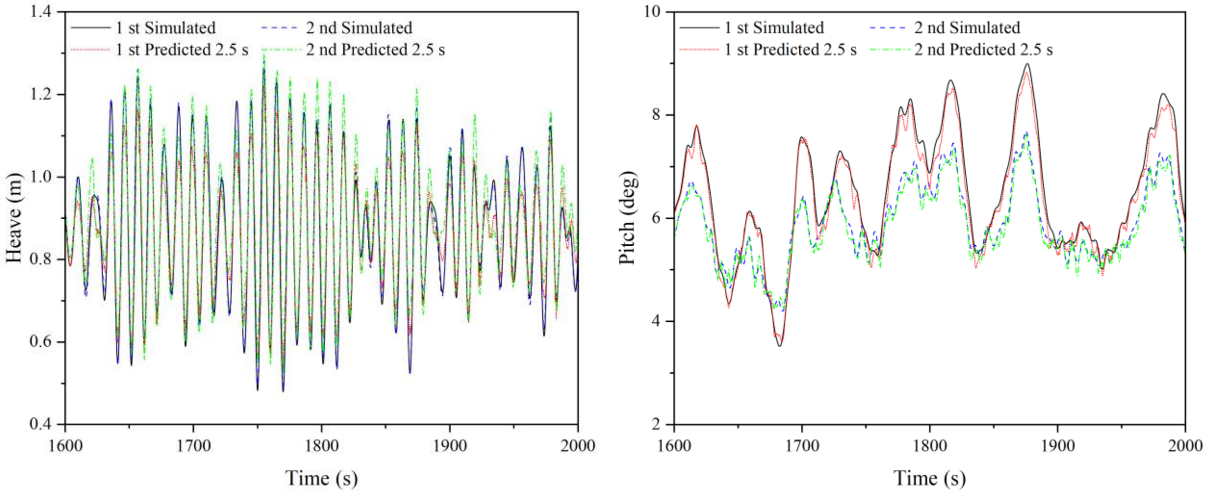

(c) (d)

Figure 21. Comparison of 1st-order and 2nd-order hydrodynamic prediction results: (a) Surge; (b) Sway; (c)Heave; (d) Pitch

According to **Figure 21**, it is observed that the motion response exhibits a stronger nonlinear characteristic under the influence of second-order hydrodynamic forces. This phenomenon is particularly evident in the surge, pitch, and sway directions, where more nonlinear fluctuations appear at the extremes of the kinematic response in all three directions. The effect of second-order hydrodynamic forces did not have much influence in the heave direction.

At the same time, in the surge, sway and pitch directions, there are significant deviations in the predicted values at the extremes of the motion response for the first-order hydrodynamics case. While in the second-order hydrodynamics case, the MI-LSTM model has better prediction at both peak and trough values. In the heave direction, the motion response of the platform in the two cases does not differ much and does not have the nonlinear characteristics in the other three directions. Therefore, the prediction effect of the MI-LSTM model in the heave direction under the influence of second-order hydrodynamics is not significantly improved.

The response spectrum analysis of the platform under the influence of second-order hydrodynamics are supplemented and chose EC 1 to plot the power spectrum density (PSD), as shown in **Figure 22**. There is a common phenomenon in all four directions, the predicted value of 2.5s is better than 5s in the performance of PSD, and both of them fit better with the PSD results of simulation values. The difference between the predicted and simulated values is mainly in the low-frequency peak of the response spectrum, while the PSD performance of the model predictions is better at the off-peak.

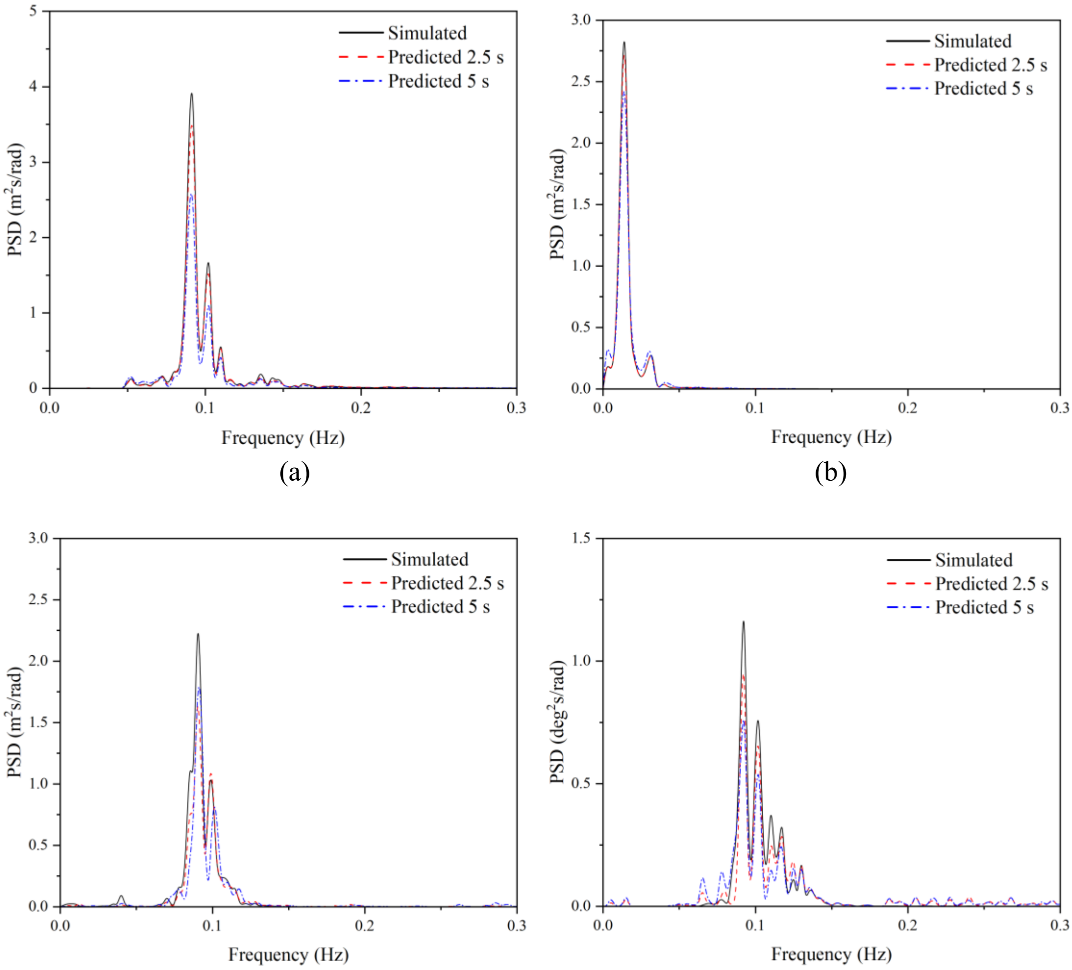

(a) (b) (c) (d)

Figure 22. Power spectral density of motion response in different directions

(a) Surge; (b) Sway; (c)Heave; (d) Pitch

Under the influence of second-order hydrodynamics, this section also analyzes the individual statistics of the prediction results and calculates the overall accuracy of each direction of motion response, shown in **Table 4**.

Table 4. The accuracy of each statistic under the influence of second-order hydrodynamics

Mode	Statistics	EC 1				EC 2				EC 3			
		Heave	Pitch	Surge	Sway	Heave	Pitch	Surge	Sway	Heave	Pitch	Surge	Sway
Multi-input 2.5 s	Max	96.5%	99.4%	99.6%	98.7%	92.6%	96.3%	99.5%	92.2%	98.0%	98.9%	98.8%	91.8%
	Min	88.5%	99.2%	98.5%	99.1%	90.9%	90.7%	99.2%	97.0%	90.2%	96.2%	99.1%	94.9%
	Average	98.8%	98.8%	98.9%	96.5%	98.0%	97.6%	99.7%	99.0%	99.9%	99.0%	98.9%	99.2%
	STD	89.9%	96.2%	96.1%	98.6%	95.8%	96.5%	99.6%	94.6%	98.6%	99.2%	96.7%	92.8%
	Overall	**93.4%**	**98.4%**	**98.3%**	**98.2%**	**94.3%**	**95.3%**	**99.5%**	**95.7%**	**96.7%**	**98.3%**	**98.4%**	**94.7%**
Multi-input 5 s	Max	87.0%	99.5%	97.6%	71.0%	97.1%	97.5%	96.6%	63.4%	94.2%	97.2%	97.8%	77.1%
	Min	94.3%	95.5%	96.5%	97.5%	89.5%	82.5%	97.4%	97.0%	94.3%	93.4%	94.4%	94.9%
	Average	98.6%	98.1%	97.3%	80.7%	94.6%	96.5%	99.3%	98.2%	94.5%	98.8%	99.6%	99.0%
	STD	87.9%	92.3%	91.4%	98.1%	93.1%	92.5%	90.9%	80.4%	92.6%	98.0%	91.3%	84.1%
	Overall	**92.0%**	**96.3%**	**95.7%**	**86.8%**	**93.6%**	**92.3%**	**96.0%**	**84.8%**	**93.9%**	**96.9%**	**95.8%**	**88.8%**

According to the results given in **Table 4**, it can be seen that the accuracy of the predicted results in all directions under the influence of second-order hydrodynamics is still at a high level, overall accuracy exceeds 90% at PAT of 2.5 s and 85% at PAT of 5 s. This phenomenon verifies the conclusions of Section 4 and confirms that an increase in PAT leads to a decrease in prediction accuracy.

The overall accuracy of the 4 degrees of freedom directions calculated from **Table 4** is shown in **Figure 23**. At PAT of 2.5 s, the difference in prediction accuracy between the second-order hydrodynamics and the first-order hydrodynamics is more obvious in surge and sway. At PAT of 5 s, in the direction of surge, heave, and pitch, the prediction accuracy in the second-order hydrodynamics case is about 3% higher than that in the first-order hydrodynamics.

By comparing with the results in the first-order hydrodynamics in Section 4, it can be found that the MI-LSTM model in the second-order hydrodynamics case not only has a good ability to learn multi-factor relationships and platform response prediction but also has a higher prediction accuracy than the first-order hydrodynamics case.

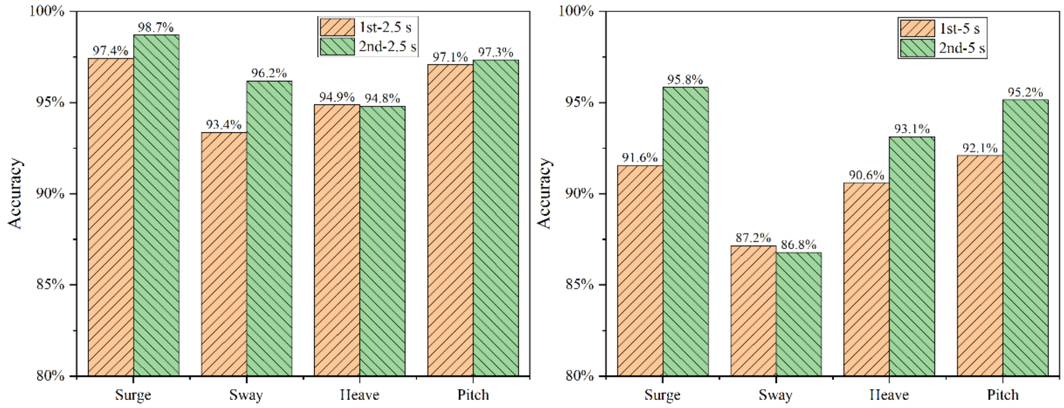

(a) (b)

Figure 23. Overall accuracy under different PATs: (a) 2.5 s; (b) 5 s

6. Comparison with the MI1D-CNN model

6.1 Predicted results with MI1D-CNN model

Currently, the mainstream deep learning methods mainly include the CNN method and the RNN method, and the MI-LSTM model established in Section 4 belongs to the RNN method. CNN methods are mostly used in image recognition and text recognition. As a representative method to deal with time series problems in CNN, a one-dimensional convolutional neural network (1D-CNN) has a certain effect on short-term prediction by adding a pooling layer.

In this section, a multi-input one-dimensional convolutional neural network (MI1D-CNN) is built to compare the CNN method with the LSTM method for the motion response prediction problem, using the same training data as in Section 4. The training of the MI1D-CNN model is completed, and the results obtained from the multi-input LSTM model are compared in Section 6.2 in terms of training time and overall accuracy. The prediction results obtained by the MI1D-CNN model are shown in **Figures 24-26**.

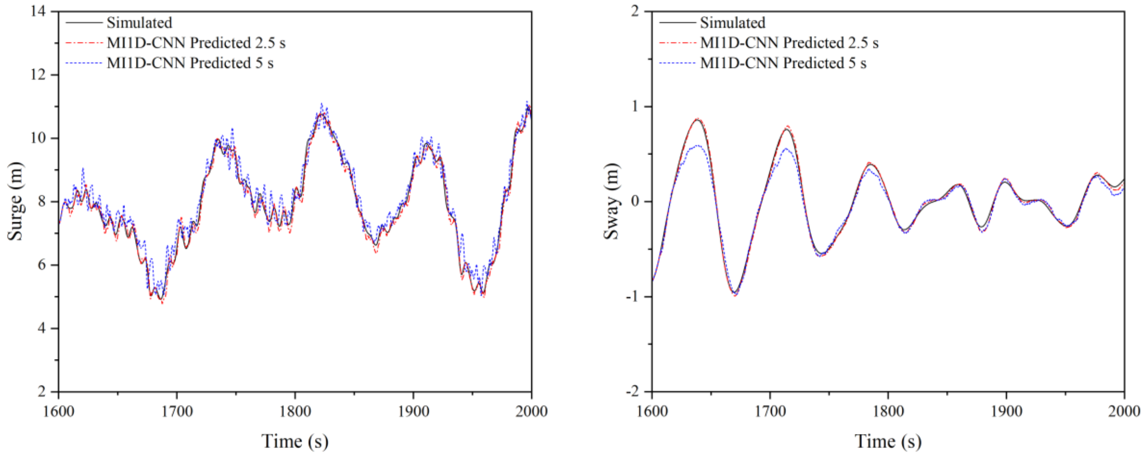

(a) (b)

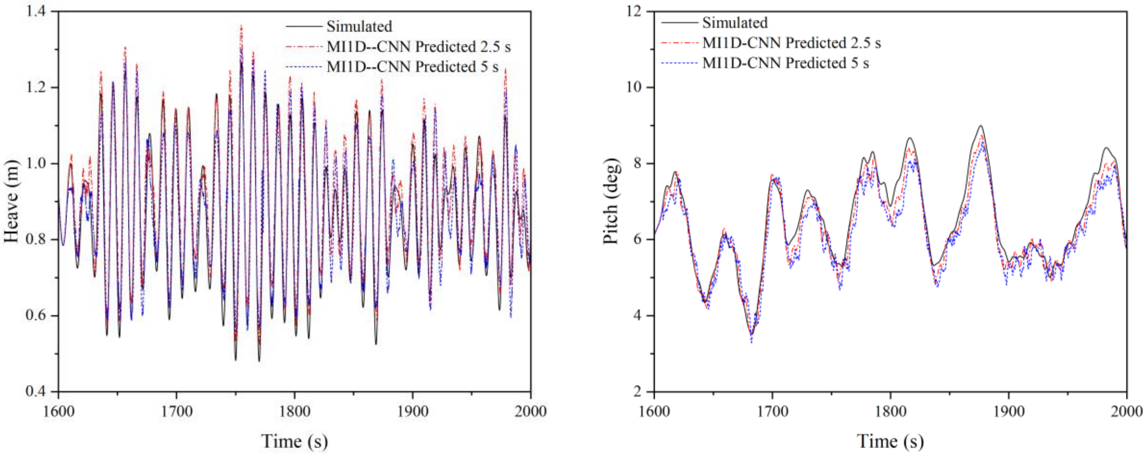

(c) (d)

Figure 24. Simulated and predicted values of EC 1 at 2.5 s and 5 s:

(a) Surge; (b) Sway; (c) Heave; (d) Pitch

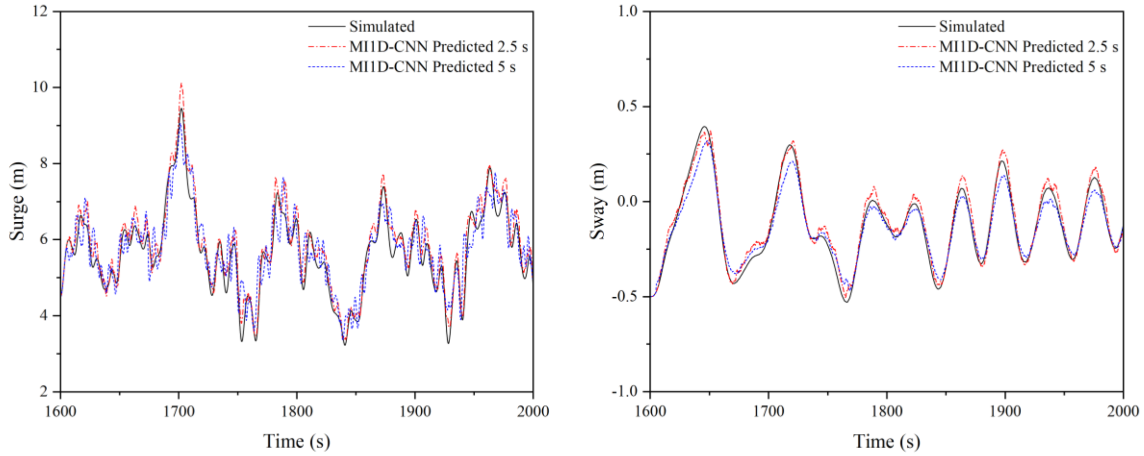

(a) (b)

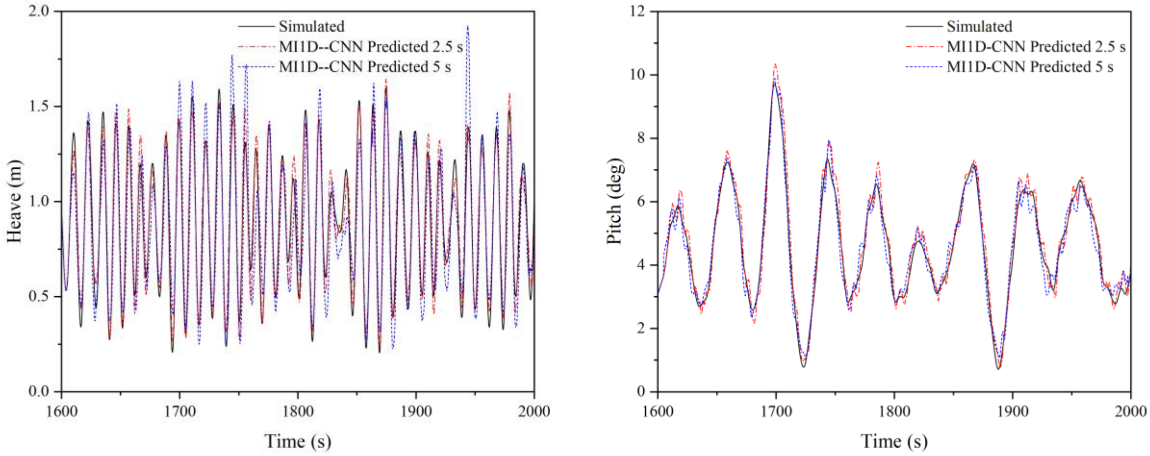

(c) (d)

Figure 25. Simulated and predicted values of EC 2 at 2.5 s and 5 s:

(a) Surge; (b) Sway; (c) Heave; (d) Pitch

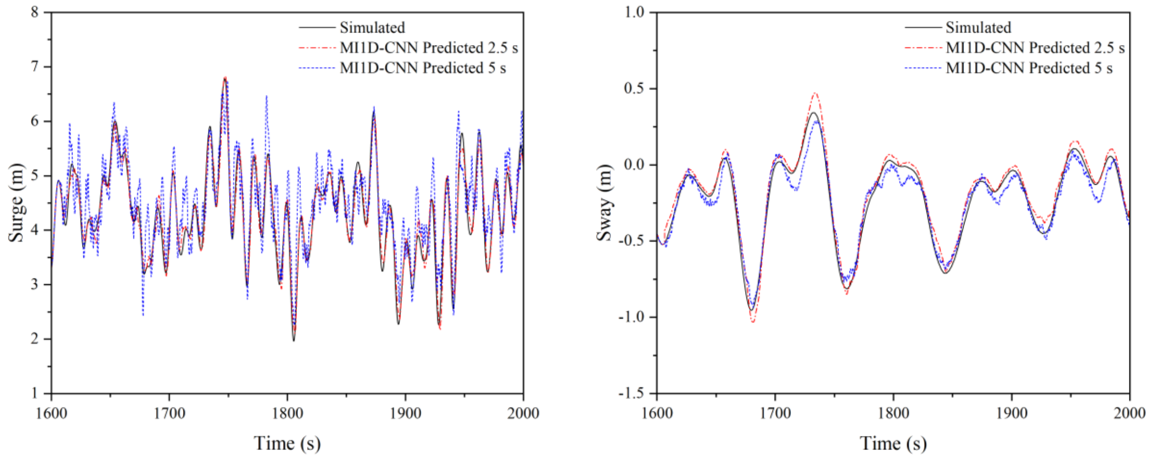

(a) (b)

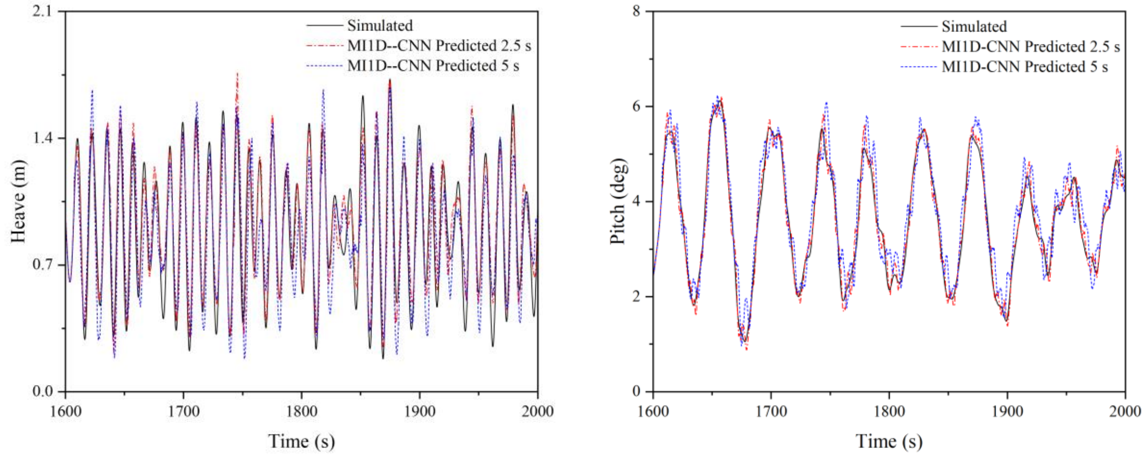

(c) (d)

Figure 26. Simulated and predicted values of EC 3 at 2.5 s and 5 s:

(a) Surge; (b) Sway; (c) Heave; (d) Pitch

According to **Figures 24-26**, and compared with **Figures 11-13** in Section 4.3, it can be found that the motion response predicted by the MI1D-CNN model produces a large number of serrations in surge and pitch of each environmental condition, especially at PAT of 2.5 s. At the same time, the prediction result at PAT of 5 s in sway does not fit well with the simulation results. To further compare the results of the MI-LSTM model with the MI1D-CNN model, it is further explained from the aspects of training time and overall accuracy in Section 6.2.

6.2 Comparison with Multi-input LSTM Model

By counting the Loss values during the training of the MI1D-CNN model, we show the decrease of the model training Loss for EC 1, shown in **Figure 27**. One can observe that, unlike the change process of the MI-LSTM model's Loss value, the oscillation phase of the MI1D-CNN model's Loss value is not obvious in the decreasing process. the MI1D-CNN model's Loss value stops changing when the number of training rounds reaches 50 rounds, which indicates that the model training has been completed and the performance is satisfactory. To further observe the imitative effect between the predicted values obtained by the two models and the simulated values, EC1 is selected and the results are summarized as shown in **Figure 28**.

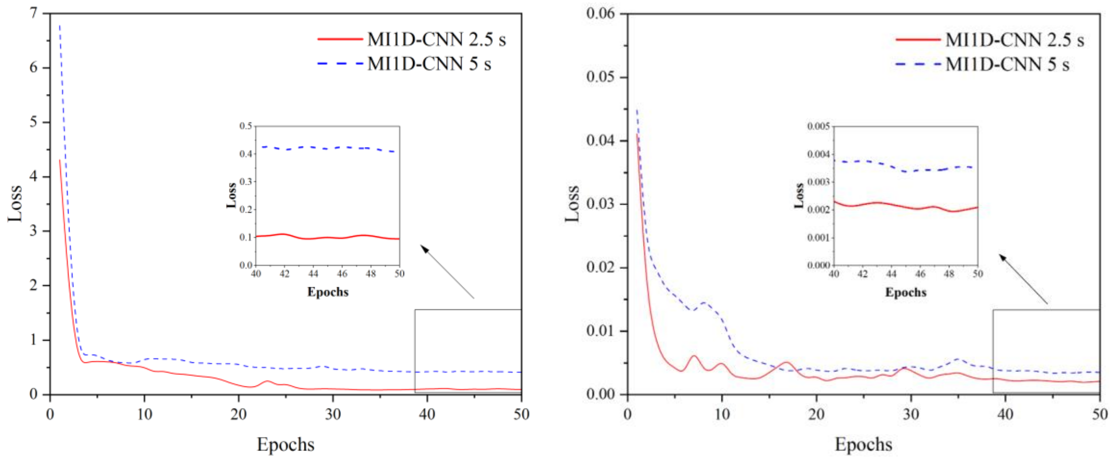

(a) (b)

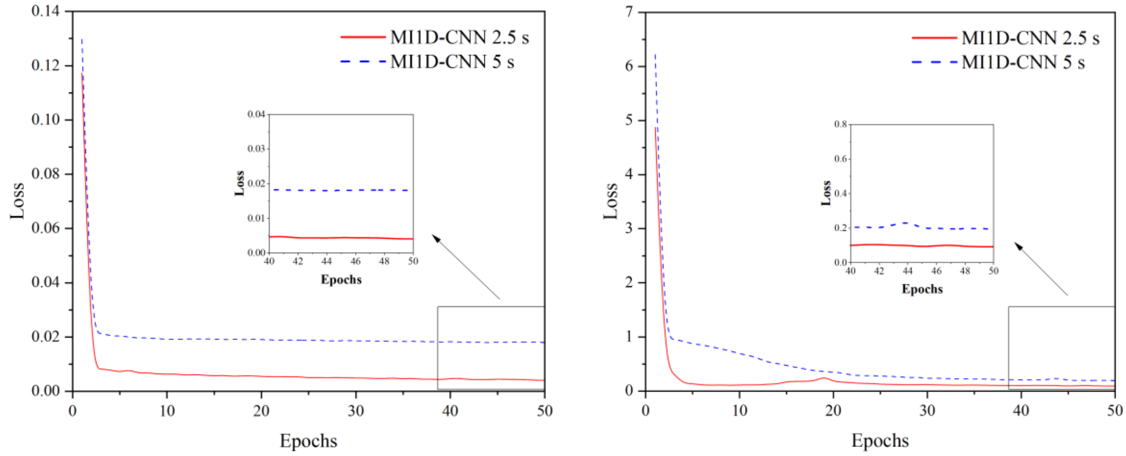

(c) (d)

Figure 27. The curve of Loss affected by Epochs for different directions:

(a) Surge; (b) Sway; (c) Heave; (d) Pitch

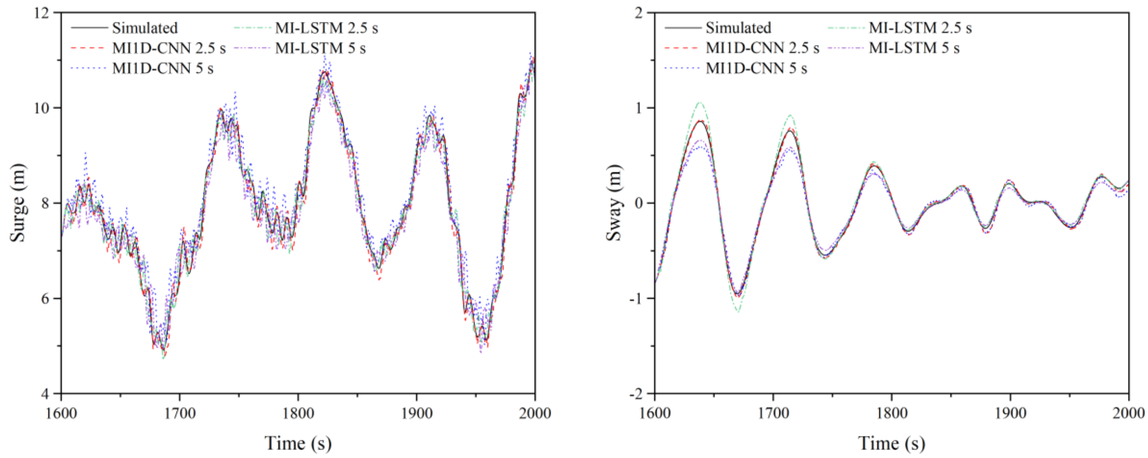

(a) (b)

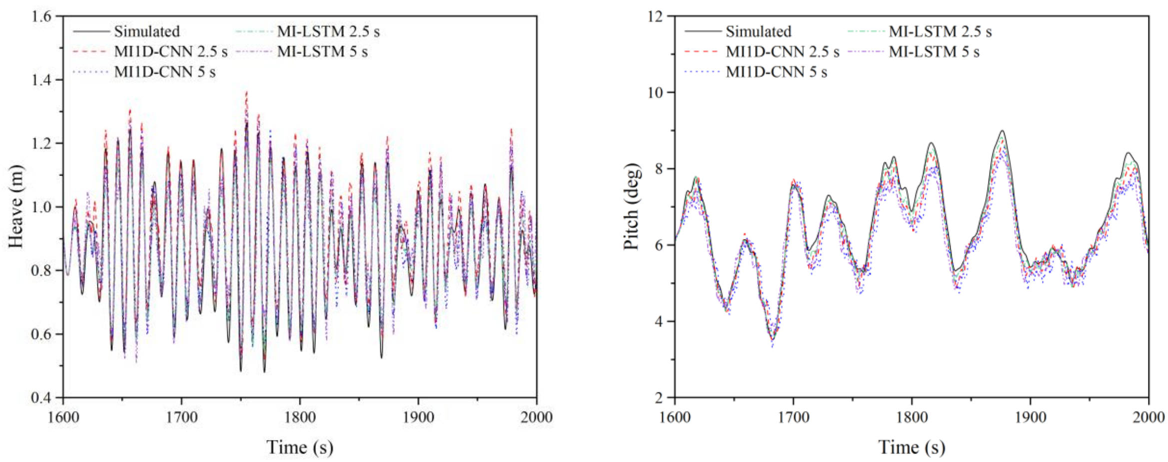

(c) (d)

Figure 28. The results of the MI1D-CNN model and the MI-LSTM model are compared: (a) Surge; (b) Sway; (c) Heave; (d) Pitch

According to **Figure 28**, from the overall imitative effect of the time series curve, the prediction results of both models fit well with the simulation results at PAT of 2.5 s. However, at PAT of 5 s, the result of the MI1D-CNN model is slightly inferior to the MI-LSTM model result, and when the PAT is at 5 s, the predicted value of the former has a large fluctuation. This volatility does not exist in the simulation value, particularly in **Figures 28(a**) and **(d)**. The time series of the platform response has a certain smoothness in sway, so both models' imitative effects are good. While the time series of the platform response itself is more volatile in heave, the imitative effects of the peak are not as good as in other directions.

To find out the difference between the MI1D-CNN model and the MI-LSTM model, the overall accuracy of the MI1D-CNN model is calculated by combining each operating condition. Then compare the overall accuracy of the MI1D-CNN model with the MI-LSTM model proposed in Section 4 and the result is shown in **Figure 29**.

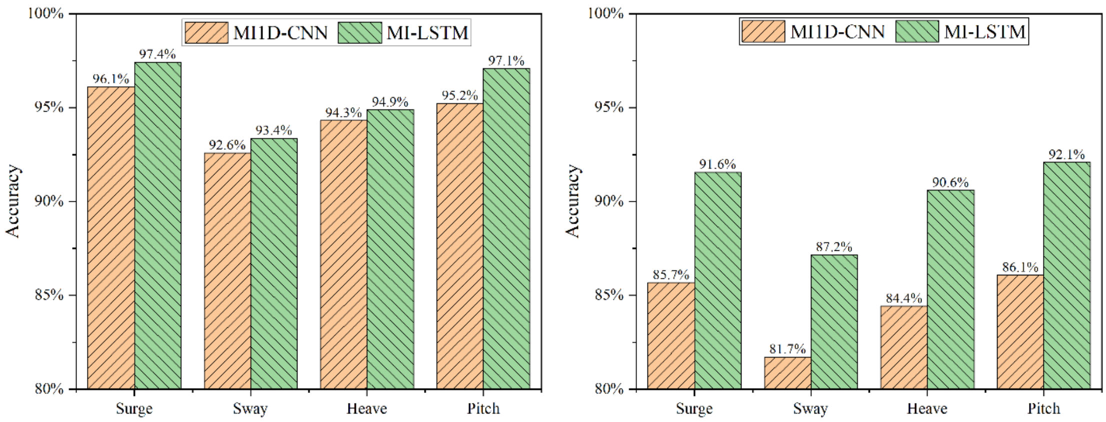

(a) (b)

Figure 29. Comparison of the overall accuracy of different models in each direction: (a) 2.5 s; (b) 5s

According to **Figure 29**, it can be found that there is no significant difference between the results of the two models when PAT is at 2.5 s, the overall effect of the MI-LSTM model is slightly better than the MI1D-CNN model, and the accuracy of the former is 1%-2% higher than the latter in all directions. But at PAT of 5 s, the situation is very different, the MI-LSTM model performs much better than the MI1D-CNN model, and the accuracy of the former is about 5% higher than the latter in all directions.

It can be seen that when the corresponding period of the prediction platform becomes longer, the traditional CNN model is not satisfactory, while the MI-LSTM model proposed in this paper performs well. Since 1D-CNN only performs convolution operations on time series information within the length of a convolution, heritability in time series information is only reflected in a single convolutional neuron. Therefore, when PAT is small, the effect on the MI1D-CNN model and the MI-LSTM model is insignificant. However, with the increase of PAT, the disadvantage of the MI1D-CNN model in processing temporal genetic information will become significant.

In addition, the training time of the two models is also recorded, as shown in **Table 5**. According to **Table 5**, the training time of the MI1D-CNN model is much shorter than that of the MI-LSTM model, which is related to the learning and calculation method of the model itself. The training time of the MI1D-CNN model is short, but it sacrifices a part of the accuracy, and the training time of the MI-LSTM model is relatively long, but the accuracy is greatly improved.

Table 5. Statistics on the training duration of the two models

Modes	PAT (s)	Epochs	Time (s)
MI-LSTM	2.5	50	912
	5	50	1053
MI1D-CNN	2.5	50	108
	5	50	157

In summary, balancing training time and accuracy has always been an important issue in deep learning. If the goal is ultra-short-term forecasting of the FOWT motion response and the accuracy requirement is relatively low, the MI1D-CNN model can be chosen. However, to increase the time span of motion response forecasting and maintain prediction accuracy, the MI-LSTM model is a better choice.

7. Conclusion

Based on the motion response data of the Braceless platform, the MI-LSTM prediction model is established by the RNN deep learning method and is trained for different degrees of freedom under different environmental conditions. The accuracy of prediction results under different PAT and input methods are determined and compared using statistics. Based on the analysis and discussions, the conclusion can be made as follows:

(1)Taking the previous data of platform motion response, mooring force, and wave elevation as input, after 50 rounds of training with two LSTM models, the Loss no longer decreases, resulting in accurate prediction results. The Loss of the MI-LSTM model is slightly better than the SI-LSTM model. The MI-LSTM model more comprehensively learns the relationship between multiple factors and the target output.

(2)Based on the established and trained LSTM neural network model, the prediction results of the model fit well with the simulated value. The prediction accuracy with PAT at 2.5 s is slightly higher than the accuracy with PAT at 5 s and the overall performance of the MI-LSTM model is better than the SI-LSTM model. The additional two factors can positively improve the accuracy of the final prediction result.

(3) The established MI-LSTM model is applied to the situation where the platform is affected by second-order hydrodynamics, and it is found that the model has a better predictive effect on the response of the Braceless platform affected by second-order hydrodynamics. The MI-LSTM model has a better performance for the case where the nonlinearity phenomenon is more pronounced.

(4) The MI-LSTM model established in this paper is compared with the traditional MI1D-

CNN model, and the advantages and disadvantages of the two models are clarified from the aspects of training time and overall accuracy. When the PAT is small, the difference between the results of the two models is not significant, while when the PAT increases, the results obtained by the MI-LSTM model are better than those obtained by the MI1D-CNN model.

Acknowledgment

This research is funded by the National Natural Science Foundation of China (Grant No. 52071058, 51939002). This paper is also partially funded by the Central Guidance on Local Science and Technology Development Fund of Shenzhen (2021Szvup018) and the Open Research Fund of Hunan Provincial Key Laboratory of Key Technology on Hydropower Development (PKLHD202003). The last author is now supported by the National Natural Science Foundation of China (Grant No. 52201379).

Reference

[1] Gao W, Li C, Ye Z. The current situation and latest research of deep-sea floating wind turbine. Engineering Sciences 2014; 16(2): 79-87.

[2] Ren, ZR, Zhou HY, Li BB, Hu ZZ, Yu MH, Shi W. Localization and topological observability analysis of a moored floating structure using mooring line tension measurements, Ocean Engineering 2022; 266P5: 112706. https://doi.org/10.1016/j.energy.2022. 112706

[3] Liu Y, Hu C, Sueyoshi M, Yoshida S, Iwashita H, Kashiwagi M. Motion response characteristics of a Kyushu-University semi-submersible floating wind turbine with trussed slender structures: Experiment vs. numerical simulation. Ocean Engineering 2021; 232: 109078. https://doi.org/10.1016/j.oceaneng.2021.109078

[4] Zeng YX, Shi W, Michailides C, Ren ZR, Li X. Turbulence model effects on the hydrodynamic response of an oscillating water column (OWC) with use of a computational fluid dynamics model. Energy 2022; 261:124926. https://doi.org/10.1016/j.energy.2022.124926

[5] Zhang LX, Shi W, Zeng YX, Michailides C, Zheng SM, Li Y. Experimental Investigation on the hydrodynamic effects of Heave Plates for application of floating offshore wind turbine. Ocean Engineering 2023; 267C:113103. https://doi.org/10.1016/j.oceaneng.2022.113103

[6] Shi W, Zhang L, Karimirad M, Michailides C, Jiang Z, Li X. Combined effects of aerodynamic and second-order hydrodynamic loads for three semisubmersible floating

wind turbines in different water depths. Applied Ocean Research 2023; 130: 103416 https://doi.org/10.1016/j.apor.2022.103416

[7] Zhang Y, Shi W, Li DS, Li X, Duan YF, Verma, AS. A novel framework for modeling floating offshore wind turbines based on the vector form intrinsic finite element (VFIFE) method. Ocean Engineering 2022; 262:112221. https://doi.org/10.1016/j.oceaneng.2022.112221

[8] Shi W, Zeng XM, Feng XY, Shao YL, Li X. Numerical study of higher-harmonic wave loads and runup on monopiles with and without ice-breaking cones based on a phase-inversion method. Ocean Engineering 2023; 267: 113221.

[9] Zeng XM, Shi W, Feng XY, Shao YL, Li X. Investigation of higher-harmonic wave loads and low-frequency resonance response of floating offshore wind turbine under extreme wave groups. Marine Structures 2023; 89:103401.

[10] Stetco A, Dinmohammadi F, Zhao X, Robu V, Flynn D, Barnes, M. Machine learning methods for wind turbine condition monitoring: a review. Renewable Energy 2019; 133: 620-635. https://doi.org/10.1016/j.renene.2018.10.047.

[11] Huang LF. Research On Online Prediction of Nonstationary Nonlinear Ship Motion in Ocean Waves. Harbin Engineering University, 2016.

[12] Li HB, Xiao LF, Wei HD. Research on Online Prediction of Floating Offshore Platform Motions based on LSTM Network. Journal of Ship Mechanics 2021; 25:576-585. https://doi.org/10.3969/j.issn.1007-7294.2021.05.006.

[13] Bahdanau D, Cho K, Bengio Y. Neural machine translation by jointly learning to align and translate. Computer Science 2014; 1: 1409.0473.

https://doi.org/10.48550/arXiv.1409.0473.

[14] Wang ZM, Qiao DS, Yan J, Tang GQ. A new approach to predict dynamic mooring tension using LSTM neural network based on responses of floating structure. Ocean Engineering 2022;249: 110905. https://doi.org/10.1016/j.oceaneng.2022.110905

[15] Khan A, Bil C, Marion KE. Ship motion prediction for launch and recovery of air vehicles. Oceans 2005:1640198. https://doi.org/10.1109/OCEANS.2005.1640198.

[16] Gu M, Liu CD, Zhang JF. Extreme short-term prediction of ship motion based on chaotic theory and RBF neural network. Journal of Ship Mechanics 2013; 17(10): 1147-1152. https://doi.org/10.3969/j.issn.1007-7294.2013.10.007.

[17] Liu Y, Duan W, Huang L, Duan S. The input vector space optimization for LSTM deep learning model in real-time prediction of ship motions. Ocean Engineering 2020; 213: 107681. https://doi.org/10.1016/j.oceaneng.2020.107681.

[18] Pena B, Huang L. Wave-GAN: A deep learning approach for the prediction of nonlinear regular wave loads and run-up on a fixed cylinder. Coastal Engineering (Amsterdam) 2021; 167: 103902. https://doi.org/10.1016/j.coastaleng.2021.103902.

[19] Lian LK, Zhao YP, Bi CW, Xu ZJ, Du H. Research on Damage Detection Method of Flat Fishing Net Based on Digital Twin Technology. Fishery Sciences 2022; 43: 19663. https://doi.org/10.19663/ j. issn.2095-9869.20210825001.

[20] Bjørni F, Lien S, Midtgarden T, Kulia G. Prediction of dynamic mooring responses of a floating wind turbine using an artificial neural network. IOP Conference Series. Materials Science and Engineering 2021; 1201(1): 12023. https://doi.org/10.1088/1757-899X/1201/1/012023.

[21] Zhang F, Guo Z, Sun, X. Short-term wind power prediction based on EMD-LSTM combined model. IOP Conference Series: Earth and Environmental Science 2020; 514(4): 042003. https://doi.org/10.1088/1755-1315/514/4/042003.

[22] Sutskever I, Vinyals O, Le Quoc V. Sequence to sequence learning with neural networks. Advances in neural information processing systems 2014; 27.

[23] Cho K, Van Merriënboer B, Gulcehre C. Learning phrase representations using RNN encoder-decoder for statistical machine translation. Computer Science 2014;1406.1078. https://arxiv.org/abs/1406.1078

[24] Vinyals O, Le Q. A Neural Conversational Model. Computer Science 2015; 1506.05869. https://arxiv.org/abs/1506.05869

[25] Liu Y, Li D. Research on User Gender Prediction of Chinese Microblog Based on Short Text Analysis. IEEE 2018: 775-779. https://doi.org/10.1109/ICIVC.2018.8492759

[26] Hochreiter S, Schmidhuber J. Long short-term memory. Neural Computation 1997; 9(8): 1735-1780. https://doi.org/10.1162/neco.1997.9.8.1735

[27] Graves A. Supervised sequence labelling with recurrent neural networks. Studies in Computational Intelligence, 2013; 385.

[28] Hurst HE. Long-term storage capacity of reservoirs. Transactions of the American society of civil engineers, 1951, 116(1): 770-799. https://doi.org/10.1061/TACEAT.0006518

[29] Graves A. Generating sequences with recurrent neural networks. Computer Science 2013. https://doi.org/10.48550/arXiv.1308.0850

[30] Kingma D, Ba J. Adam: a method for stochastic optimization. Computer Science 2014. https://doi.org/10.48550/arXiv.1412.6980

[31] Srivastava N, Hinton G, Krizhevsky A, Sutskever I, Salakhutdinov R. Dropout: a simple way to prevent neural networks from overfitting. Journal of Machine Learning Research 2014; 15(1): 1929-1958.

[32] Hinton G, Srivastava N, Krizhevsky A, Sutskever I. Improving neural networks by preventing co-adaptation of feature detectors. Computer Science 2012. https://doi.org/10.48550/arXiv.1207.0580

[33] Li L, Gao Z, Moan T. Joint Distribution of Environmental Condition at Five European Offshore Sites for Design of Combined Wind and Wave Energy Devices. Journal of Offshore Mechanics and Arctic Engineering 2015; 137(3): 031901(16). https://doi.org/10.1115/1.4029842

[34] Zhang LX, Shi W, Karimirad M, Michailides C, Jiang ZY. Second-order Hydrodyn amic Effects on the Response of Three Semisubmersible Floating Offshore Wind T urbines. Ocean Engineering 2020; 207.C: 107371. Web. https://doi.org/10.1016/j.oc eaneng.2020.107371

Short-term Motion Prediction of floating offshore wind turbine Based on Muti-input LSTM Neural Network

Wei Shi[1,2,3], Lehan Hu[1], Zaibin Lin[4], Lixian Zhang[1], Jun Wu[5], Wei Chai[6*]

[1]DeepWater Engineering Research Centre, Dalian University of Technology, China;

[2] State Key Laboratory of Coastal and Offshore Engineering, Dalian University of Technology, Dalian, China;

[3] Research Institute of Dalian University of Technology in Shenzhen, Shenzhen, China;

[4]School of Engineering, University of Aberdeen, UK

[5] School of Naval Architecture and Ocean Engineering, Huazhong University of Science and Technology, Wuhan, China

[6] School of Naval Architecture, Ocean and Energy Power Engineering, Wuhan University of Technology, Wuhan 430063, China;

* Corresponding author: Prof. Wei Chai, Email: chaiwei@whut.edu.cn

Abstract: The motion response of an offshore floating wind turbine (FOWT) platform is closely related to the control operation regarding the safety of a wind turbine. It is affected by various factors such as sea state environments and mooring systems. In practice, how to predict the motion response of the wind turbine platform in the short term has always been a concern of engineering practice. At present, the development of deep learning technology has brought some potential solutions to this problem. In this paper, a Multi-Input Long-Short Term Memory (MI-LSTM) neural network method is proposed to predict the short-term motion response of a floating offshore wind turbine platform. Specifically, the numerical simulation of the 5MW Braceless platform is carried out under different environmental conditions, and the data of

platform motion response, wave elevation, and mooring force are selected as input variables. Then the training and test groups are established after post-processing data. Subsequently, a Single-Input LSTM (SI-LSTM) model and a Multi-Input LSTM (MI-LSTM) model are established to learn the input data. After comparing the overall accuracy of the results, it is found that the additional mooring force and wave elevation positively affects the platform response prediction results. From the aspects of discreteness and overall accuracy, it is verified that the established MI-LSTM model is also applicable, considering the influence of second-order hydrodynamics. Lastly, compared with the prediction results obtained by the multi-input one-dimensional convolutional neural network (MI1D-CNN), the advantages of the two different models are expounded from the perspectives of training time and accuracy, which provides ideas for the optimization of the FOWT motion response prediction model. This study sheds insights on the short-term motion response forecast and platform positioning of a FOWT. Short-term forecasts of a FOWT can be achieved under various sea conditions by combining the global positioning system.

Keywords: Floating offshore wind turbine; deep learning; response prediction; multi-input LSTM model; second-order hydrodynamic

1. Introduction

With the rapid development of the global economy, energy has become a critical factor in determining social and economic development. To meet the Net Zero target by utilizing sustainable energy, the vigorous growth of renewable energy has become an essential part of the development strategy worldwide. Due to its high energy conversion ability, offshore wind power has been gradually installed in various countries recently. Different foundations of floating offshore wind turbines have been proposed, including spar, tension leg platform (TLP) shape, semi-submersible, and barge [1]-[3]. Substantial research has been carried out in terms of hydrodynamics, mooring systems, stability, performance, and survivability of a FOWT [4]-

[9].

Compared with the onshore wind turbine structure, a FOWT encounters a more complex ocean environment. The motion response of a FOWT occurs in six degrees of freedom (6DOF) and leads to significant challenges in design and assessment [10]. Therefore, it is of great significance to propose an accurate prediction method for the motion response of the FOWT to guide the design and assess structural safety. In the deep learning model, motion response prediction is generally based on the historical data of motion response and many other results from numerical and experimental measurements. In general, deep learning technology is applied to predict the motion response of structures in the next few seconds [11]. According to the length of the forecast time, motion response prediction can be categorized as short-term and safe-period motion prediction. Short-term prediction plays a vital role in improving dynamic positioning control performance, and it provides early warning in extreme sea conditions to reduce platform damage to a certain extent. A short-term forecast's prediction advanced time (PAT) is generally a few seconds, and it requires high forecast accuracy [12].

In recent years, the application of deep learning technology in offshore structures has gradually expanded. The research is mainly carried out by the convolutional neural network (CNN) and the recurrent neural network (RNN) methods [13]-[21]. Wang et al. [14] proposed the Low-frequency adds wave-frequency responses (LAWR) method to predict the mooring line tension of a semi-submersible platform. Combined with the LSTM method, accurate results are obtained to predict mooring line tension under different cases. Pena et al. [18] proposed the Wave-Generative Adversarial Network (Wave-GAN) technology, combined with CNN convolutional neural network and CFD method, to predict the load of nonlinear waves on fixed structural columns. Pena et al. [18] concluded the maximum error between the Wave-GAN predicted value and CFD simulated value of 1.5%-2% by adjusting several parameters, and the mean absolute error (MAE) of the test group is about 0.014. Lian et al. [19] constructed the digital twin of mesh clothing and established the deep neural network (DNN) to predict whether the mesh clothing is damaged. The average accuracy of the final identification model is 94.3%. Bjørni et al. [20] predicted the mooring line tension in the next 30 s by making use of the platform motion response in the first 60 s as input and constructed a three-layer deep neural network with bias term. It is concluded that the average error of anchor chain tension is 0.46% through cross-sectional comparisons. According to the combined prediction method of the Extreme Learning Machine (ELM), the Empirical Mode Decomposition (EMD), and LSTM neural network, Zhang et al. [21] proved that the combined prediction method presented higher prediction accuracy than the single LSTM model and ELM-LSTM model. However, when considering the influence of environmental factors and mooring force, there is limited research on predicting the motion response of a FOWT. At the same time, in practice, it needs to assess the motion response of a FOWT under the influence of various complex factors and consider the impact of second-order hydrodynamic force. Moreover, the amount of research on the motion response prediction of a FOWT under the effect of the second-order hydrodynamic force is also limited.

To investigate the short-term motion prediction of a FOWT, the MI-LSTM Neural Network model is used. This paper is organized as follows: Section 2 introduces the basic principles of the RNN. The architecture and differences between the established SI-LSTM model and the MI-LSTM model are explained in detail. The hyperparameters of the model and the selection of the training and test groups are also given in this section. Then, in Section 3, the structure size of the 5 MW Braceless platform model is shown. A detailed comparison is made between the prediction results of the SI-LSTM and MI-LSTM models under different environmental conditions in Section 4. This proves the positive excitation of the increased input factor numbers on the prediction results and illustrates the advantages and benefits of the MI-LSTM model. In Section 5, the applicability of the proposed model is demonstrated when the second-order hydrodynamic force is considered. Given that there are few comparisons between the RNN model and CNN model regarding time domain problems, in Section 6, by comparing the prediction results of the proposed model with the multi-input one-dimensional convolutional neural network (MI1D-CNN) model, the advantages of the two models are illustrated from the perspectives of overall accuracy and training time. Finally, the conclusions and recommendations are made for the future optimization of the platform response prediction model.

2. Long-Short Term Memory (LSTM) Neural Network

2.1. Recurrent Neural Network (RNN)

Recurrent neural network (RNN) is gradually emerging in the interdisciplinary field as a typical representative of deep learning technology. RNN takes time series data as input and performs recursion in the evolution direction of the sequence, where all nodes (cyclic units) are linked in a chain [22]. RNN has memorization, parameter sharing, and turning completeness [23]-[25], so it has clear advantages in learning the nonlinear features in sequences. RNNs are widely used in natural language processing, such as speech recognition, language modeling, and time series prediction. RNN performs outstandingly in solving scheduling problems, and motion response prediction is the typical time domain problem. Therefore, in this paper, RNN is selected for model architecture.

Since the motion of the platform at time t is affected by the motion at the previous time $t-1$, meanwhile, the motion at current time t will also have an impact at forward time $t+1$, platform motion response is a continuous process with time dependence. Considering this characteristic, the traditional deep neural network (DNN) cannot convey information precisely in the time sequence, but the RNN is developed to overcome this problem. Training input data from a FOWT system to predict the motion response in the next few seconds can be viewed as an adaptive function mapping. The input is the previous time series information of different input factors, and the output is the motion response in the future. Hence, the trained deep learning model can achieve prediction in a short time.

The timeline expansion of the RNN is shown in **Figure 1**, where x is the network input layer, s is the network node hiding layer, and o is the network node output layer. After the network receives the input x_t at time t, the value of the hidden layer is s_t and the output value is o_t. The value of s_t depends not only on x_t, but also on s_{t-1}. In other words, s inherits the information from each node.

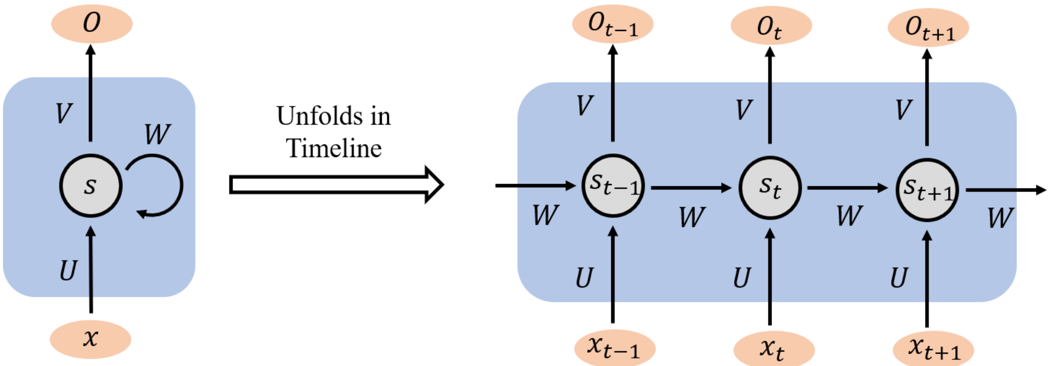

Figure 1. An unfolded RNN network

The calculation method of the RNN network is shown in Equations 1-2:

$$o_t = \boldsymbol{g}(\mathbf{V} \cdot s_t) \tag{1}$$

$$s_t = \boldsymbol{f}(\mathbf{U} \cdot x_t + \mathbf{W} \cdot s_{t-1}) \tag{2}$$

where **V** is the weight matrix of the output layer, ***g*** is the activation function for the output layer, **U** is the weight matrix of the input layer *x*, and **W** is the weight matrix of the last value, which is the input of the present time, and ***f*** is the activation function for the hidden layer. Common activation functions, such as sigmoid, tanh, Rectified Linear Unit (ReLU), and linear activation function, can be selected according to data characteristics and experimental effects. The sigmoid activation function is generally selected for hidden layer activation function ***f***, while the linear activation function is generally chosen for output layer activation function ***g***. Equation 1 is the calculation formula of the output layer. The output layer is fully connected, indicating that every node in the output layer is connected to every node in the hidden layer. Equation 2 is the calculation formula of the hidden layer.

2.2. Long-Short Term Memory (LSTM) Network

LSTM is first proposed by Hochreiter and Schmidhuber [25]. Compared with traditional RNN, the LSTM network has improved the gradient explosion and gradient extinction. It has been one of the most popular RNN models and is widely applied in many fields, such as speech recognition, image description, and natural language processing. The internal structure of the LSTM node is shown in **Figure 2** [27].

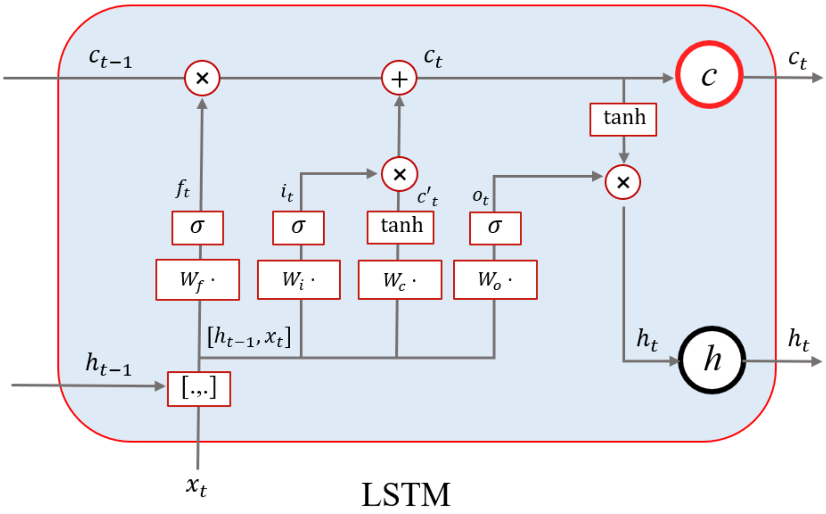

Figure 2. LSTM node unit internal structure

At time t, the LSTM network has three inputs: current time input value x_t, LSTM output value h_{t-1} at the last time, and the unit state c_{t-1} at the previous time. The output of LSTM has two parts: the output value of LSTM at the current time h_t, and the unit state at the current time c_t. x, h, and c are vectors. In addition, LSTM uses the concept of a Gate to control the state of the unit [27]. Gate is a full connection layer that controls information transmission between input and output. Its input is a vector of time series information, and its output is a vector of real numbers between 0 and 1. The gate can be expressed as:

$$G(x) = \boldsymbol{\sigma}(\boldsymbol{W} \cdot \boldsymbol{x} + \mathbf{b}) \quad (3)$$

where $\boldsymbol{W}$ is the weight matrix of the gate, $\mathbf{b}$ is the bias term, and $\boldsymbol{\sigma}$ is the generally sigmoid activation function.

The output vector of the gate is multiplied by the element and the vector is controlled to achieve the gate effect. The gated output is a vector of real numbers between 0 and 1. When the gated output is 0, any vectors multiplied by the output will get the 0 vectors, indicating that no information can pass through. When the gated output is 1, no changes are applied by multiplying, indicating that any information can pass through. Because $\boldsymbol{\sigma}$ has a range of (0,1), the gate is an intermediate state.

LSTM relies on two gates to control the content of the cell state: (1) one is the forget gate that determines the amount of the cell state c_{t-1} at the last moment. c_{t-1} is used to retain the current moment c_t; (2) one is the input gate that determines the amount of the current network input x_t, which is saved to the unit state c_t. Meanwhile, LSTM uses an output gate to control the amount of unit state c_t that is generated from the current output value h_t. The governing equations of each gate are given as follows:

$$f_t = \boldsymbol{\sigma}(\mathbf{W_f} \cdot [\boldsymbol{h_{t-1}}, \boldsymbol{x_t}] + \mathbf{b_f}) \tag{4}$$

$$i_t = \boldsymbol{\sigma}(\mathbf{W_i} \cdot [\boldsymbol{h_{t-1}}, \boldsymbol{x_t}] + \mathbf{b_i}) \tag{5}$$

$$c_t = f_t \cdot c_{t-1} + i_c \cdot tanh(\mathbf{W_C} \cdot [\boldsymbol{h_{t-1}}, \boldsymbol{x_t}] + \mathbf{b_c}) \tag{6}$$

$$o_t = \boldsymbol{\sigma}(\mathbf{W_o} \cdot [\boldsymbol{h_{t-1}}, \boldsymbol{x_t}] + \mathbf{b_o}) \tag{7}$$

$$h_t = o_t \cdot tanh(\boldsymbol{c_t}) \tag{8}$$

where f_t is the forgetting gate equation, $\mathbf{W_f}$ is the weight matrix of the forgetting gate, $[h_{t-1,} x_t]$ is joining two vectors into a longer vector, $\mathbf{b_f}$ is the biased term of the forgetting gate, i_t is the input gate equation, $\mathbf{W_i}$ is the weight matrix of the input gate, $\mathbf{b_i}$ is the offset term of the input gate, c_t is the current moment element state equation, o_t is the output gate control equation, h_t is the final output equation determined by the output gate and unit state.

The unique Gate structure in the LSTM model effectively improves the phenomenon of gradient explosion and gradient disappearance. the activation function of the gate structure in the LSTM model is the sigmoid function, and the Sigmoid function controls the value of the forgetting gate between 0 and 1. When the output of the gate is 1, the forgetting gate is saturated, at this time the long-range information gradient does not disappear, and the gradient can be well passed in the LSTM, largely mitigating the probability of gradient disappearance occurring; when the output of the gate is 0, at this time the model is blocking the gradient flow and forgetting the previous information, indicating that the information of the previous moment does not affect on the current moment. Through the gate structure and sigmoid activation function, the LSTM model can effectively solve the gradient disappearance and gradient explosion problems.

Existing LSTM network prediction modes mainly fall into the following four types [28]: point-to-point, point-to-sequence, sequence-to-point, and sequence-to-sequence, as shown in **Figure 3**:

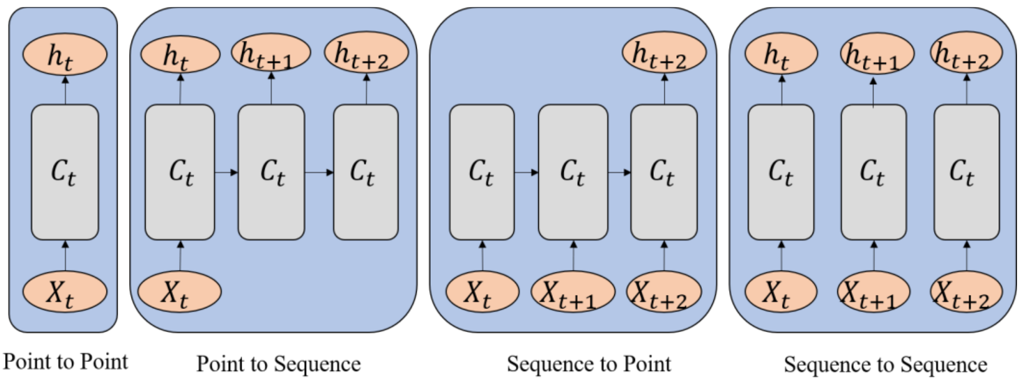

Figure 3. LSTM network prediction modes

The LSTM network in this paper is set up by using sequence-to-point mode for a prediction model, which uses forecasting point response from previous time series after the selected data input mode is adopted in the form of the sliding window. Each window length has 200 time points and the 10 s surge motion. The sliding window form is shown in **Figure 4**, where the mapping relationship between the data input and output is presented when the forecast time is 5 s. Therefore, the response at $t+5$ is predicted based on the response from t-10 to t.

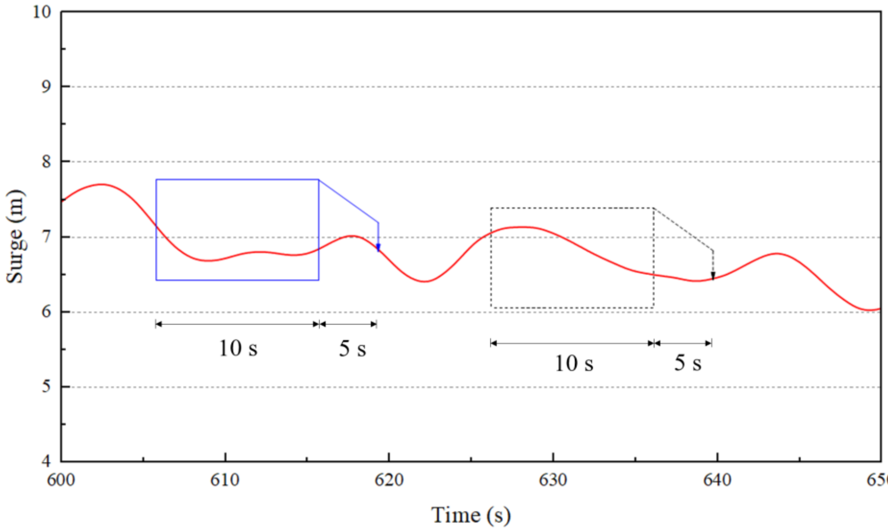

Figure 4. Sliding windows for data input and output

2.3. LSTM Model Structure

The LSTM network model established in this paper has three hidden layers and one fully connected output layer, shown in **Figure 5**. The data sampling frequency is 20 Hz. The input time step of the LSTM network contains 200 time series points with a motion response of 10s. The batch size is set to 256 sample sets, which are also the input for training and updating internal parameters. The number of neurons is set to 200. These two parameters are hyperparameters and can be adjusted according to the performance of the actual test.

Input layer: input time series with a window of 200 data points, representing the motion response of 10s. The input dimension of the single-input model is 1, and that of the multi-input model is 3.

Hidden layer: The hidden layer has 200 nodes.

Output layer: The output layer is dense, the activation function is linear, and the output result is the motion response at the target time.

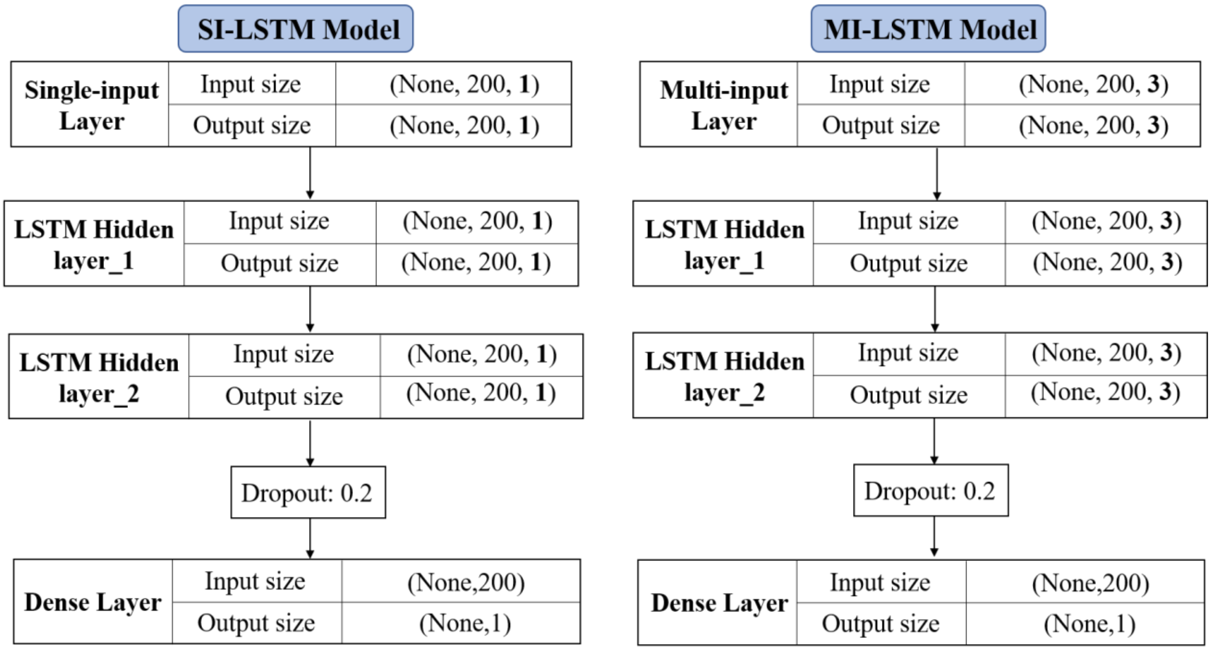

Figure 5. LSTM network model structure and data transfer format

The Adam algorithm is configured for the LSTM network [30]. Adam algorithm is an advanced Stochastic Gradient Descent (SGD) algorithm, which introduces an adaptive learning rate for each parameter. The adaptive learning method and the Momentum method are combined. The learning rate is dynamically adjusted by the first and second moment estimation of the gradient. The gradient descent process is relatively stable and suitable for most non-convex optimization problems in large data sets and high-dimensional space.

Simultaneously, the Dropout layer is added after the input layer and the hidden layer to prevent overfitting [31-[32], and the Dropout_1 and Dropout_2 are set to 0.2. Overfitting may occur due to a large number of unknown network parameters or training times. The principle of dropout is that during the neural network training, some neurons are randomly discarded and not used for training at this round to avoid overfitting and accelerate loss convergence.

In this paper, the LSTM neural network is constructed, and the input data consists of three parts, including time series of previous motion response, mooring force, and wave elevation. And the current motion response is set as the output data. The process of using the LSTM neural network model to predict the motion response is shown in **Figure 6.** The process of predicting motion response by LSTM neural network.

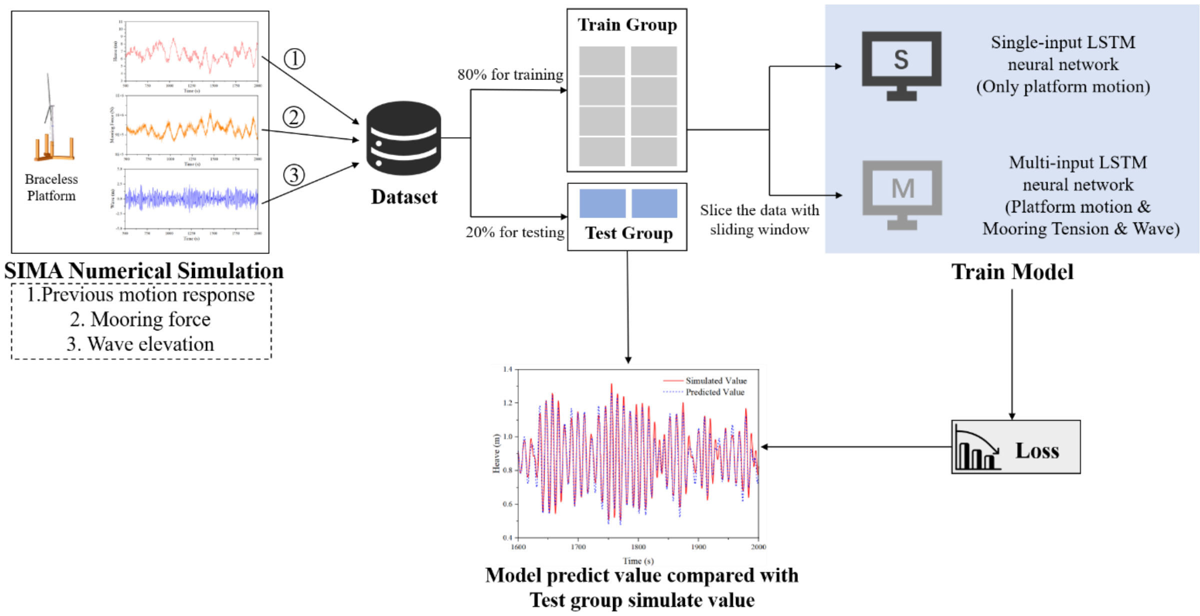

Figure 6. The process of predicting motion response by LSTM neural network

3. Braceless Platform model

The 5 MW Braceless model is established by SIMA, and the time domain response is obtained by numerical simulation. SIMA is developed for the analysis of flexible marine riser systems, but it is also suited for any slender structures, such as mooring lines, umbilicals, steel pipelines, and conventional risers. The data used in training in this paper came from the FOWT model of a 5 MW Braceless semi-submersible platform in the water depth of 100 m. The Braceless platform consists of one central column, three side columns, and three pontoons, shown in **Figure 7**.

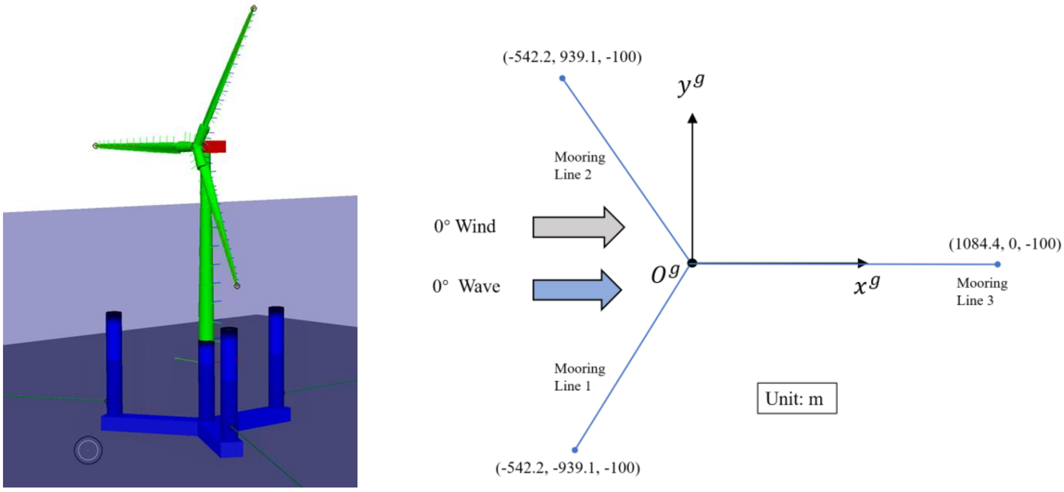

Figure 7. Schematic of 5-MW Braceless platform

Three side columns are evenly distributed around the central column at 120°. They are connected to the bottom of the central column by a floating buoy to form a Braceless semi-submersible platform. The three-point mooring system is adopted, and the anchor chain is set at the bottom of the side column. 0° wave-wind misalignment is considered in the simulation. The main parameters of the Braceless platform are shown in **Table 1.** Parameters of the 5 MW Braceless Platform:

Table 1. Parameters of the 5 MW Braceless Platform

Parameter	Value
Central column diameter (m)	6.5
Side column diameter (m)	6.5
Buoy height (m)	6
Buoy bottom width (m)	9
Buoy short radius (m)	41
Buoy long radius (m)	45.5
Depth of the draft (m)	30
Displacement (t)	10555
Steel weight (t)	1804

Equivalent thickness (m)	0.03

Based on the data given in Ref. [33], site 5 in Norway was selected as a representative site for the simulation. In the following cases, the water depth is 100 m. The average wind speed V_t, effective wave height H_S, and spectrum peak period T_p at the selected cabin height are listed. The JONSWAP spectrum is used to describe random ocean waves, and the JONSWAP spectrum is shown in Equations 9-1 to 9-3. The Kaimal wind speed spectrum is used to describe the offshore wind conditions.

$$S_{(f)} = \alpha \frac{{H_S}^2}{{T_p}^4 f^5} exp\left[-\frac{5}{4}(T_p f)^{-4}\right] \gamma^{exp\left[-\frac{(T_p f-1)}{2\sigma^2}\right]} \quad (9\text{-}1)$$

where f is the wave frequency, γ is the shape parameter, and σ and α are shown below,

$$\sigma = \begin{cases} 0.09 & f \geq f_p \\ 0.07 & f < f_p \end{cases} \quad (9\text{-}2)$$

$$\alpha = \frac{0.0624}{0.230 + 0.0336\gamma - 0.185/(1.9+\gamma)} \quad (9\text{-}3)$$

Table 2. Environment matrix

Case	Vt (m/s)	γ	Hs (m)	Tp (s)
EC 1	9.8	3.3	2.9	9.98
EC 2	14.8	3.3	4.5	11.81
EC 3	16	3.3	5.3	12.81

4. Single-input and Multi-input

4.1. Data Partitioning and Error Measurement

The sampling frequency of the Braceless platform simulation test is 20 Hz. The total sampling length of motion response (surge, pitch, and sway) is 2000 s. The collected time series

contains 40000 data points. In the training model, the first 32000 points of response data are the training groups and the last 8000 points of response data are the test groups. Three test cases (EC1, EC2, and EC3) are selected, and each test case contained 2000 s surge, pitch, and sway motion data.

The training group data is used to train and obtain the neural network model. The relationship between training Epochs and Loss is observed through the Loss function. Then the test group data is imported into the trained neural network model to verify the accuracy and performance of the trained model.

The Loss function adopted in this paper is the Mean Squared Error (MSE), which is the averaged squared difference between the predicted value and the measured value as shown in Equation 10:

$$MSE = \frac{\Sigma(y_t' - y_t)^2}{n} \tag{10}$$

where y_t' is the predicted value of the motion response at time t, y_t is the measured value of the motion response at time t, and n is the total number of predicted values 8000 in this study.

4.2. Single-input Predicted Results

Single-input LSTM (SI-LSTM) model is used to train the motion response data in the training group in terms of the heave, surge, sway, and pitch. The training input of the model is only based on the previous motions. The output of the model is compared and analyzed with the data of the test group. The predicted advance time is set as 2.5 s and 5 s respectively. The actual and predicted values are shown in **Figures 8-10**.

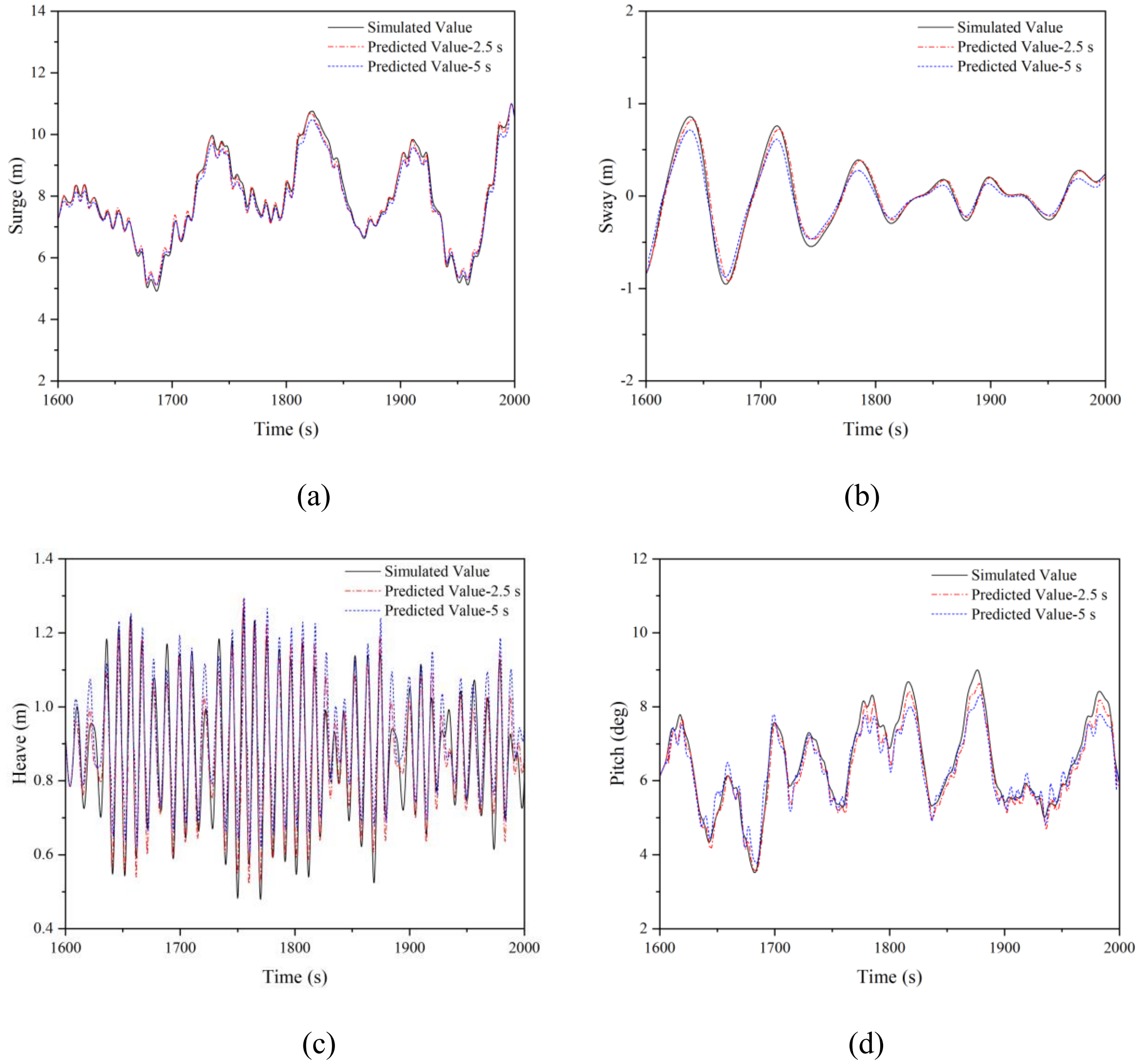

Figure 8. Simulated and predicted values of EC 1 at 2.5 s and 5 s:

(a) Surge; (b) Sway; (c) Heave; (d) Pitch

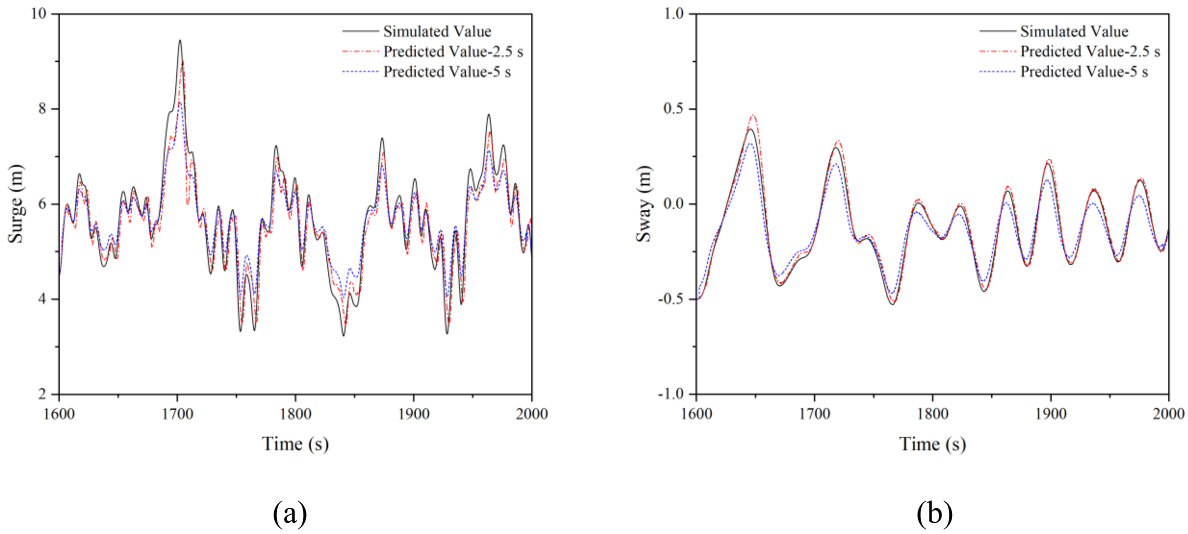

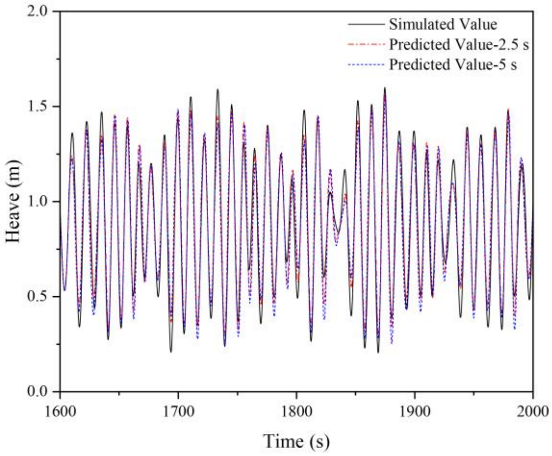

(c)

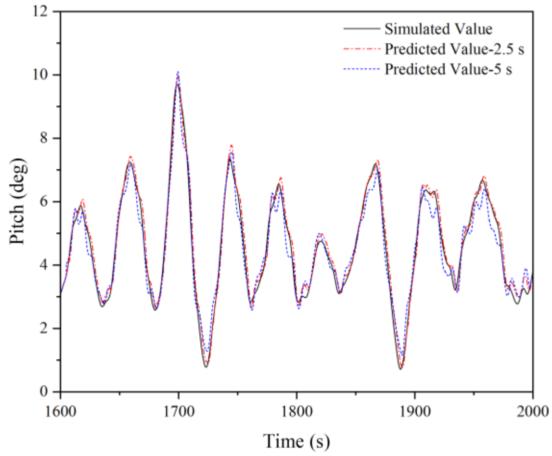

(d)

Figure 9. Simulated and predicted values of EC 2 at 2.5 s and 5 s:

(a) Surge; (b) Sway; (c) Heave; (d) Pitch

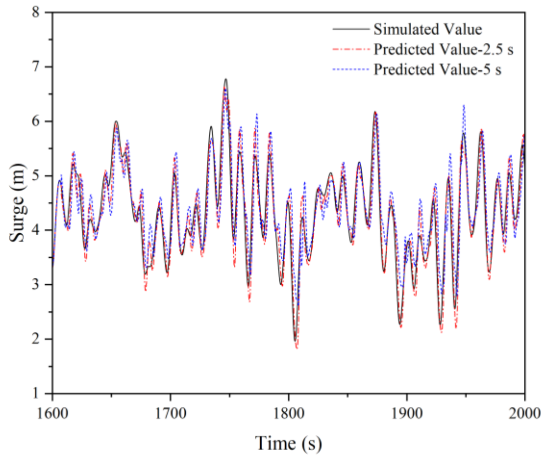

(a)

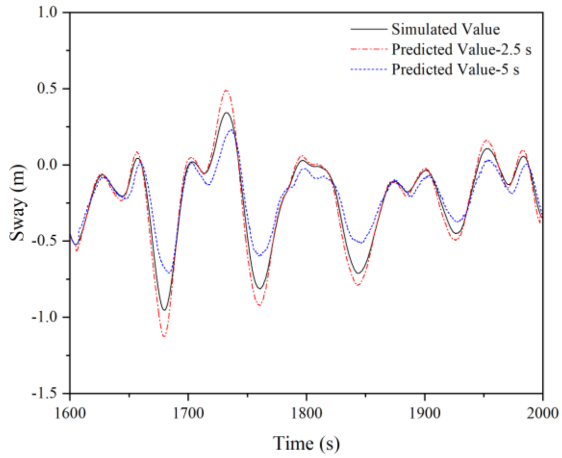

(b)

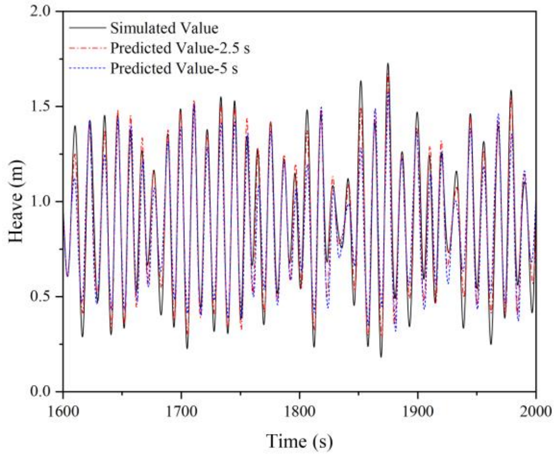

(c)

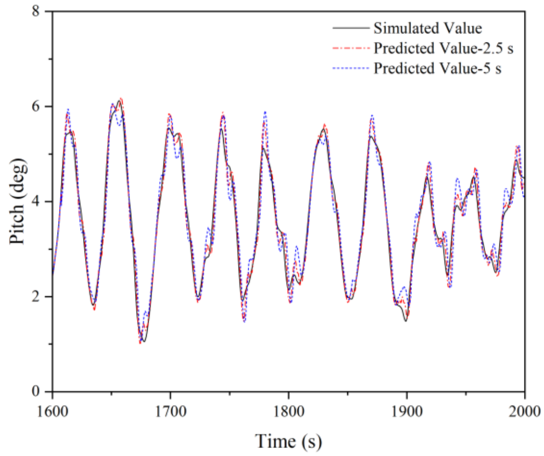

(d)

Figure 10. Simulated and predicted values of EC 3 at 2.5 s and 5 s:

(a) Surge; (b) Sway; (c) Heave; (d) Pitch

It can be seen from **Figures 8-10** that when the previous motion response is used as the single input, the predicted value at PAT of 2.5 s is closer to the simulated value. Due to the large amplitude of motion in the surge, the predicted results in **Figure 8(a)** agree well with the simulation results, apart from the minor discrepancy at the peak of the surge in **Figures 9-10(a)**. Due to the small amplitude in sway, the predicted results under the two PATs generally agree with simulated results compared to the agreement between predicted and simulated surge. Similarly, there is also a minor discrepancy at the peak. The amplitude of heave motion is the smallest among the three motions, but it contains higher frequency components. The predicted heave motion in three test cases in **Figures 8-10** presents better agreement with simulated results at PAT of 2.5 s, but a minor discrepancy can be noted at the peak and trough at PAT of 5 s. The peak value of pitch in **Figures 8-10(d)** is also large, but there is higher-order fluctuation at the peak and trough due to the nonlinear motion induced by wind and waves. Single-input LSTM model learned the nonlinear features from the training data group, so the predicted value agrees well with the simulated results.

In summary, compared with the simulated values, the predicted values in all motions have very minor discrepancies at peak and trough, but a fairly good agreement has been presented. The discrepancy at peak and trough can be attributed to the limited input factors to train the neural network. To unravel this, the multi-input network structure is investigated in detail in Section 4.3.

4.3. Muti-input Predicted Results

A multi-input model is trained to explore the effects of multiple factors as input conditions on the predicted results. Unlike the single-input model, the training input of the multi-input LSTM (MI-LSTM) model is based on the previous motions, mooring forces, and wave

elevation. The output of the model is compared and analyzed with the data of the test group. The predicted advance time is set as 2.5 s and 5 s respectively. The test and predicted results are shown in **Figures 11-13**:

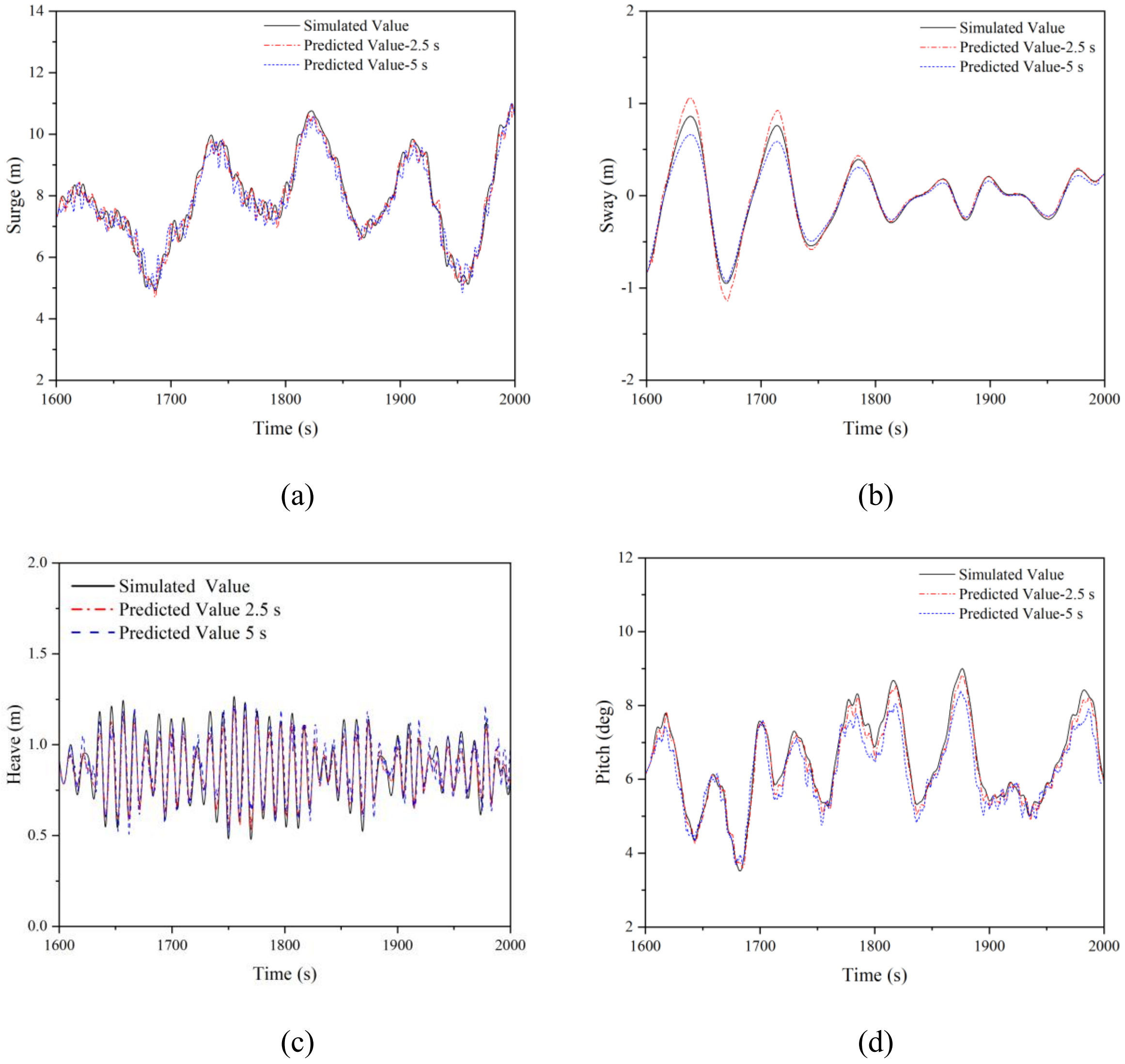

Figure 11. Simulated and predicted values of EC 1 at 2.5 s and 5 s:

(a) Surge; (b) Sway; (c) Heave; (d) Pitch

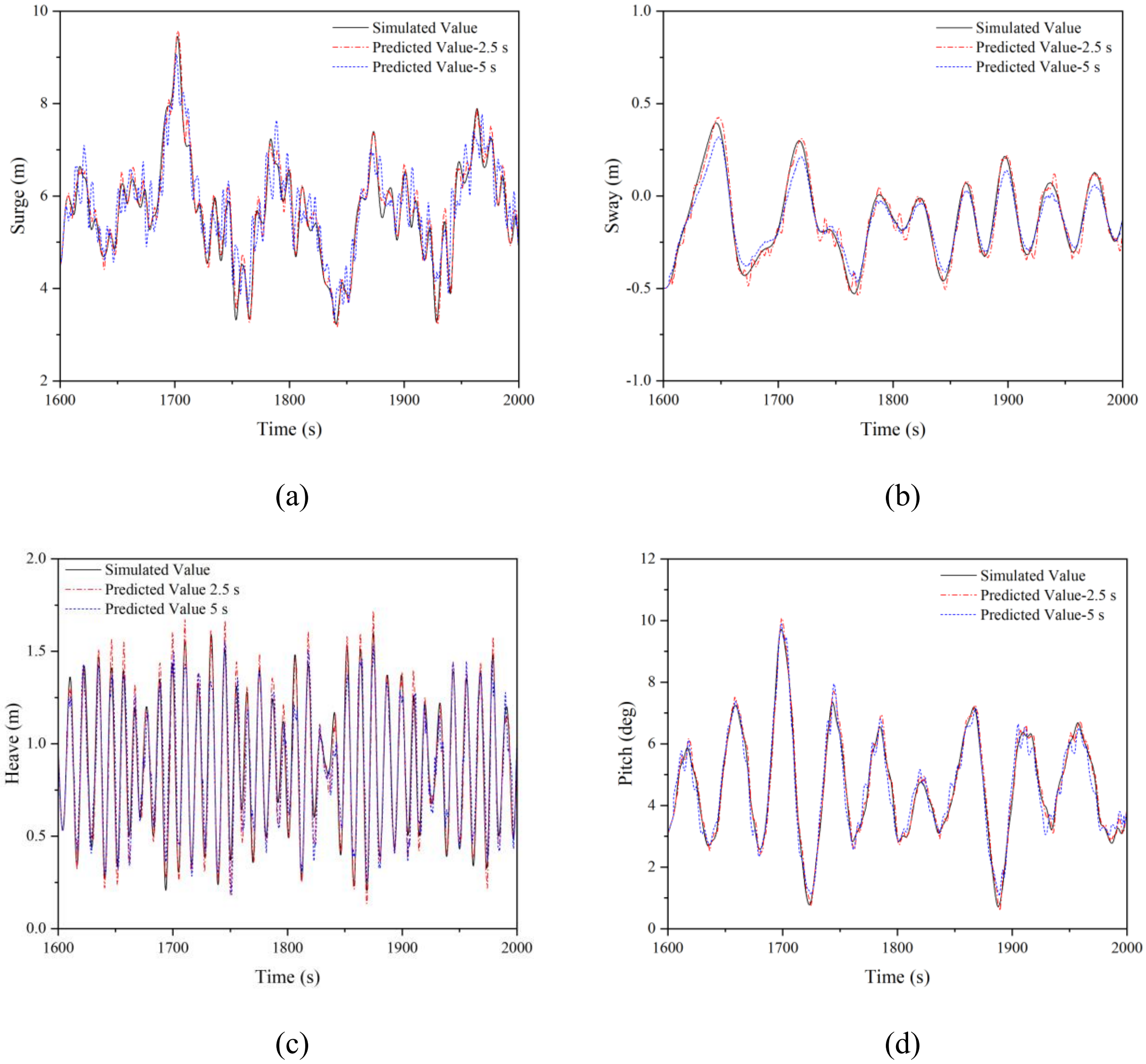

Figure 12. Simulated and predicted values of EC 2 at 2.5 s and 5 s:

(a) Surge; (b) Sway; (c) Heave; (d) Pitch

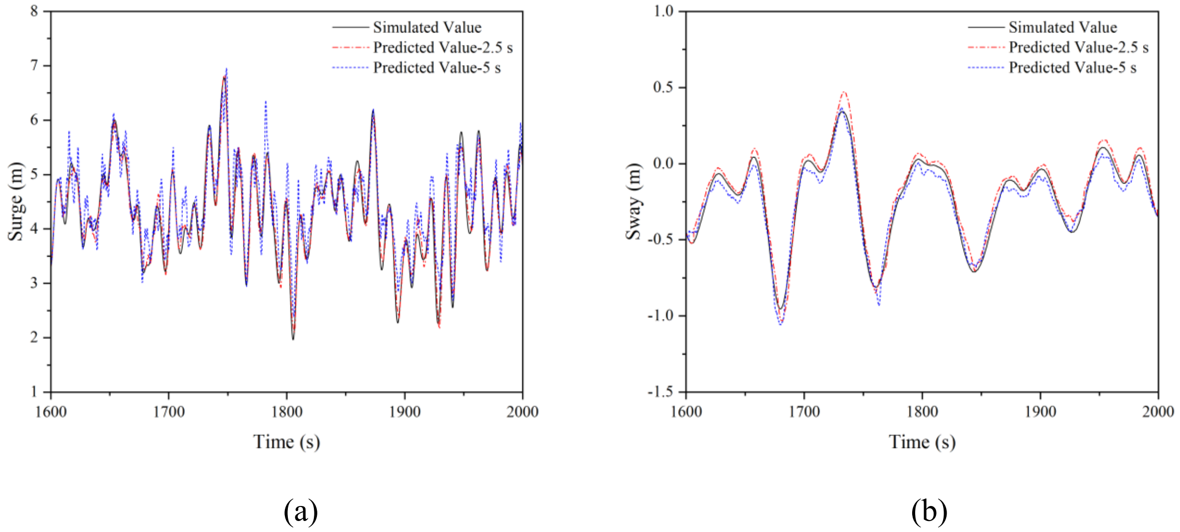

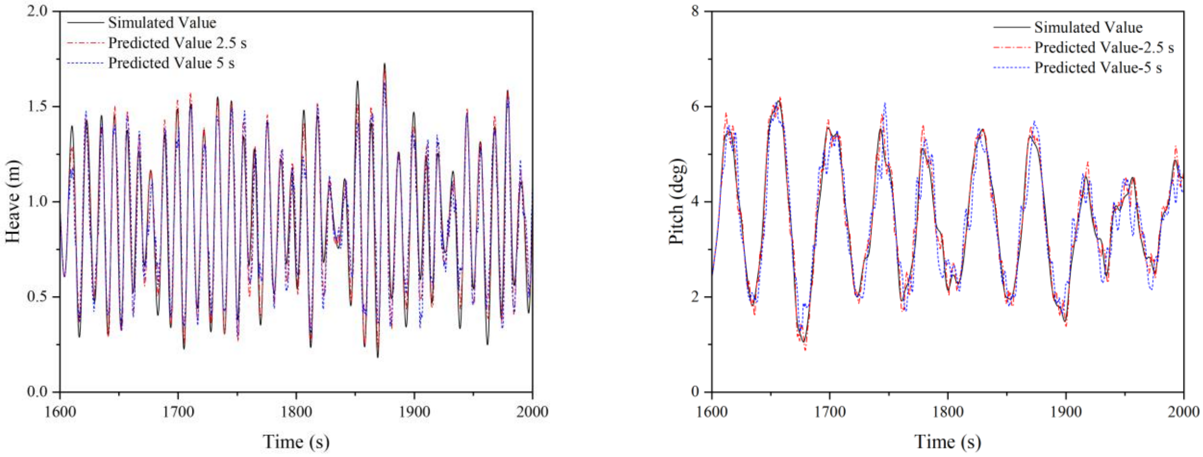

(c) (d)

Figure 13. Simulated and predicted values of EC 3 at 2.5 s and 5 s:

(a) Surge; (b) Sway; (c) Heave; (d) Pitch

When the model input factors become multiple, i.e., adding mooring force and wave elevation, a better agreement between the predicted value and the simulated value is obtained compared with the single input case. Improved agreement of surge prediction at peak in **Figure 12(a)** is presented compared to **Figure 9(a)**. But in the case of multiple inputs, the fluctuations can also be noticed from the predicted surge. Sway and heave are not significantly improved due to their less sensitivity to mooring force. With the additional input factors, the accuracy of the predicted pitch has been improved significantly as pitch motion is sensitive to mooring forces, comparing **Figure 9(d)** and **12(d)**. It can be found that in the period 1900s-2000s, the discrepancy of the single-input model can be found, while the multi-input model presented better performance with additional input data sets. Similar to the pitch, better agreements have been achieved for the predicted surge.

In a word, after adding the additional input factors to train the multi-input model, better performance in predicting the FOWT motion response has been demonstrated. However, the saw-tooth effect of the MI-LSTM model is more obvious, caused by the deep learning of the additional input information. The saw tooth effect is further analyzed after analyzing the scatterplot of discrete situations in Section 4.4.

4.4 Error Analysis

In this study, the number of Epochs is set to 50 rounds. It is shown in **Figure 14** the trend of the Loss function changing with the Epochs is generated and recorded during the training. It can be noted that with the increment of Epochs, Loss decreases rapidly in the beginning. Then after the rapid decrease stage, Loss finally tended to be stable. After the Epochs reaches 50, Loss remains unchanged. It can be concluded that the network training effect will not be further improved after 50 rounds and a neural network model with good accuracy is generated. The model has completed learning about the relationship between the input and output data.

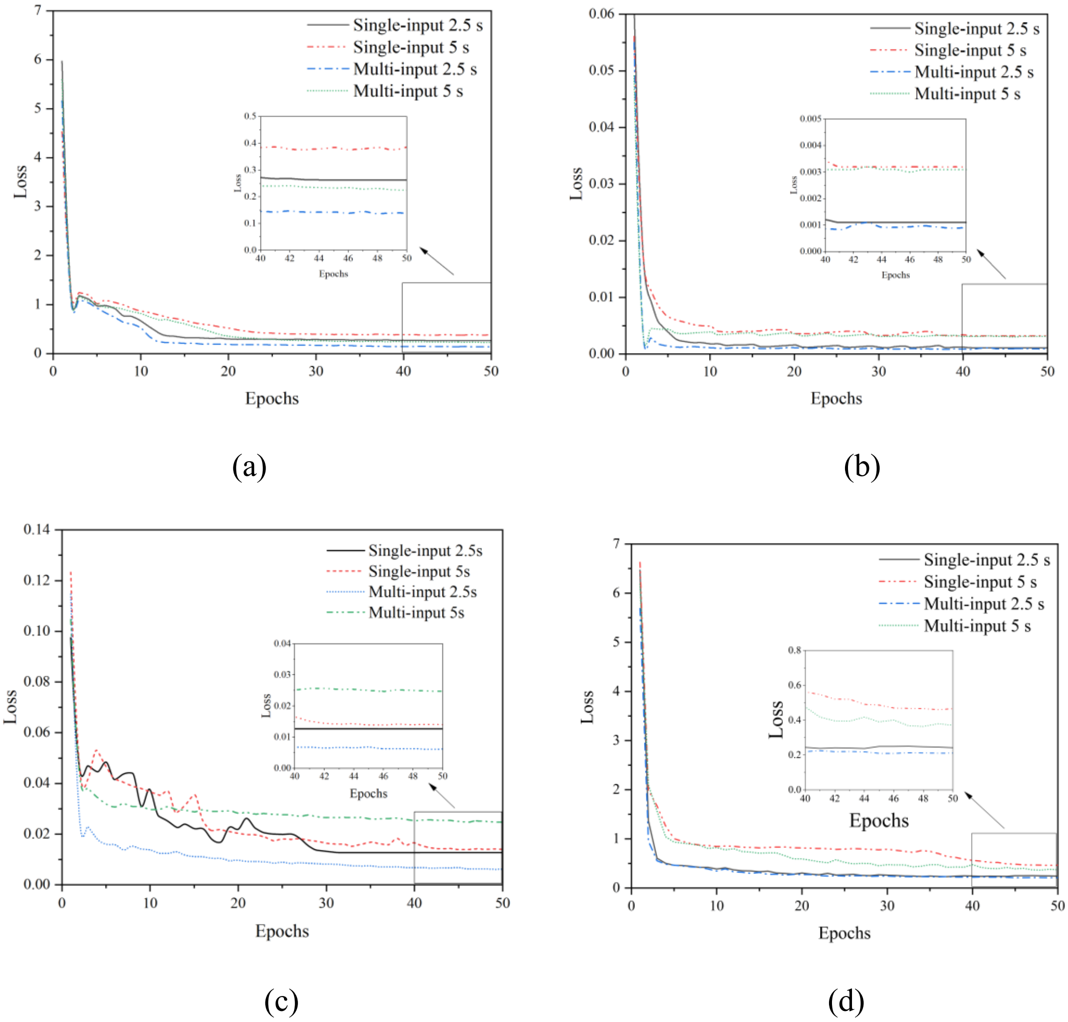

Figure 14. The curve of Loss affected by Epochs for different directions:

(a) Surge; (b) Sway; (c) Heave; (d) Pitch

At the same time, the Loss of the MI-LSTM model is found to be lower than that of the

SI-LSTM model both in 2.5 s and 5 s. It can be considered that the learning ability of the model is improved after additional factors are added to the training. The predicted results are shown in sections 4.2 and 4.3 and compared with simulation data. It is difficult to observe their overall discretization, so a scatter plot of the prediction results in different input modes is plotted in this section, as shown in **Figure 15.**

According to **Figure 15**, comparing the SI-LSTM model with the MI-LSTM model under the different cases, it can be found that after adding two additional input factors, the discrete situation of the MI-LSTM model prediction results is significantly smaller than that of the SI-LSTM model prediction results. This phenomenon is more evident in the sway and heave of EC1, surge and sway of EC2, and sway and heave of EC3. The use of the MI-LSTM model is beneficial in reducing the discrete nature of predicted results.

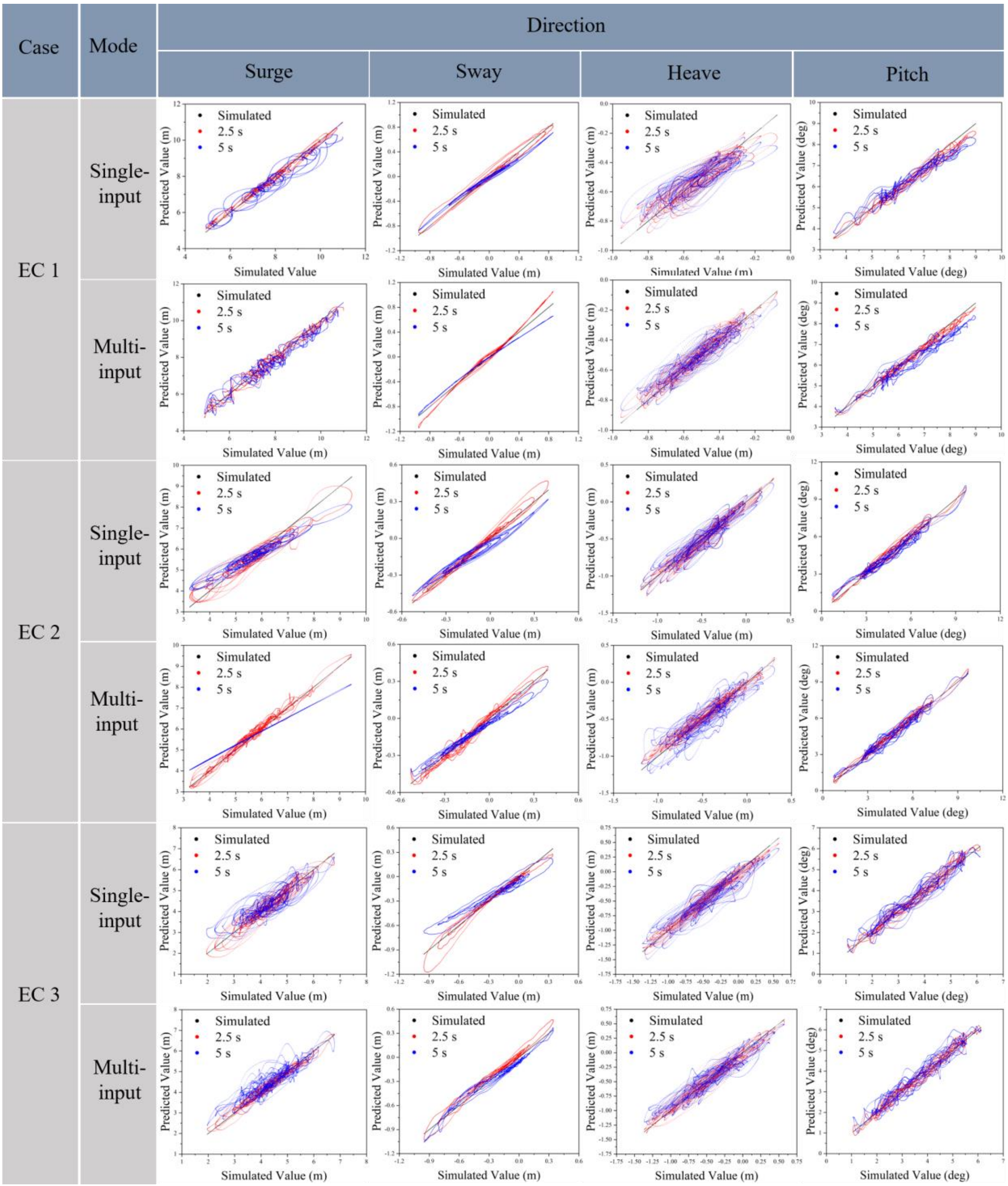

Figure 15. The discrete scatter plot of prediction results with two models

Comparing the prediction results of the SI-LSTM model with the MI-LSTM model on the same image, the comparison results for EC 1 are shown in **Figure 16**. From the figure, one can find that the prediction results of both SI-LSTM model and MI-LSTM model have high accuracy. For the surge motion, both models have the best results and have a good fit in both peak and trough positions as well. For the sway motion, the MI-LSTM model predicts a certain absolute value bias at the response extremes, while the SI-LSTM model predicts a certain absolute value bias at the response extremes. For the heave motion, since the SI-LSTM model does not take into account the effect of wave elevation, and the response in the heave direction happens to be most affected by the wave, the accuracy of the SI-LSTM model in this direction is not as good as that of the MI-LSTM model. For the pitch motion, the results of both models are similar to those of the surge direction, but the predicted values are smaller at the peak, which is more obvious in the SI-LSTM model.

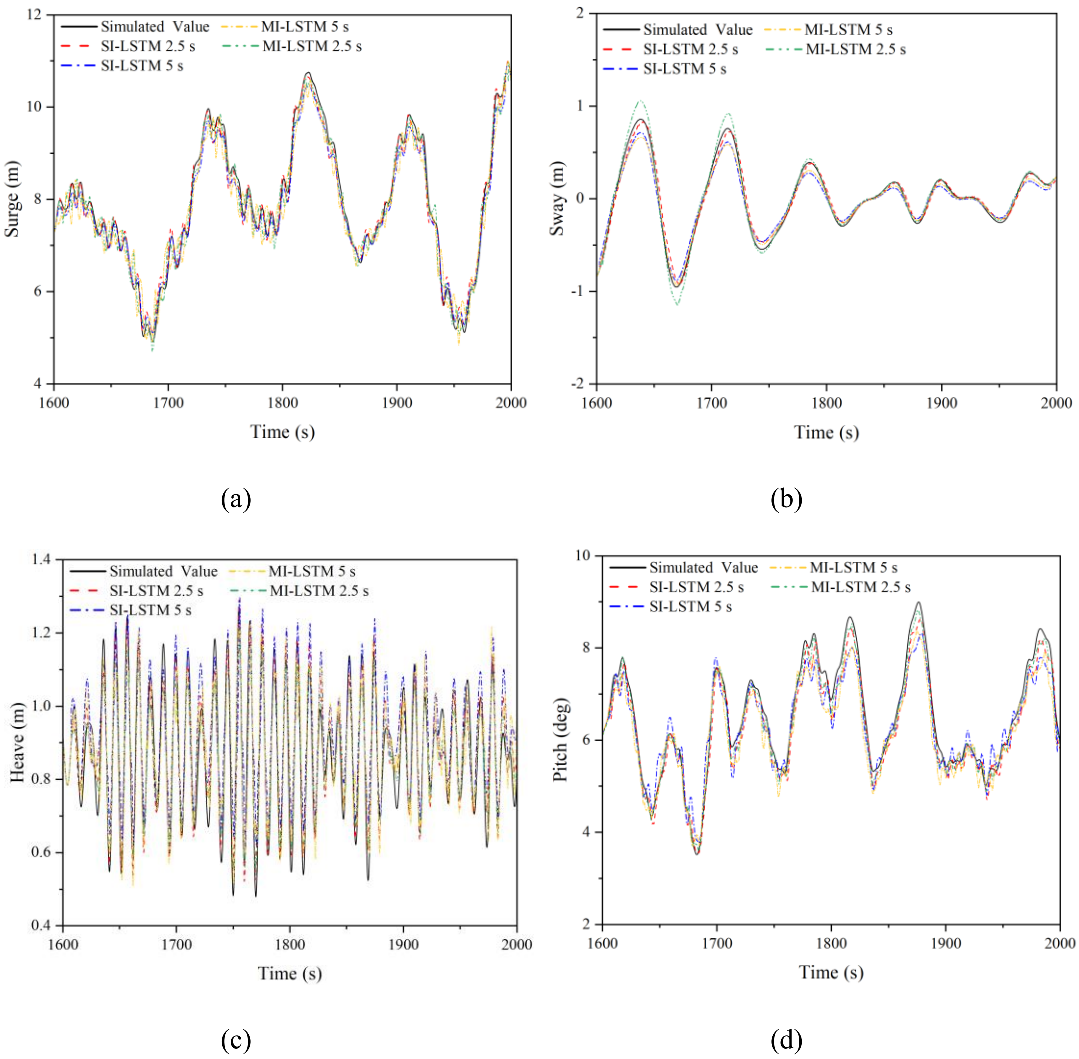

Figure 16. Comparison of 1st-order and 2nd-order hydrodynamic prediction results: (a) Surge; (b) Sway; (c)Heave; (d) Pitch

In addition to the impact of discrete situations, the overall accuracy of the MI-LSTM model and the single-input model is also important. The individual statistics for predicting the final result of the FOWT motion response using both models are listed in Table 3. The overall accuracy of both models is presented in **Figure 17**.

Based on Table 3 and Figure 16, the results at PAT of 2.5 s present better agreements than at PAT of 5 s. After adopting the MI-LSTM model, the accuracy of the prediction results in pitch and heave has been significantly improved. With the increment of PAT, the period between input and output becomes larger, so the time correlation between the two decreases and the uncertainty increases. The upper limit of learning ability decreases as the correlation between input and output information decreases. Therefore, the accuracy at PAT of 5 s is lower than that of 2.5 s.

Mode	Statistics	EC 1				EC 2				EC 3			
		Heave	Pitch	Surge	Sway	Heave	Pitch	Surge	Sway	Heave	Pitch	Surge	Sway
Single-input 2.5 s	Max	73.2%	95.9%	99.9%	96.7%	96.2%	92.6%	95.3%	81.2%	84.3%	98.8%	97.8%	81.0%
	Min	92.3%	99.0%	96.2%	96.2%	93.4%	92.4%	93.0%	97.1%	96.8%	96.2%	92.4%	76.9%
	Average	99.7%	97.2%	99.8%	88.6%	95.6%	92.4%	98.5%	90.6%	96.9%	93.3%	96.5%	94.9%
	STD	87.5%	93.7%	94.3%	94.0%	97.7%	98.9%	83.7%	90.6%	96.0%	92.1%	93.5%	97.7%
	Overall	**88.2%**	**96.4%**	**97.6%**	**93.9%**	**95.7%**	**94.1%**	**92.6%**	**89.9%**	**93.5%**	**95.1%**	**95.0%**	**87.6%**
Multi-input 2.5 s	Max	73.2%	98.0%	97.6%	97.1%	97.4%	96.1%	96.8%	92.5%	95.8%	98.5%	99.4%	82.9%
	Min	96.0%	97.8%	95.8%	89.6%	93.3%	93.9%	98.2%	98.7%	98.3%	93.5%	96.6%	91.9%
	Average	97.5%	98.2%	99.4%	88.6%	96.0%	98.5%	98.9%	96.6%	99.2%	98.2%	99.0%	92.4%
	STD	97.3%	95.3%	96.8%	97.9%	97.8%	98.8%	95.6%	95.5%	96.6%	98.1%	94.9%	96.6%
	Overall	**91.0%**	**97.3%**	**97.4%**	**93.3%**	**96.1%**	**96.8%**	**97.4%**	**95.8%**	**97.5%**	**97.1%**	**97.5%**	**91.0%**
Single-input 5 s	Max	73.2%	92.5%	98.7%	83.2%	82.9%	95.9%	86.1%	81.1%	69.7%	88.9%	97.4%	67.9%
	Min	89.3%	93.0%	96.7%	92.2%	91.4%	80.1%	74.9%	94.4%	90.8%	89.5%	67.2%	74.3%
	Average	98.9%	97.7%	97.8%	75.0%	93.0%	89.0%	89.8%	91.7%	92.3%	93.5%	98.3%	92.9%
	STD	75.6%	81.5%	88.3%	82.6%	93.3%	89.8%	76.2%	78.7%	90.4%	87.3%	85.3%	70.2%
	Overall	**84.3%**	**91.2%**	**95.4%**	**83.3%**	**90.1%**	**88.7%**	**81.8%**	**86.5%**	**85.8%**	**89.8%**	**87.1%**	**76.3%**
Multi-input 5 s	Max	73.2%	93.3%	98.1%	76.8%	82.5%	98.2%	87.8%	80.8%	85.3%	89.1%	97.4%	82.1%
	Min	91.3%	95.1%	98.5%	98.4%	96.0%	76.5%	85.7%	94.4%	91.0%	94.3%	78.4%	89.0%
	Average	97.7%	95.5%	98.6%	83.7%	96.9%	89.8%	88.4%	91.9%	98.0%	97.5%	96.4%	89.3%
	STD	89.7%	86.2%	91.3%	85.3%	97.0%	98.0%	90.8%	81.0%	88.8%	91.6%	87.2%	93.2%
	Overall	**88.0%**	**92.5%**	**96.7%**	**86.1%**	**93.1%**	**90.6%**	**88.2%**	**87.0%**	**90.8%**	**93.1%**	**89.8%**	**88.4%**

Table 3. The accuracy of each statistic under the different input model

At the same time, the overall prediction result of the MI-LSTM model is better than the SI-LSTM model. The additional input factors increase the dimension of information, which enables the MI-LSTM model to explore more relationships between different input factors and the motion response of the target output. MI-LSTM model also adds more details to the final prediction results, improving the overall accuracy of the prediction results. In other words, there is a positive correlation between mooring force, wave elevation, and the motion response of the platform.

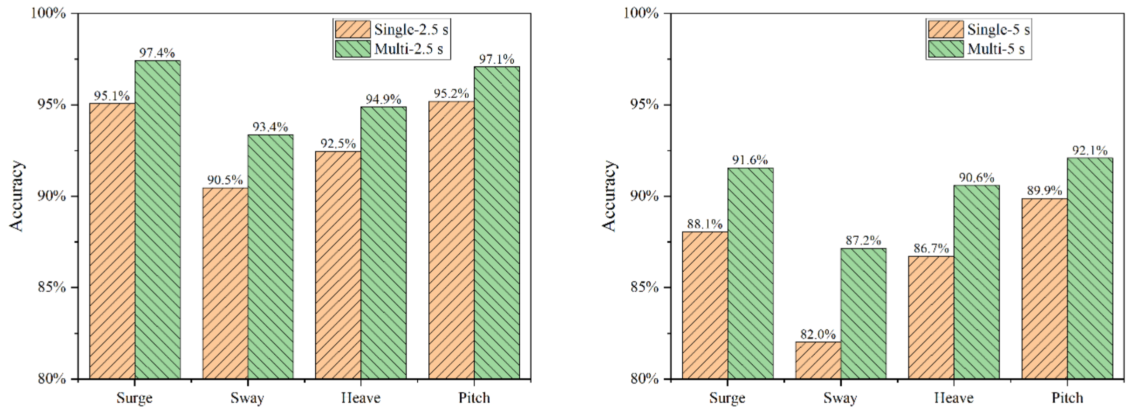

(a) (b)

Figure 17. Overall accuracy under different PATs: (a) 2.5 s; (b) 5 s

5. Second-order Hydrodynamic Effects

5.1 Prediction results under the influence of second-order hydrodynamic effects

The influence of second-order hydrodynamics is significant for the load prediction of a FOWT [34]. EC1-EC3 are again simulated considering second-order hydrodynamic effects, the simulation data is imported into the MI-LSTM model for training. The prediction results under the second-order hydrodynamic force are obtained after the training, shown in **Figures 18-20.**

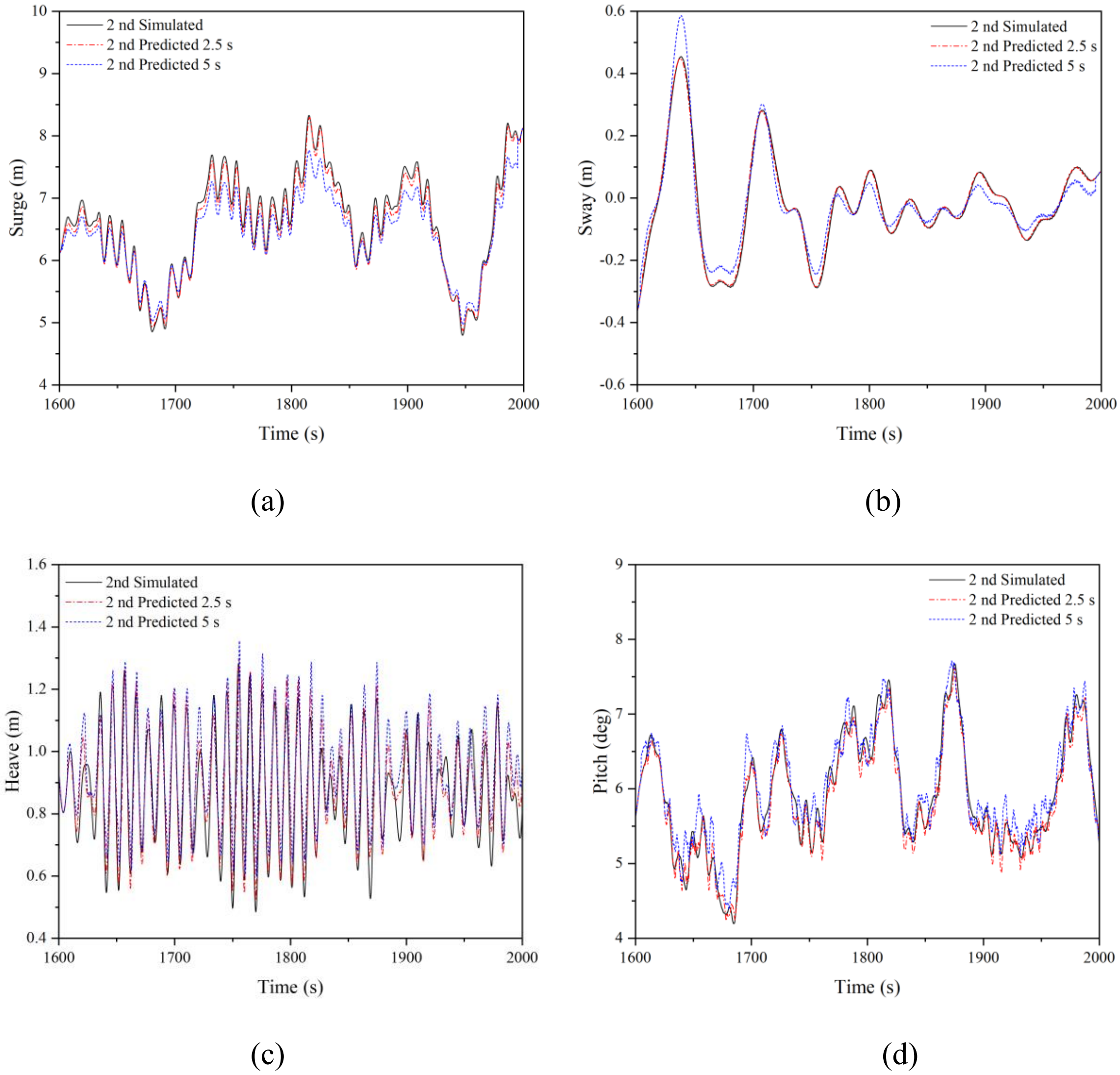

Figure 18. Simulated and predicted values of EC 1 at 2.5 s and 5 s:

(a) Surge; (b) Sway; (c) Heave; (d) Pitch

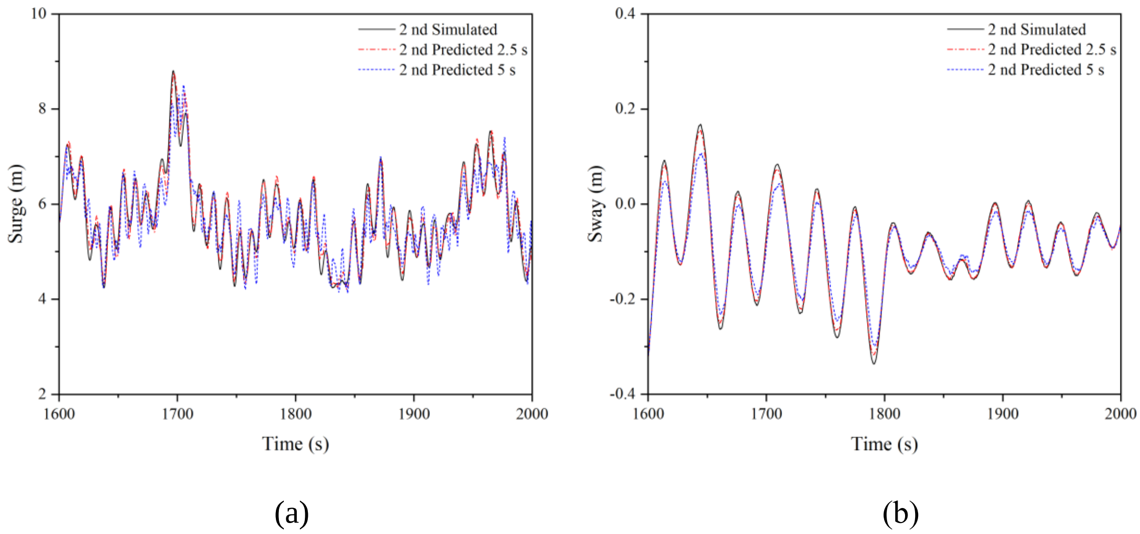

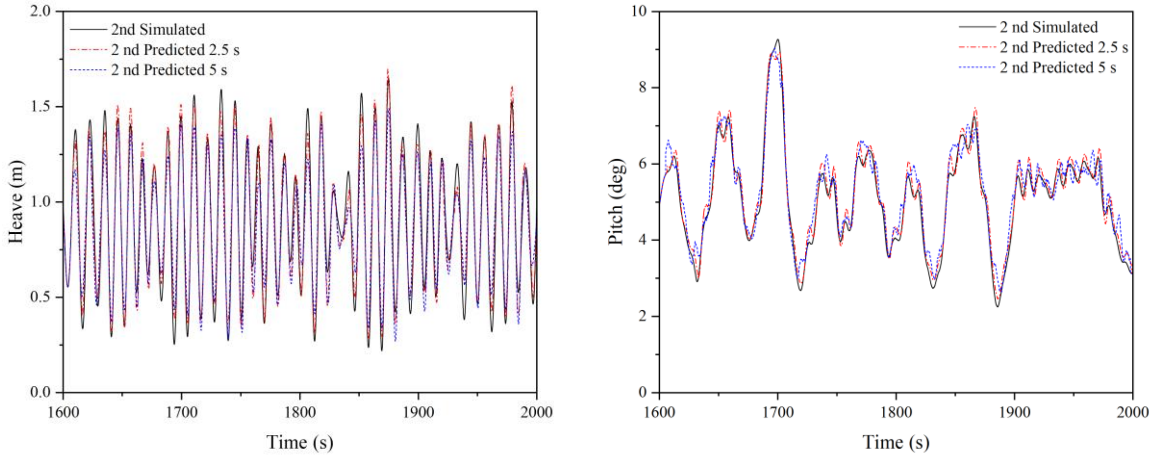

(c) (d)

Figure 19. Simulated and predicted values of EC 2 at 2.5 s and 5 s:

(a) Surge; (b) Sway; (c) Heave; (d) Pitch

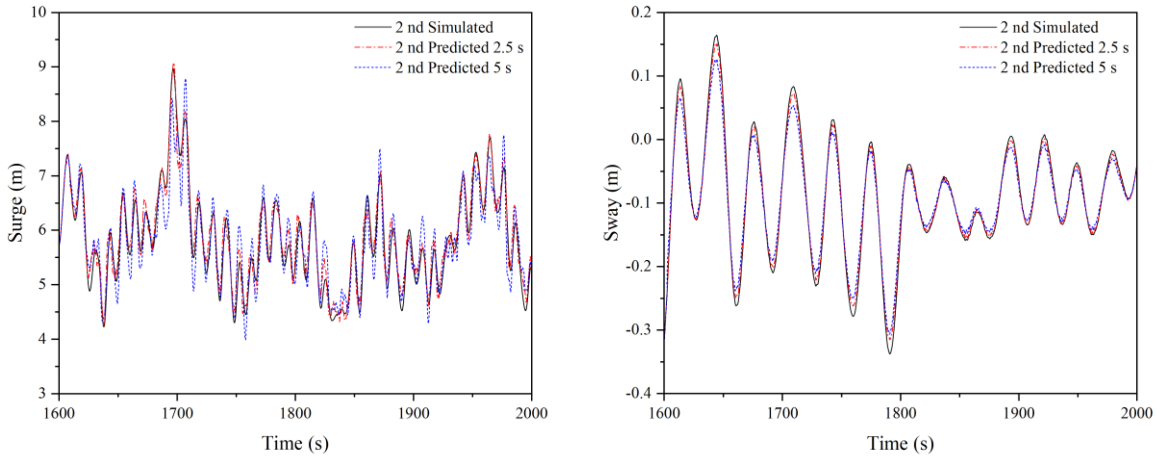

(a) (b)

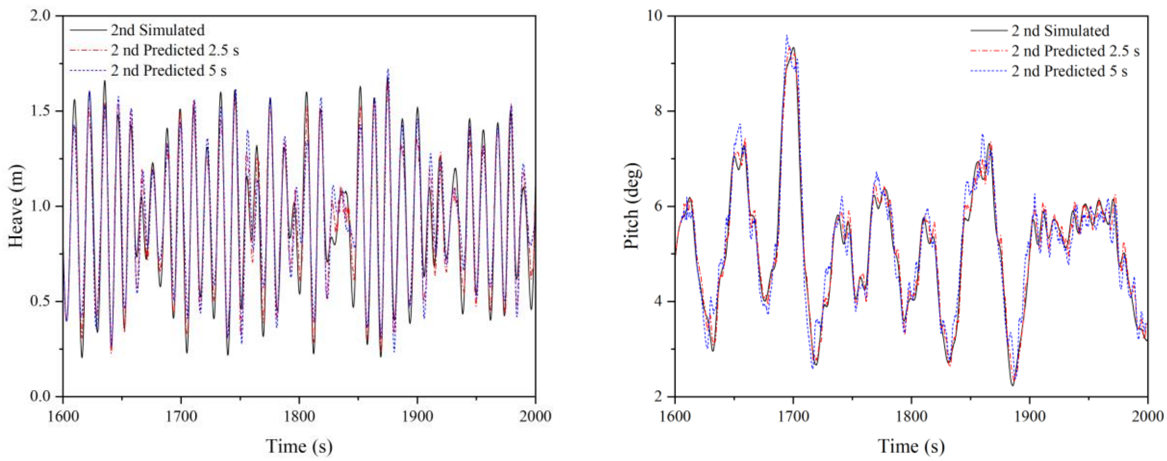

(c) (d)

Figure 20. Simulated and predicted values of EC 3 at 2.5 s and 5 s:

(a) Surge; (b) Sway; (c) Heave; (d) Pitch

Figures 18-20 show that the peak fitting in all directions at 5 s is weaker than that of 2.5 s, similar to the case when the platform model is affected by first-order hydrodynamic forces. Compared with the first-order hydrodynamic influence, the prediction results under the second-order hydrodynamics show smaller fluctuations in both surge and pitch. On the other hand, the predicted value of sway is smooth, and there is no slight fluctuation. The error of prediction results in heave mainly occurs in peaks and troughs, but it is not obvious. The statistical accuracy in each direction, as well as the overall accuracy, is further analyzed in section 5.2.

5.2. Error Analysis

To compare the short-term prediction effect of the MI-LSTM model in both first-order hydrodynamics and second-order hydrodynamics cases, the results of the PAT of 2.5 s under EC 1 are selected for comparison, shown in **Figure 21**.

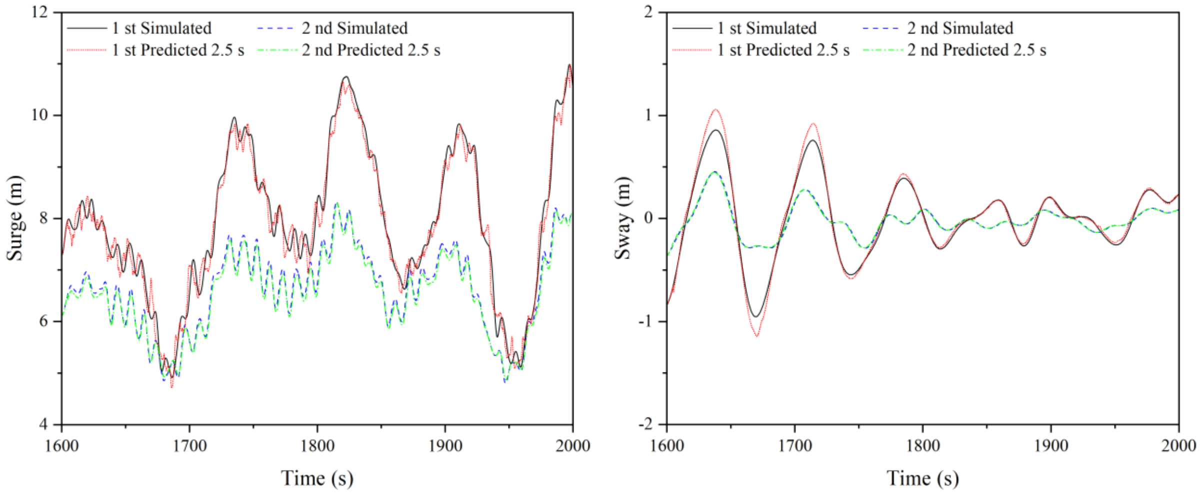

(a) (b)

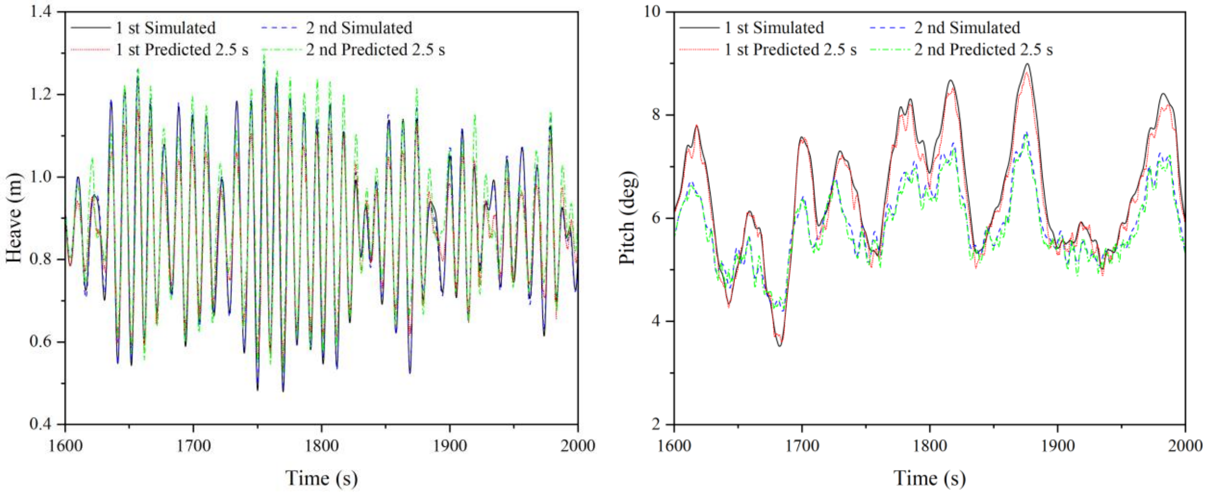

(c) (d)

Figure 21. Comparison of 1st-order and 2nd-order hydrodynamic prediction results: (a) Surge; (b) Sway; (c)Heave; (d) Pitch

According to **Figure 21**, it is observed that the motion response exhibits a stronger nonlinear characteristic under the influence of second-order hydrodynamic forces. This phenomenon is particularly evident in the surge, pitch, and sway directions, where more nonlinear fluctuations appear at the extremes of the kinematic response in all three directions. The effect of second-order hydrodynamic forces did not have much influence in the heave direction.

At the same time, in the surge, sway and pitch directions, there are significant deviations in the predicted values at the extremes of the motion response for the first-order hydrodynamics case. While in the second-order hydrodynamics case, the MI-LSTM model has better prediction at both peak and trough values. In the heave direction, the motion response of the platform in the two cases does not differ much and does not have the nonlinear characteristics in the other three directions. Therefore, the prediction effect of the MI-LSTM model in the heave direction under the influence of second-order hydrodynamics is not significantly improved.

The response spectrum analysis of the platform under the influence of second-order hydrodynamics are supplemented and chose EC 1 to plot the power spectrum density (PSD), as shown in **Figure 22**. There is a common phenomenon in all four directions, the predicted value of 2.5s is better than 5s in the performance of PSD, and both of them fit better with the PSD results of simulation values. The difference between the predicted and simulated values is mainly in the low-frequency peak of the response spectrum, while the PSD performance of the model predictions is better at the off-peak.

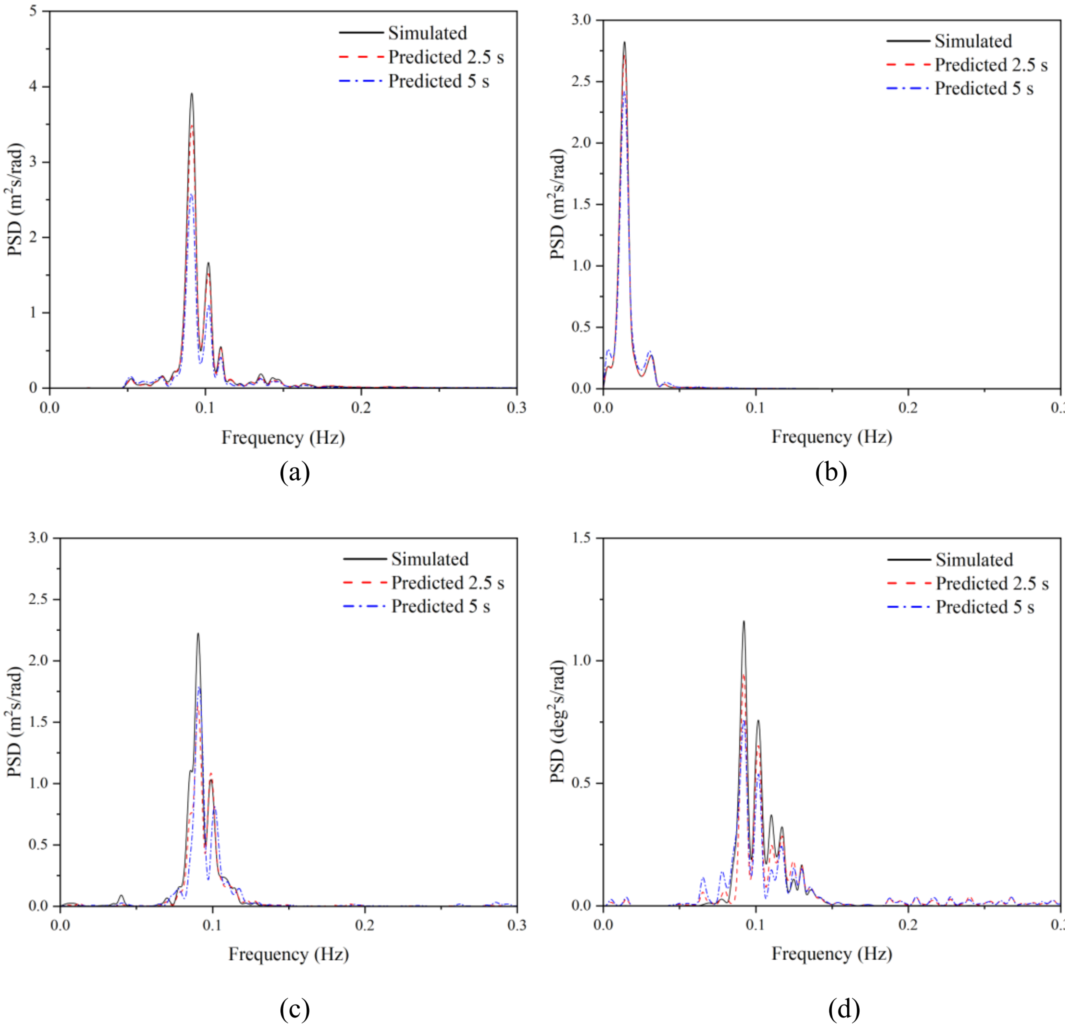

Figure 22. Power spectral density of motion response in different directions

(a) Surge; (b) Sway; (c)Heave; (d) Pitch

Under the influence of second-order hydrodynamics, this section also analyzes the individual statistics of the prediction results and calculates the overall accuracy of each direction of motion response, shown in **Table 4**.

Table 4. The accuracy of each statistic under the influence of second-order hydrodynamics

Mode	Statistics	EC 1				EC 2				EC 3			
		Heave	Pitch	Surge	Sway	Heave	Pitch	Surge	Sway	Heave	Pitch	Surge	Sway
Multi-input 2.5 s	Max	96.5%	99.4%	99.6%	98.7%	92.6%	96.3%	99.5%	92.2%	98.0%	98.9%	98.8%	91.8%
	Min	88.5%	99.2%	98.5%	99.1%	90.9%	90.7%	99.2%	97.0%	90.2%	96.2%	99.1%	94.9%
	Average	98.8%	98.8%	98.9%	96.5%	98.0%	97.6%	99.7%	99.0%	99.9%	99.0%	98.9%	99.2%
	STD	89.9%	96.2%	96.1%	98.6%	95.8%	96.5%	99.6%	94.6%	98.6%	99.2%	96.7%	92.8%
	Overall	**93.4%**	**98.4%**	**98.3%**	**98.2%**	**94.3%**	**95.3%**	**99.5%**	**95.7%**	**96.7%**	**98.3%**	**98.4%**	**94.7%**
Multi-input 5 s	Max	87.0%	99.5%	97.6%	71.0%	97.1%	97.5%	96.6%	63.4%	94.2%	97.2%	97.8%	77.1%
	Min	94.3%	95.5%	96.5%	97.5%	89.5%	82.5%	97.4%	97.0%	94.3%	93.4%	94.4%	94.9%
	Average	98.6%	98.1%	97.3%	80.7%	94.6%	96.5%	99.3%	98.2%	94.5%	98.8%	99.6%	99.0%
	STD	87.9%	92.3%	91.4%	98.1%	93.1%	92.5%	90.9%	80.4%	92.6%	98.0%	91.3%	84.1%
	Overall	**92.0%**	**96.3%**	**95.7%**	**86.8%**	**93.6%**	**92.3%**	**96.0%**	**84.8%**	**93.9%**	**96.9%**	**95.8%**	**88.8%**

According to the results given in **Table 4**, it can be seen that the accuracy of the predicted results in all directions under the influence of second-order hydrodynamics is still at a high level, overall accuracy exceeds 90% at PAT of 2.5 s and 85% at PAT of 5 s. This phenomenon verifies the conclusions of Section 4 and confirms that an increase in PAT leads to a decrease in prediction accuracy.

The overall accuracy of the 4 degrees of freedom directions calculated from **Table 4** is shown in **Figure 23**. At PAT of 2.5 s, the difference in prediction accuracy between the second-order hydrodynamics and the first-order hydrodynamics is more obvious in surge and sway. At PAT of 5 s, in the direction of surge, heave, and pitch, the prediction accuracy in the second-order hydrodynamics case is about 3% higher than that in the first-order hydrodynamics.

By comparing with the results in the first-order hydrodynamics in Section 4, it can be found that the MI-LSTM model in the second-order hydrodynamics case not only has a good ability to learn multi-factor relationships and platform response prediction but also has a higher prediction accuracy than the first-order hydrodynamics case.

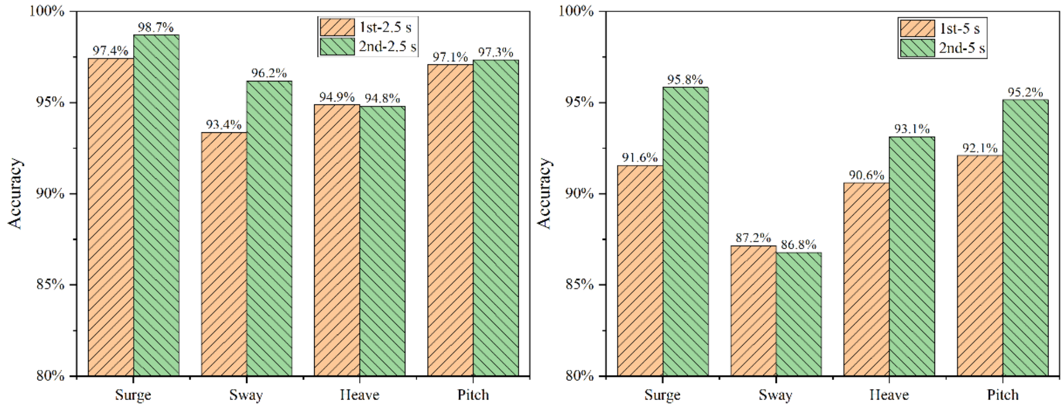

(a) (b)

Figure 23. Overall accuracy under different PATs: (a) 2.5 s; (b) 5 s

6. Comparison with the MI1D-CNN model

6.1 Predicted results with MI1D-CNN model

Currently, the mainstream deep learning methods mainly include the CNN method and the RNN method, and the MI-LSTM model established in Section 4 belongs to the RNN method. CNN methods are mostly used in image recognition and text recognition. As a representative method to deal with time series problems in CNN, a one-dimensional convolutional neural network (1D-CNN) has a certain effect on short-term prediction by adding a pooling layer.

In this section, a multi-input one-dimensional convolutional neural network (MI1D-CNN) is built to compare the CNN method with the LSTM method for the motion response prediction problem, using the same training data as in Section 4. The training of the MI1D-CNN model is completed, and the results obtained from the multi-input LSTM model are compared in Section 6.2 in terms of training time and overall accuracy. The prediction results obtained by the MI1D-CNN model are shown in **Figures 24-26**.

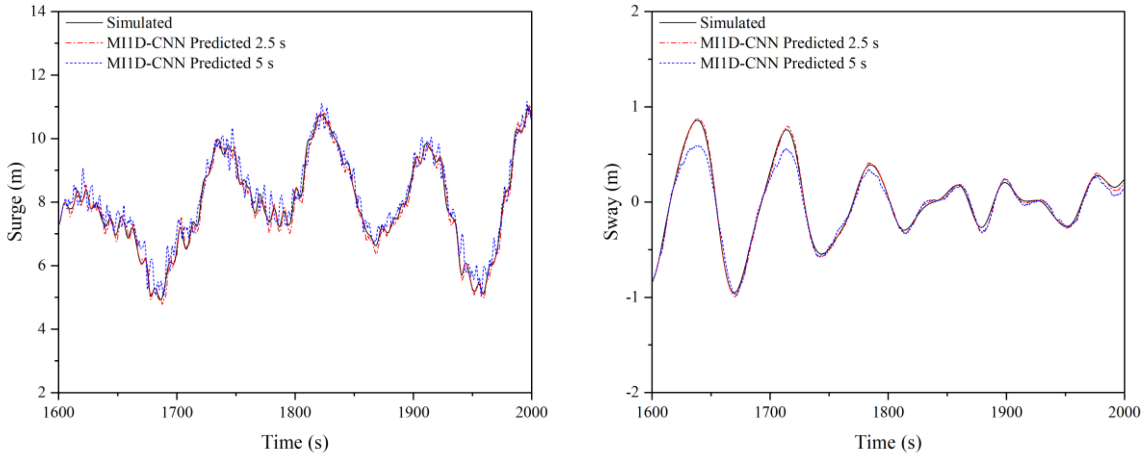

(a) (b)

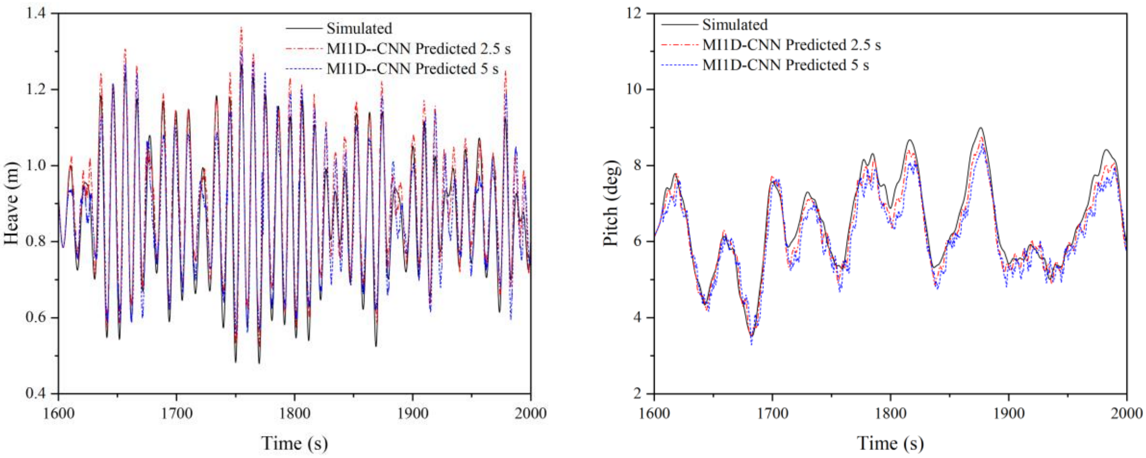

(c) (d)

Figure 24. Simulated and predicted values of EC 1 at 2.5 s and 5 s:

(a) Surge; (b) Sway; (c) Heave; (d) Pitch

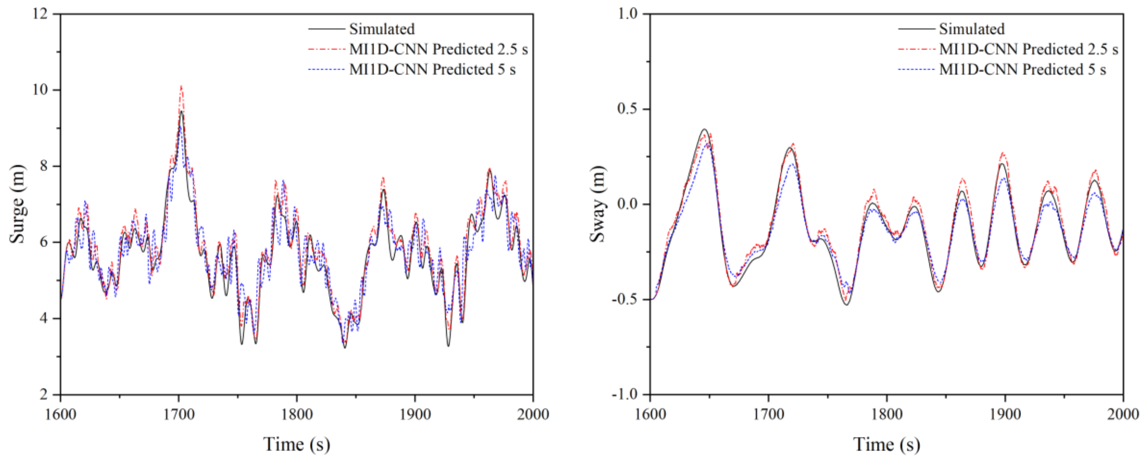

(a) (b)

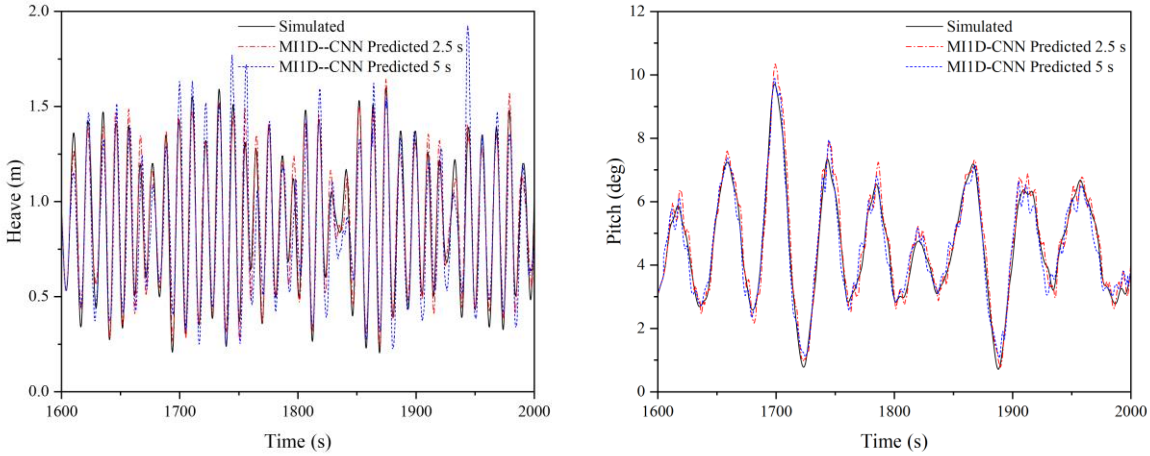

(c) (d)

Figure 25. Simulated and predicted values of EC 2 at 2.5 s and 5 s:

(a) Surge; (b) Sway; (c) Heave; (d) Pitch

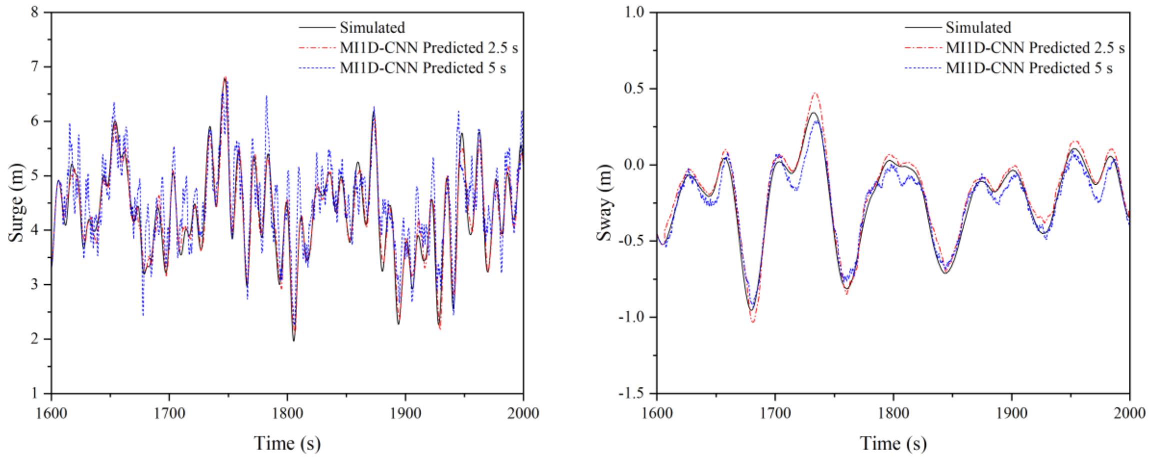

(a) (b)

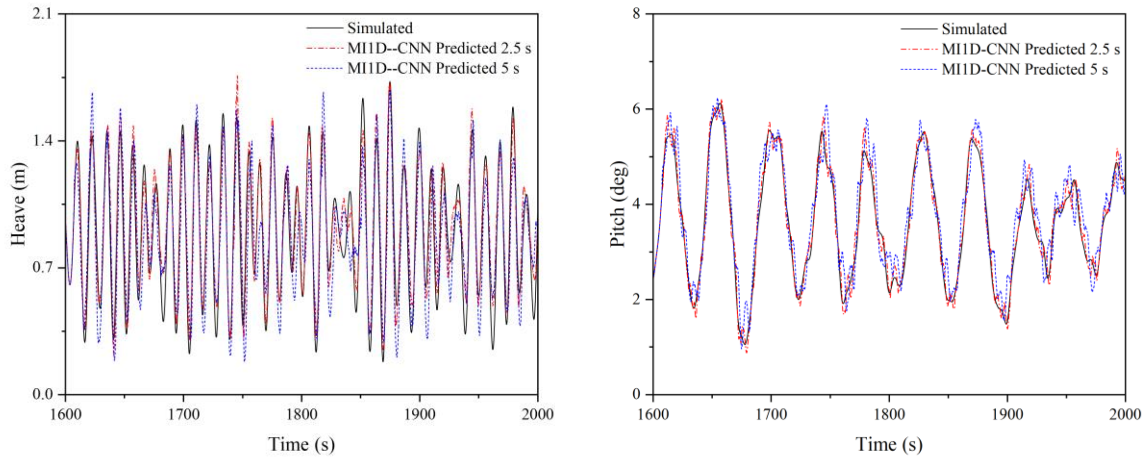

(c) (d)

Figure 26. Simulated and predicted values of EC 3 at 2.5 s and 5 s：

(a) Surge; (b) Sway; (c) Heave; (d) Pitch

According to **Figures 24-26**, and compared with **Figures 11-13** in Section 4.3, it can be found that the motion response predicted by the MI1D-CNN model produces a large number of serrations in surge and pitch of each environmental condition, especially at PAT of 2.5 s. At the same time, the prediction result at PAT of 5 s in sway does not fit well with the simulation results. To further compare the results of the MI-LSTM model with the MI1D-CNN model, it is further explained from the aspects of training time and overall accuracy in Section 6.2.

6.2 Comparison with Multi-input LSTM Model

By counting the Loss values during the training of the MI1D-CNN model, we show the decrease of the model training Loss for EC 1, shown in **Figure 27**. One can observe that, unlike the change process of the MI-LSTM model's Loss value, the oscillation phase of the MI1D-CNN model's Loss value is not obvious in the decreasing process. the MI1D-CNN model's Loss value stops changing when the number of training rounds reaches 50 rounds, which indicates that the model training has been completed and the performance is satisfactory. To further observe the imitative effect between the predicted values obtained by the two models and the simulated values, EC1 is selected and the results are summarized as shown in **Figure 28**.

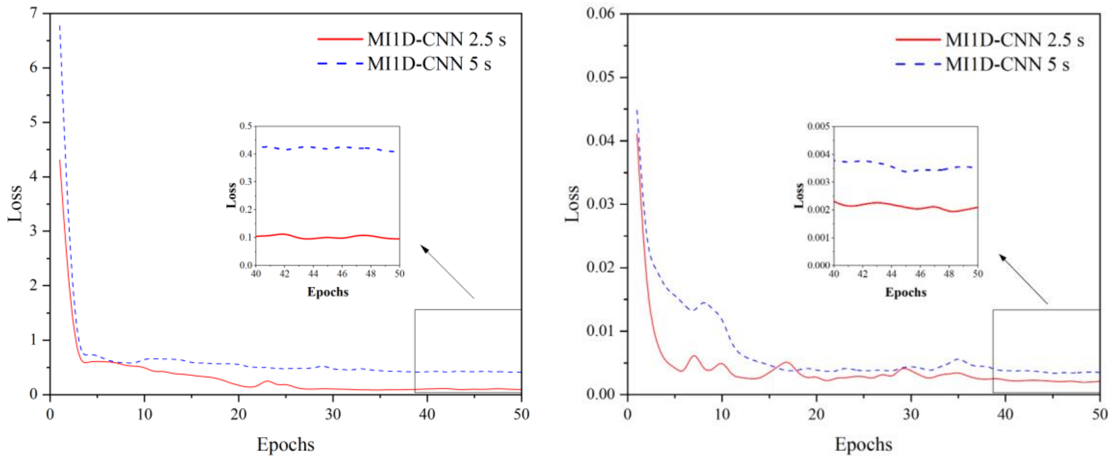

(a) (b)

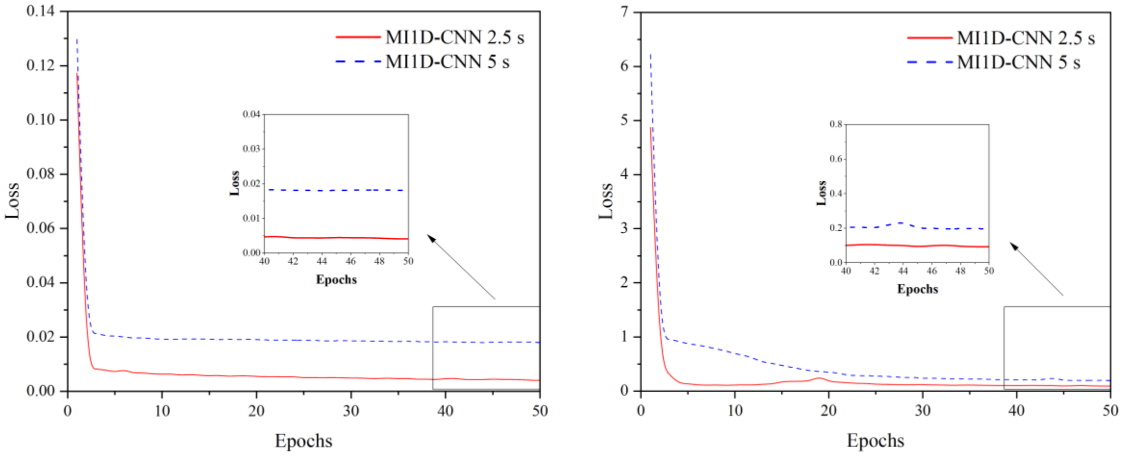

(c) (d)

Figure 27. The curve of Loss affected by Epochs for different directions:

(a) Surge; (b) Sway; (c) Heave; (d) Pitch

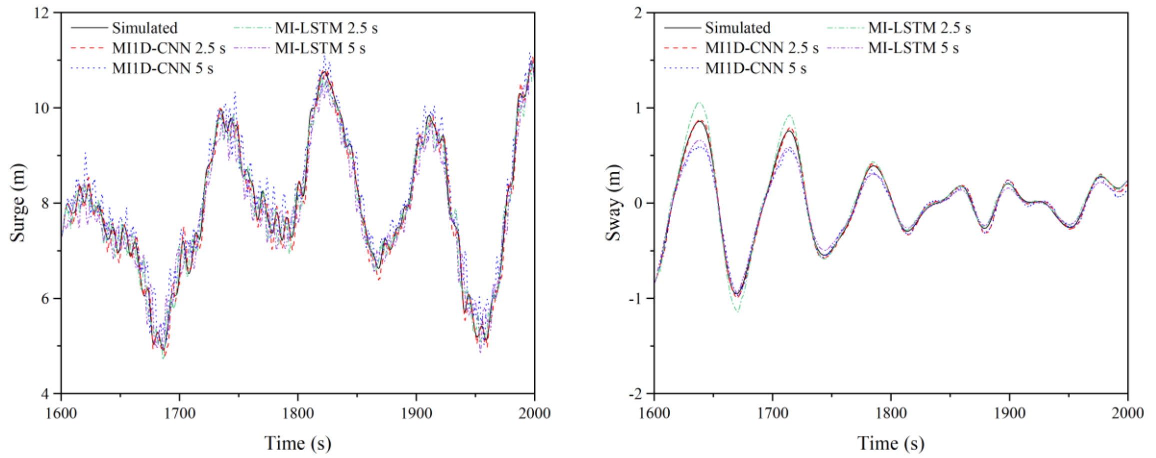

(a) (b)

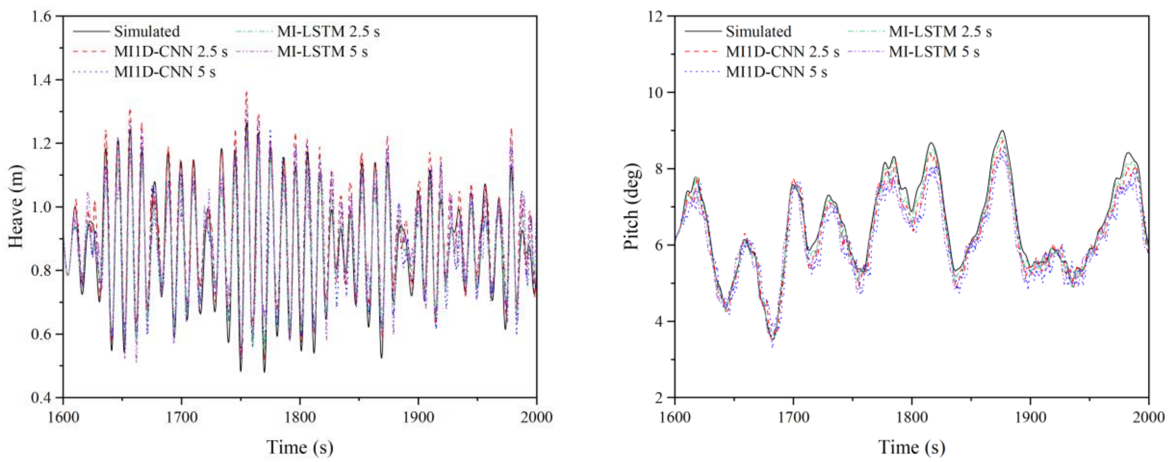

(c) (d)

Figure 28. The results of the MI1D-CNN model and the MI-LSTM model are compared: (a) Surge; (b) Sway; (c) Heave; (d) Pitch

According to **Figure 28**, from the overall imitative effect of the time series curve, the prediction results of both models fit well with the simulation results at PAT of 2.5 s. However, at PAT of 5 s, the result of the MI1D-CNN model is slightly inferior to the MI-LSTM model result, and when the PAT is at 5 s, the predicted value of the former has a large fluctuation. This volatility does not exist in the simulation value, particularly in **Figures 28(a**) and **(d)**. The time series of the platform response has a certain smoothness in sway, so both models' imitative effects are good. While the time series of the platform response itself is more volatile in heave, the imitative effects of the peak are not as good as in other directions.

To find out the difference between the MI1D-CNN model and the MI-LSTM model, the overall accuracy of the MI1D-CNN model is calculated by combining each operating condition. Then compare the overall accuracy of the MI1D-CNN model with the MI-LSTM model proposed in Section 4 and the result is shown in **Figure 29**.

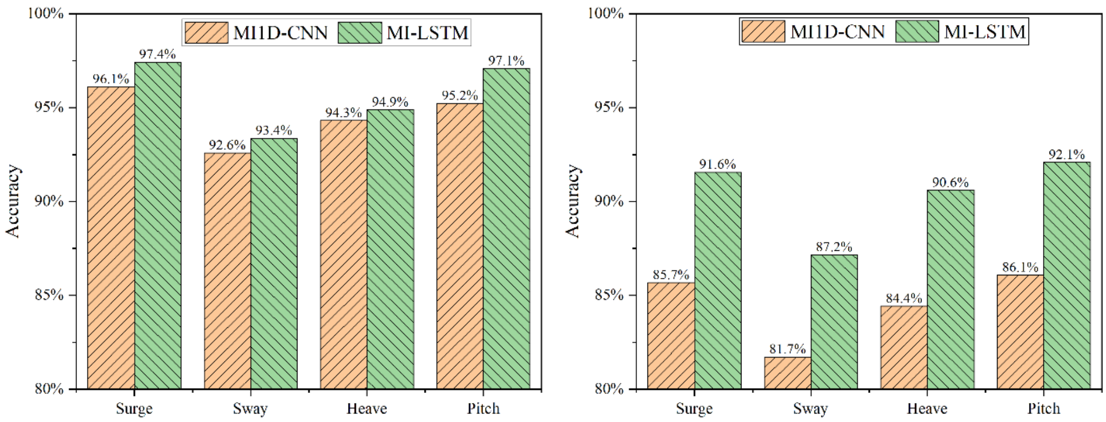

(a) (b)

Figure 29. Comparison of the overall accuracy of different models in each direction: (a) 2.5 s; (b) 5s

According to **Figure 29**, it can be found that there is no significant difference between the results of the two models when PAT is at 2.5 s, the overall effect of the MI-LSTM model is slightly better than the MI1D-CNN model, and the accuracy of the former is 1%-2% higher than the latter in all directions. But at PAT of 5 s, the situation is very different, the MI-LSTM model performs much better than the MI1D-CNN model, and the accuracy of the former is about 5% higher than the latter in all directions.

It can be seen that when the corresponding period of the prediction platform becomes longer, the traditional CNN model is not satisfactory, while the MI-LSTM model proposed in this paper performs well. Since 1D-CNN only performs convolution operations on time series information within the length of a convolution, heritability in time series information is only reflected in a single convolutional neuron. Therefore, when PAT is small, the effect on the MI1D-CNN model and the MI-LSTM model is insignificant. However, with the increase of PAT, the disadvantage of the MI1D-CNN model in processing temporal genetic information will become significant.

In addition, the training time of the two models is also recorded, as shown in **Table 5**. According to **Table 5**, the training time of the MI1D-CNN model is much shorter than that of the MI-LSTM model, which is related to the learning and calculation method of the model itself. The training time of the MI1D-CNN model is short, but it sacrifices a part of the accuracy, and the training time of the MI-LSTM model is relatively long, but the accuracy is greatly improved.

Table 5. Statistics on the training duration of the two models

Modes	PAT (s)	Epochs	Time (s)
MI-LSTM	2.5	50	912
	5	50	1053
MI1D-CNN	2.5	50	108
	5	50	157

In summary, balancing training time and accuracy has always been an important issue in deep learning. If the goal is ultra-short-term forecasting of the FOWT motion response and the accuracy requirement is relatively low, the MI1D-CNN model can be chosen. However, to increase the time span of motion response forecasting and maintain prediction accuracy, the MI-LSTM model is a better choice.

7. Conclusion

Based on the motion response data of the Braceless platform, the MI-LSTM prediction model is established by the RNN deep learning method and is trained for different degrees of freedom under different environmental conditions. The accuracy of prediction results under different PAT and input methods are determined and compared using statistics. Based on the analysis and discussions, the conclusion can be made as follows:

(1)Taking the previous data of platform motion response, mooring force, and wave elevation as input, after 50 rounds of training with two LSTM models, the Loss no longer decreases, resulting in accurate prediction results. The Loss of the MI-LSTM model is slightly better than the SI-LSTM model. The MI-LSTM model more comprehensively learns the relationship between multiple factors and the target output.

(2)Based on the established and trained LSTM neural network model, the prediction results of the model fit well with the simulated value. The prediction accuracy with PAT at 2.5 s is slightly higher than the accuracy with PAT at 5 s and the overall performance of the MI-LSTM model is better than the SI-LSTM model. The additional two factors can positively improve the accuracy of the final prediction result.

(3) The established MI-LSTM model is applied to the situation where the platform is affected by second-order hydrodynamics, and it is found that the model has a better predictive effect on the response of the Braceless platform affected by second-order hydrodynamics. The MI-LSTM model has a better performance for the case where the nonlinearity phenomenon is more pronounced.

(4) The MI-LSTM model established in this paper is compared with the traditional MI1D-

CNN model, and the advantages and disadvantages of the two models are clarified from the aspects of training time and overall accuracy. When the PAT is small, the difference between the results of the two models is not significant, while when the PAT increases, the results obtained by the MI-LSTM model are better than those obtained by the MI1D-CNN model.

Acknowledgment

This research is funded by the National Natural Science Foundation of China (Grant No. 52071058, 51939002). This paper is also partially funded by the Central Guidance on Local Science and Technology Development Fund of Shenzhen (2021Szvup018) and the Open Research Fund of Hunan Provincial Key Laboratory of Key Technology on Hydropower Development (PKLHD202003). The last author is now supported by the National Natural Science Foundation of China (Grant No. 52201379).

Reference

[1] Gao W, Li C, Ye Z. The current situation and latest research of deep-sea floating wind turbine. Engineering Sciences 2014; 16(2): 79-87.

[2] Ren, ZR, Zhou HY, Li BB, Hu ZZ, Yu MH, Shi W. Localization and topological observability analysis of a moored floating structure using mooring line tension measurements, Ocean Engineering 2022; 266P5: 112706. https://doi.org/10.1016/j.energy.2022. 112706

[3] Liu Y, Hu C, Sueyoshi M, Yoshida S, Iwashita H, Kashiwagi M. Motion response characteristics of a Kyushu-University semi-submersible floating wind turbine with trussed slender structures: Experiment vs. numerical simulation. Ocean Engineering 2021; 232: 109078. https://doi.org/10.1016/j.oceaneng.2021.109078

[4] Zeng YX, Shi W, Michailides C, Ren ZR, Li X. Turbulence model effects on the hydrodynamic response of an oscillating water column (OWC) with use of a computational fluid dynamics model. Energy 2022; 261:124926. https://doi.org/10.1016/j.energy.2022.124926

[5] Zhang LX, Shi W, Zeng YX, Michailides C, Zheng SM, Li Y. Experimental Investigation on the hydrodynamic effects of Heave Plates for application of floating offshore wind turbine. Ocean Engineering 2023; 267C:113103. https://doi.org/10.1016/j.oceaneng.2022.113103

[6] Shi W, Zhang L, Karimirad M, Michailides C, Jiang Z, Li X. Combined effects of aerodynamic and second-order hydrodynamic loads for three semisubmersible floating

wind turbines in different water depths. Applied Ocean Research 2023; 130: 103416 https://doi.org/10.1016/j.apor.2022.103416

[7] Zhang Y, Shi W, Li DS, Li X, Duan YF, Verma, AS. A novel framework for modeling floating offshore wind turbines based on the vector form intrinsic finite element (VFIFE) method. Ocean Engineering 2022; 262:112221. https://doi.org/10.1016/j.oceaneng.2022.112221

[8] Shi W, Zeng XM, Feng XY, Shao YL, Li X. Numerical study of higher-harmonic wave loads and runup on monopiles with and without ice-breaking cones based on a phase-inversion method. Ocean Engineering 2023; 267: 113221.

[9] Zeng XM, Shi W, Feng XY, Shao YL, Li X. Investigation of higher-harmonic wave loads and low-frequency resonance response of floating offshore wind turbine under extreme wave groups. Marine Structures 2023; 89:103401.

[10] Stetco A, Dinmohammadi F, Zhao X, Robu V, Flynn D, Barnes, M. Machine learning methods for wind turbine condition monitoring: a review. Renewable Energy 2019; 133: 620-635. https://doi.org/10.1016/j.renene.2018.10.047.

[11] Huang LF. Research On Online Prediction of Nonstationary Nonlinear Ship Motion in Ocean Waves. Harbin Engineering University, 2016.

[12] Li HB, Xiao LF, Wei HD. Research on Online Prediction of Floating Offshore Platform Motions based on LSTM Network. Journal of Ship Mechanics 2021; 25:576-585. https://doi.org/10.3969/j.issn.1007-7294.2021.05.006.

[13] Bahdanau D, Cho K, Bengio Y. Neural machine translation by jointly learning to align and translate. Computer Science 2014; 1: 1409.0473.

https://doi.org/10.48550/arXiv.1409.0473.

[14] Wang ZM, Qiao DS, Yan J, Tang GQ. A new approach to predict dynamic mooring tension using LSTM neural network based on responses of floating structure. Ocean Engineering 2022;249: 110905. https://doi.org/10.1016/j.oceaneng.2022.110905

[15] Khan A, Bil C, Marion KE. Ship motion prediction for launch and recovery of air vehicles. Oceans 2005:1640198. https://doi.org/10.1109/OCEANS.2005.1640198.

[16] Gu M, Liu CD, Zhang JF. Extreme short-term prediction of ship motion based on chaotic theory and RBF neural network. Journal of Ship Mechanics 2013; 17(10): 1147-1152. https://doi.org/10.3969/j.issn.1007-7294.2013.10.007.

[17] Liu Y, Duan W, Huang L, Duan S. The input vector space optimization for LSTM deep learning model in real-time prediction of ship motions. Ocean Engineering 2020; 213: 107681. https://doi.org/10.1016/j.oceaneng.2020.107681.

[18] Pena B, Huang L. Wave-GAN: A deep learning approach for the prediction of nonlinear regular wave loads and run-up on a fixed cylinder. Coastal Engineering (Amsterdam) 2021; 167: 103902. https://doi.org/10.1016/j.coastaleng.2021.103902.

[19] Lian LK, Zhao YP, Bi CW, Xu ZJ, Du H. Research on Damage Detection Method of Flat Fishing Net Based on Digital Twin Technology. Fishery Sciences 2022; 43: 19663. https://doi.org/10.19663/ j. issn.2095-9869.20210825001.

[20] Bjørni F, Lien S, Midtgarden T, Kulia G. Prediction of dynamic mooring responses of a floating wind turbine using an artificial neural network. IOP Conference Series. Materials Science and Engineering 2021; 1201(1): 12023. https://doi.org/10.1088/1757-899X/1201/1/012023.

[21] Zhang F, Guo Z, Sun, X. Short-term wind power prediction based on EMD-LSTM combined model. IOP Conference Series: Earth and Environmental Science 2020; 514(4): 042003. https://doi.org/10.1088/1755-1315/514/4/042003.

[22] Sutskever I, Vinyals O, Le Quoc V. Sequence to sequence learning with neural networks. Advances in neural information processing systems 2014; 27.

[23] Cho K, Van Merriënboer B, Gulcehre C. Learning phrase representations using RNN encoder-decoder for statistical machine translation. Computer Science 2014;1406.1078. https://arxiv.org/abs/1406.1078

[24] Vinyals O, Le Q. A Neural Conversational Model. Computer Science 2015; 1506.05869. https://arxiv.org/abs/1506.05869

[25] Liu Y, Li D. Research on User Gender Prediction of Chinese Microblog Based on Short Text Analysis. IEEE 2018: 775-779. https://doi.org/10.1109/ICIVC.2018.8492759

[26] Hochreiter S, Schmidhuber J. Long short-term memory. Neural Computation 1997; 9(8): 1735-1780. https://doi.org/10.1162/neco.1997.9.8.1735

[27] Graves A. Supervised sequence labelling with recurrent neural networks. Studies in Computational Intelligence, 2013; 385.

[28] Hurst HE. Long-term storage capacity of reservoirs. Transactions of the American society of civil engineers, 1951, 116(1): 770-799. https://doi.org/10.1061/TACEAT.0006518

[29] Graves A. Generating sequences with recurrent neural networks. Computer Science 2013. https://doi.org/10.48550/arXiv.1308.0850

[30] Kingma D, Ba J. Adam: a method for stochastic optimization. Computer Science 2014. https://doi.org/10.48550/arXiv.1412.6980

[31] Srivastava N, Hinton G, Krizhevsky A, Sutskever I, Salakhutdinov R. Dropout: a simple way to prevent neural networks from overfitting. Journal of Machine Learning Research 2014; 15(1): 1929-1958.

[32] Hinton G, Srivastava N, Krizhevsky A, Sutskever I. Improving neural networks by preventing co-adaptation of feature detectors. Computer Science 2012. https://doi.org/10.48550/arXiv.1207.0580

[33] Li L, Gao Z, Moan T. Joint Distribution of Environmental Condition at Five European Offshore Sites for Design of Combined Wind and Wave Energy Devices. Journal of Offshore Mechanics and Arctic Engineering 2015; 137(3): 031901(16). https://doi.org/10.1115/1.4029842

[34] Zhang LX, Shi W, Karimirad M, Michailides C, Jiang ZY. Second-order Hydrodynamic Effects on the Response of Three Semisubmersible Floating Offshore Wind Turbines. Ocean Engineering 2020; 207.C: 107371. Web. https://doi.org/10.1016/j.oceaneng.2020.107371